SISSA
Scuola
Internazionale
Superiore di
Studi Avanzati

Physics Area - PhD course in
Statistical Physics

Anomalous heat transport in harmonic long-range chains

Candidate:
Francesco Andreucci

Advisors:
Stefano Ruffo
Andrea Trombettoni

Academic Year 2022-2023

Contents

Acknowledgments

I would like to to express my deepest thanks to my advisors, Stefano Ruffo and Andrea Trombettoni, for their guidance during my PhD, both from the scientific and the human point of view. An heartfelt thanks also goes to Stefano Lepri, who acted as a *de-facto* third supervisor, especially for having introduced me to the wonders and the woes of numerical computations. Last but not least, a huge thanks to Carlos Mejia- Monasterio for the kind hospitality in Madrid and for all the discussions about physics and non. I learned a lot from all of you, and I am very happy that you were part of my PhD experience.
Next, I would like to thank the canteen staff of SISSA, especially Patrizia, who has the almost super-natural ability of remembering the name of everyone.
My years in Trieste would not have been as pleasant as they have been without all of the friends I met along the way. It is impossible here to mention everyone without turning these acknowledgements to a laundry list. A special thanks, though, goes to my flatmates Alessandro, Saman, Migno, Alice and Vittorio, for making *Villa Oriani* a special place. Even if now we all went our separate ways, I think that something of all the time we spent together will always remain with me.
Finally, I cannot finish this thesis without mentioning the continuous support of my family, especially during the most stressful and intense moments of my PhD, thank you for the constant encouragement.

Chapter 1

Preface

In the last two decades a lot of effort went into the study of anomalous, superdiffusive, heat transport and violations of the Fourier law in one-dimensional classical chains. Reviews on these topics are available in the literature [1, 2]. More recently, there has been interest in the study of heat transport in long-range interacting systems, i.e. systems where the interaction between constituents scales as a power-law of their distance. The long-range version of the XY model was analyzed in [3]: it was shown, by numerical integration of the equations of motion of the model, that the heat flux does not scale as the inverse of the system size (as stated by Fourier law), but as a non-trivial power of the latter which depends on the exponent of the long-range interaction. Furthermore, it was shown that if the exponent of the long-range interaction is between one and zero, then the system acts as an insulator. This puzzling behaviour was clarified in [4] where it was shown, numerically, that the poor energy conduction of the system is related to the presence of localized excitations ("discrete breathers") whose number is a decreasing function of the long-range exponent.
The long-range Fermi-Pasta-Ulam-Tsingou (FPUT) chain was analyzed for instance in [5]: thermal conductivity was numerically computed (via molecular dynamics simulations) and an anomalous scaling was found. Furthermore, it was numerically shown that, when the long-range exponent is equal to two, the discrete breathers can move freely across the system, thus boosting energy transport. This picture was also confirmed in [6]. In [7] the structure factors of the long-range FPUT model were obtained via numerical simulations of the system. The result is that these structure factors present several peaks at frequencies $\omega_{peak}(k)$: these are the low-energy, low-momentum propagating excitation, who were found to have an anomalous dispersion law. Furthermore, the numerical computation of the spatio-temporal correlation function of the energy shows that energy propagation strongly depends on the value

of the long-range exponent, suggesting once again an anomalous scaling of the thermal conductivity. Finally, both the dynamics of the long-range FPUT model and the long-range XY model when attached to two external heat baths was numerically simulated in [8]: again the result is that the heat flux does not scale as the inverse of the system size, but as a non-trivial power of the latter.
From the cursory overview we just exposed, it is evident that the understanding of anomalous transport in long-range systems is a difficult and unsolved problem, especially if one wants to obtain analytical results. Given the complexity of this task, we decided to restrict ourselves to linear long-range chains: even for these, apparently simple, cases we could not find in the literature any analytical result for transport quantities, with one exception detailed below. This PhD manuscript thus deals with the study of heat transport in long-range one-dimensional chains and contains the results I have obtained in my PhD work in this direction.
There are several methods in the literature to study heat transport in quadratic systems, like the one based on the Lyapunov equation introduced by Lebowitz [9], the Green function method by Dhar [2] and the generalized eigenvalue method [10]. As we will see, these methods can all be extended, with appropriate modifications, to the case of harmonic long-range systems. In particular the latter, which is rarely mentioned in the literature, will be instrumental to shed some light on the scaling of the heat flux in the long-range harmonic chain. Despite the apparent simplicity of these linear models, they exhibit, as we will see, highly non-trivial behaviours. For example, in the quadratic power-law long-range chain the heat flux scales with the size of the system with an anomalous exponent which depends on the long-range exponent of the chain. Furthermore, the model has an highly non-trivial "fractal-like" spectral structure.
Let us finally mention that from the study of some quadratic models, it might actually be possible to infer some qualitative aspects of the behaviour of interacting system. Indeed, in [11] a nearest-neighbours linear chain with nearest-neighbours stochastic momentum exchanges (i.e. two adjacent particles exchange their momenta at random times) was analyzed and the heat flux was computed. The result is that heat transport is anomalous, a property that is present only in interacting models for short range systems [1]. Saito and Tamaki [12] computed the thermal conductivity in a quadratic long-range chain with stochastic nearest-neighbours momentum exchanges and found that heat transport is anomalous: I extended their results to the case of long-range stochastic momentum exchanges.
The content of the manuscript is organized as follows.
In Chapter 2 we describe the main known properties about long-range systems, in particular we will focus on the consequences of the loss of additivity, the main equi-

librium properties (Peierls argument, Landau action and critical exponents) and the existence of a proper continuum limit.
In Chapter 3 we collect and revise the three main methods used in the literature to study heat transport in quadratic systems in two different contexts. At first, we consider heat transport in the stationary state of systems brought out of equilibrium by coupling to two external heat baths: this case can be studied with a method introduced by Lieb, Lebowitz and Lieb [9] or the so-called Green function method [2] by Dhar. The final part of the chapter is devoted to the computation of the thermal conductivity using the Green-Kubo formula in an isolated quadratic system with stochastic collisions.
In Chapter 4 we consider heat transport in the nonequilibrium steady-state of a fully-coupled network of N quantum harmonic oscillators, interacting with two heat reservoirs. We will consider two different cases: one in which the number of particles coupled to the baths is fixed and another in which it is proportional to N. In both cases we compute the asymptotic scaling with N of the heat flux and the temperature profile using the Green function method. This chapter is based on the results obtained in [13]
In Chapter 5 we study, numerically, the transport properties of a long-range (but not fully-connected) chain coupled with two heat reservoirs. In particular, we show that the heat flux scales as a power-law of the system size N and we discuss the relation between the spectral properties of the system and the value of the scaling exponent. This chapter is based on the results of [14]
In Chapter 6 we discuss the determination of thermal conductivity using the Green-Kubo formula in a quadratic long-range chain with stochastic collisions. In particular we consider both the case of nearest-neighbours collisions, recovering known results, and then we extend our analysis to the case of long-range collisions which was not studied before. The results of this chapter will be the focus of a future publication [15].
In Chapter 7 we present our conclusion and some further lines of development.

Chapter 2

Long-range interacting systems

In this chapter we recall some properties of long-range interacting systems that will be useful in the other chapters of this manuscript. In section 2.1 we explore some generic properties of long-range systems related to the loss of additivity with respect to the usual short-range interactions. In sections 2.2 we briefly describe the peculiarities of the critical behaviour of long-range systems and in section 2.3 we show how the properties of the spectrum of a long-range system can drastically change its behaviour in the thermodynamic limit. Finally, in section 2.4 we recall some examples of experimental realizations of this kind of systems. For a more detailed picture on the physics of long-range systems we refer to the reviews [16, 17] for the classical case and [18, 19] for the quantum case, respectively.

2.1 Extensivity and additvity in long-range systems

In long-range interacting systems the interaction between two constituents $U(r)$ scales as a power-law $U(r) \sim r^{-\alpha}$ for large r, being r the inter-constituent distance. Consider for instance a gas of long-range-interacting particles in a d-dimensional box of linear dimension R and volume $V \sim R^d$. If we assume that they are distributed with uniform density ρ, then the energy per particle e can be estimated as [16]:

$$e = \int_V d^d r\, \rho U(r) \sim \int_a^R \rho r^{d-1} dr\, r^{-\alpha} \sim \frac{\rho}{d-\alpha} \left[R^{d-\alpha} - a^{d-\alpha} \right], \tag{2.1}$$

where the length a encodes some short-range regularization of the potential, such as an hard-core interaction which does not affect in any way the long-rage properties

of the system. As we can see, in the thermodynamic limit we get two different behaviours for e, (and thus for the total energy $E = Ve$) according to the value of α:

$$e \sim \begin{cases} R^{d-\alpha} \sim V^{1-\alpha/d}, & \alpha < d \\ R^0, & \alpha > d \end{cases}, \quad E \sim \begin{cases} V^{2-\alpha/d}, & \alpha < d \\ V, & \alpha > d \end{cases}. \tag{2.2}$$

We immediately notice that if $\alpha < d$ the energy is super-extensive and this regime is called *strong-long-range*. Irrespective of the long-range nature of the interaction, the number of accessible states for the systems still scales factorially with the number of constituents, and thus the entropy is still extensive and can never compete with the super-extensive energy. It follows that this kind of systems cannot exhibit any form of phase transition. However, it should also be noted that we typically deal with finite systems and in the case of long-range interactions we expect the effect of boundaries to be important. For example, in globular stellar clusters, provided the temperature is high enough, the TS term can compete with the energy. A simpler way to study this regime is to make the energy extensive by scaling the interaction U as $U \to V^{\alpha/d-1}$: this procedure is called Kac rescaling[20], and allows us to study the system in the usual thermodynamic limit.
For what concerns systems with $\alpha > d$, it turns out[17] that there is a critical value α^* such that if $\alpha > \alpha^*$ the systems behaves for all purposes as a short-range one and the non-local nature of the interaction is immaterial. On the other hand, if $d < \alpha < \alpha^*$ the non-locality of interactions changes the universality class and the generic behaviour of the system, for example the velocity of propagation of excitations can become unbounded (as we discuss in section 2.2.2) and the usual Lieb-Robinson bound for the spreading of information does not apply [21]. This latter case is called *weak-long-range* regime.
It is important to note that, while Kac rescaling allows us to recover extensivity, systems with $\alpha < d$ remain non-additive, while systems with $\alpha > d$ are additive. We remind that a system is additive if, after splitting it in two halves, the total energy is approximately given by the sum of the energies of the two halves. This in turn means that the surface energy contribution of the interface between the two regions is negligible and, thus, that the interactions have to decay sufficiently fast. Consider now for example the Curie-Weiss model:

$$H_{CW} = -\frac{J}{2N} \sum_{ij} \sigma_i \sigma_j, \quad \sigma_i = \pm 1. \tag{2.3}$$

This is a fully-connected model with $\alpha = 0$ which includes the Kac rescaling (in fact, H_{CW} is extensive). Now we split the system in two halves: in the first all the

spins are up, $\sigma_i = 1$ and in the other where all spins are down $\sigma_i = -1$. The total energy is zero, but the energy of each region is $-(J/8)N$ and thus the system is non-additive. Lack of additivity has a series of dramatic consequences for the thermodynamic properties of strong-long-range systems. In particular it can be proven that non-additivity leads to non-concave entropy and thus ensemble inequivalence. For example, the microcanonical specific heat can be negative, as is the case of self-gravitating objects such as stars.
Strong-long-range and weak-long-range systems also differ greatly in the properties of their dynamics. In particular, strong-long-range systems possess long-lived metastable states whose lifetime diverges with the system's size[22], so that they never thermalize in the thermodynamic limit, a feature that is absent for weak-long-range systems that thermalize in a time which does not depend on the system's size. There are evidences that these metastable states persists also if we couple the system with external heat reservoirs [23].

2.2 Long-range systems at criticality

In this section we analyze the behaviour of long-range systems near criticality. For what concerns strong-long-range systems, there are numerical and analytical evidences that the critical exponents are given by the ones of the fully connected case $\alpha = 0$ for any $0 < \alpha < d$ [22].
We will now give a brief overview of what happens for weak-long-range systems, considering spin models as an example. Since we are considering $\alpha > d$, it is useful, and customary in the literature, to define $\sigma = \alpha - d > 0$. A first observation is that we expect ferromagnetic long-range interactions to favour the creation of large magnetic domains and thus in general to be more ordered than their short-range versions. Let us see a simple example of this phenomenon.

2.2.1 Peierls argument for the $1d$ long-range Ising model

One of the first long-range spin model introduced in the literature is the Dyson model [24], which is essentially a long-range version of the well-known one-dimensional Ising model :

$$H = -\sum_{ij} J_{ij} s_i s_j, \quad J_{ij} = J|i-j|^{-\alpha}, \quad s_i = \pm 1, \quad \alpha > 1. \tag{2.4}$$

We now apply Peierls argument to this model [25], namely we compute the change in the free energy of the system after the creation of a domain wall. For instance,

starting from the configuration with all of the N spins aligned (the ground state), we create a domain-wall excitation by flipping the first L spins. The energy of this configuration is:

$$\Delta E = 2\sum_{i=1}^{L}\sum_{j=L+1}^{N} J_{ij} = 2J\sum_{n=L+2}^{L+N}\sum_{m=1}^{N-L} m^{-\alpha} \approx N^{2-\alpha}, \tag{2.5}$$

where in the step we introduced $n = i + j$ and $m = j - i$. Since we have N ways to choose the value of L the entropy associated with the domain-wall excitation is $\Delta S = k_B \ln N$, which has to be compared with (2.5) in the thermodynamic limit:

$$\begin{cases} \alpha < 2: & \Delta E > \Delta S \to T_c \neq 0 \\ \alpha > 2: & \Delta E < \Delta S \to T_c = 0. \end{cases} \tag{2.6}$$

We thus see that if $\alpha > 2$ the system behaves as the short-range Ising model and there is no phase transition at finite temperature in one dimension. However, if $\alpha < 2$, we can have an ordered ferromagnetic phase even in one dimension.

2.2.2 Landau theory and Ginzburg criterion for long-range interacting systems

In this section we study the Landau theory of a weak-long-range interacting system with a Z_2 symmetry, such as the Dyson model introduced in (2.4), in particular we want to compute the upper critical dimension using the Ginzburg criterion. As is well known, Landau theory completely neglects the role of fluctuations: this is in general correct only for $d > d_c$, where d_c is the so-called upper critical dimensions. In order to analyze the effect of fluctuations and go beyond the mean-field case, it is necessary to consider a coarse-grained order parameter which depends on the space point $\boldsymbol{x}$ that we will indicate as $\varphi(\boldsymbol{x})$[1]. Note that this approach is possible if the system has

[1]To construct the order parameter $\varphi(\boldsymbol{x})$, we first divide the volume V of the system in smaller cells of volume v. Then, called N_v the number of spins in a given cell and $\boldsymbol{x}$ the center of said cell, we define the coarse-grained order parameter as:

$$\varphi(\boldsymbol{x}) = \frac{1}{N_v}\sum_{i\in v}\langle s_i\rangle\,, \tag{2.7}$$

where the sum runs only on the sites belonging to the cell. Notice that the linear dimension of the cell must be bigger than the lattice spacing, but smaller than the correlation length, otherwise we lose the local correlation when we take the average and all of the $\varphi(\boldsymbol{x})$ would be uncorrelated.

a proper continuum description: as we will see in section 2.3 this is possible if $\alpha > d$. The Landau-Ginzburg action for the kind of model we are considering is:

$$S = \int d^d\boldsymbol{x} d^d\boldsymbol{y} \frac{\varphi(\boldsymbol{x})\varphi(\boldsymbol{y})}{|\boldsymbol{x}-\boldsymbol{y}|^\alpha} + \int d^d\boldsymbol{x}(t\varphi(\boldsymbol{x})^2 + u\varphi(\boldsymbol{x})^4), \tag{2.8}$$

where t is the reduced temperature $t = (T - T_c)/T_c$ and $u > 0$ is the coupling.
Let us, for the moment, only study quadratic fluctuation and neglect the interacting term by putting $u = 0$. It is convenient to work in Fourier space, where the action (2.8) reads as:

$$S = \int \frac{d^d\boldsymbol{q}}{(2\pi)^d}(t + \omega(\boldsymbol{q}))\varphi(\boldsymbol{q})\varphi(-\boldsymbol{q}), \tag{2.9}$$

where $\omega(\boldsymbol{q})$ is the Fourier transform of the long-range quadratic interaction:

$$\omega(\boldsymbol{q}) = \int_{|\boldsymbol{r}|>a} d^d\boldsymbol{r}|\boldsymbol{r}|^{-\alpha} e^{i\boldsymbol{q}\cdot\boldsymbol{r}}, \tag{2.10}$$

where a is the lattice spacing that regularizes the integral in the ultra-violet. Since we are working in the continuum limit, we are interested in the low-momentum behaviour of (2.10) which is worked out in Appendix 1. The result is:

$$\omega(\boldsymbol{q}) \approx c_3 + \begin{cases} c_1 q^\sigma, & 0 < \sigma < 2, \\ c_2 q^2, & \sigma > 2, \end{cases} \qquad q = |\boldsymbol{q}|, \quad \sigma = \alpha - d > 0. \tag{2.11}$$

Notice that if $\sigma > 2$ we recover the usual short-range quadratic dispersion relation and the system falls into the universality class of the short-range Ising model. We also remark that in section 2.2.1 we found that the value of σ discriminating between short-range and long-range behaviour is $\sigma = 1$. This should not surprise us since here we are neglecting interactions and it is well known that the short-range Ising model is not described by the short-range Gaussian model. The same happens in their long-range counterparts. We also note that the c_3 constant is immaterial as it can be safely absorbed in the critical temperature, while, as it can be seen from (A.6), c_1 and c_2 are positive in the region of parameters were they are relevant. Finally, note that if $0 < \sigma < 1$ the velocity of propagation of excitation diverges at low momentum.
We now consider the case $\sigma < 2$, the action is given by:

$$S = \int \frac{d^d\boldsymbol{q}}{(2\pi)^d}(t + c_1 q^\sigma)\varphi(\boldsymbol{q})\varphi(-\boldsymbol{q}). \tag{2.12}$$

From (2.12) we can immediately read the two-point function for the order parameter as:

$$\langle \varphi(\boldsymbol{x})\varphi(0)\rangle = \int_{|\boldsymbol{q}|<1/a} \frac{e^{i\boldsymbol{q}\cdot\boldsymbol{x}}}{t + c_1 q^\sigma}. \tag{2.13}$$

On the other hand, the Landau action per unit volume (that completely neglects the spatial dependence of the order parameter) is given by:

$$L = t\varphi^2 + u\varphi^4, \tag{2.14}$$

where now φ is an homogeneous order parameter which can be thought as the average of the magnetization over the whole system. The values of the order parameter at equilibrium are given by the minima of (2.14) and are:

$$\bar{\varphi} = \begin{cases} 0, & t > 0, \\ \sqrt{-t/2u}, & t < 0. \end{cases} \tag{2.15}$$

The first one corresponds to the disordered phase and the second one corresponds to the ordered phase. Now we consider Gaussian fluctuation in the ordered phase near the critical point ($t = 0^-$), we thus consider the action (2.8) with $u = 0$, we expand the order parameter as:

$$\varphi(\boldsymbol{x}) = \bar{\varphi} + \delta\varphi(\boldsymbol{x}), \tag{2.16}$$

and we plug it in (2.8) with $u = 0$ to find the action for the fluctuations. The result, up to irrelevant constant terms, is:

$$S_{fluct} = \int d^d\boldsymbol{q}(|t| + c_2 q^\sigma)\delta\varphi(\boldsymbol{q})\delta\varphi(-\boldsymbol{q}), \tag{2.17}$$

from which we can immediately read the correlation function of fluctuations:

$$\langle \delta\varphi(\boldsymbol{x})\delta\varphi(\boldsymbol{y})\rangle = \int_{q<1/a} d^d\boldsymbol{q} \frac{e^{i\boldsymbol{q}\cdot(\boldsymbol{x}-\boldsymbol{y})}}{|t| + c_2 q^\sigma} \to \langle \delta\varphi(\boldsymbol{x})^2\rangle = \int_{q<1/a} d^d\boldsymbol{q} \frac{1}{|t| + c_2 q^\sigma} \propto |t|^{d/\sigma - 1} \tag{2.18}$$

In order to assess whether fluctuations are important we consider the ratio:

$$\varepsilon = \frac{\langle \delta\varphi(\boldsymbol{x})^2\rangle}{\bar{\varphi}^2} \propto |t|^{d/\sigma - 2}, \tag{2.19}$$

where we used (2.18) and (2.15). If $\varepsilon \ll 1$ then the fluctuations are negligible and Landau theory is correct. We then see that if $\sigma < d/2 \equiv \bar{\sigma}$ fluctuations are irrelevant and the system falls in the mean-field universality class. On the other hand, if

$\sigma > d/2$ then fluctuations are important and the critical exponents are in general functions of σ which interpolate between mean-field values and short-range values. These results can also be read the other way around: for $d > 2\sigma$ the system is mean-field, and thus the upper critical dimension is $d_c = 2\sigma$. Notice that for $\sigma = 2$ we recover the short-range result $d_c = 4$.
At the end of this analysis we are thus left with the following picture [26]:

- $-d < \sigma < 0$ The universality class is the one of the fully-connected model $\sigma = -d$
- $0 < \sigma < \bar{\sigma}$ The universality class is the one of the mean-field model obtained with the Landau action (2.14).
- $\bar{\sigma} < \sigma < \sigma^*$ The critical exponents are functions of σ that interpolate between the mean-field and the short-range values.
- $\sigma > \sigma^*$ The critical exponents are the ones of the short-range model.

In our case we found $\bar{\sigma} = d/2$ and $\sigma^* = 2$, but we worked at the Gaussian level: let us now consider the full interacting action (2.8). Dimensional analysis tells us that the field $\varphi(\boldsymbol{x})$ has dimension $(\sigma - d)/2$. This in turn means that the interaction $\varphi(\boldsymbol{x})^4$ has dimension $2(\sigma - d)$ and thus it is irrelevant for $\sigma < d/2$, so it does not affect our analysis in the mean-field region. On the other hand, for $\sigma > d/2$ interactions are relevant and can change the critical exponents as it happens, for instance, in the long-range one-dimensional Ising model we saw in section 2.2.1, where $\sigma^* = 1$. A pioneering work in this direction was the one by Sak [27], where, by Renormalization Group techniques, he argued that $\sigma^* = 2 - \eta_{SR}$, where η_{SR} is the anomalous dimension of the short-range model. It should be remarked, however, that Sak criterion has not been conclusively confirmed numerically. Its consistency has been investigated numerically in several works, see e.g. [28, 29, 30], finding good agreement, but there are also works that seem to point at a different value of σ^* [31].

2.3 Thermodynamic limit of long-range interacting systems

In this section we want to point out another important property of long-range interacting systems, namely the relation between the energy spectrum of the system and the existence of the continuum limit of the latter [32]. Consider a one-dimensional

long-range quadratic chain (with periodic boundary conditions):

$$H = \sum_{l=1}^{N} \frac{p_l^2}{2m} + \frac{1}{N_\sigma} \sum_{l=1}^{N} \sum_{r=1}^{N/2} \frac{(x_l - x_{l+r})^2}{r^{1+\sigma}}, \tag{2.20}$$

where N_σ is the Kac factor defined as:

$$N_\sigma = \sum_{l=1}^{N/2} l^{-1-\sigma}. \tag{2.21}$$

In the large N limit, (2.21) correctly scale to make the Hamiltonian (2.20) extensive:

$$N_\sigma \approx \begin{cases} \zeta(1+\sigma), & \sigma > 1, \\ ln(N), & \sigma = 0, \\ -2^\sigma/\sigma N^\sigma, & -1 < \sigma < 0. \end{cases} \tag{2.22}$$

Now we move to Fourier space and we find:

$$H = \sum_n \left(\frac{p_{k_n} p_{-k_n}}{2m} + \frac{\omega_{k_n}}{2} x_{k_n} x_{-k_n}\right), \quad k_n = \frac{2\pi}{N} n, \quad n = -N/2+1, ..., N/2, \tag{2.23}$$

where the spectrum of the system is given by:

$$\omega_{k_n} = \frac{1}{N_\sigma} \sum_{r=1}^{N/2} \frac{4 \sin^2(k_n r)}{r^{1+\sigma}}. \tag{2.24}$$

Now we want to take the thermodynamic limit: we need to distinguish between the cases $\sigma > 0$ and $-1 < \sigma < 0$.
If $\sigma > 0$ we can replace k_n with a continuous variable $k \in (-\pi, \pi]$ and replace the sum in (2.24) with an integral:

$$\omega_{k_n} \to \frac{4}{\zeta(1+\sigma)} \int_1^\infty dr \frac{\sin^2(kr)}{r^{1+\sigma}} \equiv \omega(k), \tag{2.25}$$

and the spectrum becomes a continuous function of the momentum k. This is the typical case for "usual" (i.e. short-range) systems. However, let's now look at the

case $-1 < \sigma < 0$. In this case for large N the spectrum (2.24) becomes:

$$\omega_{k_n} = \frac{|\sigma| 2^{|\sigma|}}{N^\sigma} \sum_{r=1}^{N/2} \frac{4 \sin^2(2\pi n r/N)}{r^{1+\sigma}} \tag{2.26}$$

$$= \frac{|\sigma| 2^{|\sigma|}}{N} \sum_{r=1}^{N/2} \frac{4 \sin^2(2\pi n r/N)}{(r/N)^{1+\sigma}} \tag{2.27}$$

$$\approx |\sigma| 2^{|\sigma|} \int_0^{1/2} d\rho \frac{4 \sin^2(2\pi n \rho)}{\rho^{1+\sigma}} \equiv \omega_n. \tag{2.28}$$

So in the strong-long range regime the spectrum remains discrete even in large N limit. This means that it is not possible in this case to define a continuous momentum variable and it is thus not possible to give a continuous description of the system[32]. Furthermore, the spectrum is made of isolated points and the only accumulation point is $n = \infty$ around which the spectrum ω_n goes as:

$$\omega_n \sim N^{-|\sigma|} \tag{2.29}$$

so all the eigen-energies of the system accumulate around zero.

2.4 Experimental realizations

We want to emphasize the fact that these systems are not merely an academic curiosity, but they have experimental realizations in a plethora of different contexts, both classical and quantum. Let us start from the former. The most famous examples of long-range interactions are the gravitational and Coulombian ones, although it should be mentioned that the latter are really long-range only in systems such as one-component plasmas [33], otherwise screening effects make the interaction effectively short-range. Other cases of long-range interaction in classical systems are given by the logarithmic interaction between vortices in $2d$ hydrodynamics [34], or the stress field around a slit in a plane in the context of $2d$ elasticity [35].
In the quantum regime, long-range systems can nowadays be realized thanks to the advancements in experimental techniques in the context of AMO systems. A first example is given by trapped ions systems. These systems consist in ions interacting via Coulomb interaction and trapped in an external potential, which are then laser cooled. At low temperatures, they organize themselves as a Wigner crystal [36]. This crystal is subjected to a spin-dependent optical force, which induces an effective spin-spin interaction which can be tuned to be a power-law $r^{-\alpha}$ of the distance

between the spins r, with $0 < \alpha < 3$ [37, 38].
Another way to simulate long-range interaction is with quantum gases coupled to cavity modes. These systems consist in Bose condensates trapped in a cavity interacting with a standing wave laser with frequency far detuned with respect to the frequency of atomic excitations so that can only be scattered by the condensate. Furthermore the laser's frequency is very close to the frequency of a cavity mode, so that most of the scattered phonons will scatter in that mode. Then the long-range effective coupling between atoms is mediated by phonons scattering off an atom in the cavity mode and then off another atom [39]. With this method we can simulate fully connected systems, since phonon is delocalized over the cavity mode. For example, it is possible to simulate the Hamiltonian of the hamiltonian mean-field model [40], one of the most studied fully-connected model in the literature of long-range systems [22].

Chapter 3

Heat transport in quadratic systems

In this chapter we are going to describe several methods to study heat transport in quadratic systems that we will extend to long-range systems in later Chapters. We will be interested in the general quadratic Hamiltonian:

$$H = \sum_i \frac{p_i^2}{2m_i} + \frac{1}{2}\sum_{ij} \Phi_{ij} x_i x_j, \tag{3.1}$$

where the matrix Φ is a symmetric matrix which specifies the form of the interaction we are considering. We will mainly consider the following protocol to study heat transport: we attach the system (3.1) to two external baths, one on the left (on the side of site 1) with temperature T_L and one on the right (on the side of site N) with temperature T_R. Then, after a transient, the system will reach a stationary state, characterized by the presence of a net heat current J flowing through the chain and a temperature profile T_i. The methods described in sections 3.1, 3.2 and 3.3 are related to this protocol.
In section 3.4 we introduce a class of systems which, despite being quadratic, are believed to share some traits with interacting systems. We then describe a method based on the Green-Kubo formula to compute the thermal conductivity κ.

3.1 Rieder-Lebowitz-Lieb method

One of the first methods to study heat transport in quadratic systems was introduced by Rieder, Lebowitz and Lieb in their seminal work [9] in order to describe the steady-

state of a nearest-neighbours chain coupled to two external heat baths.
We model the effect of the baths as white noise terms in the equations of motion[1]:

$$\ddot{x}_n = -\sum_j \Phi_{nj} x_j + \delta_{1,n}(\xi_L - \lambda \dot{x}_1) + \delta_{N,n}(\xi_R - \lambda \dot{x}_N) \tag{3.2}$$

$$\langle \xi_{R/L}(t)\xi_{R/L}(t')\rangle = 2k_B T_{R/L}\lambda\delta(t-t'), \tag{3.3}$$

where λ is the coupling between the system and the baths. We also added friction terms in order to reach a steady-state in which the fluctuation-dissipation relation is satisfied. It is convenient to convert the Langevin equations (3.2) into a Fokker-Planck equation [41]. The result is:

$$\frac{\partial P(y,t)}{\partial t} = A_{ij}\frac{\partial}{\partial y_i}(y_j P) + \frac{1}{2}D_{ij}\frac{\partial^2 P}{\partial y_i \partial y_j}, \quad \boldsymbol{y}^T = (x_1, ...x_N, p_1, ...p_N), \tag{3.4}$$

where the drift matrix A and the diffusion matrix D are given by:

$$A = \begin{pmatrix} \mathbb{O} & -\mathbb{I} \\ \Phi & \lambda R \end{pmatrix}, \quad D = \begin{pmatrix} \mathbb{O} & \mathbb{O} \\ \mathbb{O} & 2k_B\lambda T(R+\eta S) \end{pmatrix}, \tag{3.5}$$

$$R_{ij} = \delta_{ij}(\delta_{i1} + \delta_{iN}), \quad S_{ij} = \delta_{ij}(\delta_{i1} - \delta_{iN}), \tag{3.6}$$

$$T = \frac{T_L + T_R}{2}, \quad \eta = \frac{T_R - T_L}{T} = \Delta T/T. \tag{3.7}$$

The general solution to equation (3.4) is a Gaussian distribution:

$$P(\boldsymbol{y},t) = \frac{1}{(2\pi)^N\sqrt{\det(C)}}\exp(-\boldsymbol{y}^T C^{-1}\boldsymbol{y}/2), \quad C_{ij} = \langle y_i y_j\rangle . \tag{3.8}$$

where C is the matrix of covariances of the canonical coordinates. Inserting the ansatz (3.8) into the Fokker-Planck equation (3.4) we get an equation for the matrix C:

$$\dot{C} = D - AC - CA^T, \tag{3.9}$$

which in the stationary state becomes the celebrated Lyapunov equation:

$$AC + CA^T = D. \tag{3.10}$$

[1]This is tantamount to neglecting the effect of the dynamics of the system on the baths, see [1]

Once we solve (3.10) we know all the correlators in the steady-state and we can compute both the heat-flux and the temperature profile. It is convenient to introduce the matrices U, V and Z:

$$C = \begin{pmatrix} U & Z \\ Z^T & V \end{pmatrix}, \quad U_{ij} = \langle x_i x_j \rangle , \quad V_{ij} = \langle \dot{x}_i \dot{x}_j \rangle , \quad Z_{ij} = \langle \dot{x}_i x_j \rangle . \tag{3.11}$$

As a check, note that if the baths have the same temperature $T_L = T_R = T$, the following is a solution of (3.10):

$$U = T\Phi^{-1}, \quad V = T\mathbb{I}, Z = 0, \tag{3.12}$$

which corresponds to the equilibrium solution and energy equipartition among the normal modes at temperature T. Once we solve the Lyapunov equation (3.10) we can compute both the heat flux and the temperature profile in the stationary state. Indeed, the temperature profile can be computed from its kinetic definition:

$$T_i = \langle \dot{x}_i^2 \rangle = V_{ii}, \tag{3.13}$$

while the heat flux can be expressed as the rate of energy flowing from the left bath to the first site:

$$J = \lambda(T_L - T_1) = \lambda(T_L - V_{11}). \tag{3.14}$$

We conclude with two comments. First, one can relax the condition that the baths are coupled only to the first and last site. Assume, for example, that the left-hand bath is coupled to the first N_L sites and the right-hand one is coupled to the last N_R sites. Then all one has to do is to change the R matrix defined in (3.4) with:

$$R_{ij} = \delta_{ij}(\delta_{1i}\delta_{2i}...\delta_{N_L i} + \delta_{N-N_R+1,i}\delta_{N-N_R+2,i}\delta_{Ni}) \tag{3.15}$$

Second, it should be noted that, in general, finding analytical solution to the Lyapunov equation (3.10) is quite difficult. However this method can be easily implemented numerically thanks to the many routines that solve the Lyapunov equation, such as the one in the SciPy library in Python [42] and one can easily reach system's sizes of $N \sim 10^3$.

3.1.1 Nearest-neighbours harmonic chain

One of the few cases where an analytical solution of (3.10) is known is the nearest-neighbours chain considered by Rieder, Lebowitz and Lieb in [9], which corresponds to a matrix Φ proportional to the discrete Laplacian:

$$\Phi = \omega^2 G, \quad \boldsymbol{G} = (2\delta_{ij} - \delta_{i,j+1} - \delta_{i,j-1}). \tag{3.16}$$

The derivation of the solution to the Lyapunov equation corresponding to (3.16) is discussed in some detail in Appendix 2. Let φ_j be the function:

$$\varphi_j = \frac{\sinh[(N-j)\alpha]}{\sinh(N\alpha)}, \quad e^{\alpha} = 1 + \frac{\omega^2}{2\lambda^2} - \frac{\omega^2}{2\lambda^2}\sqrt{1 + \frac{4\lambda^2}{\omega^2}}. \tag{3.17}$$

Then the heat flux (3.14) is given by:

$$J = \frac{\omega^2 k_B \Delta T}{2\lambda^2}\varphi_1, \tag{3.18}$$

which in the thermodynamic limit becomes (using (B.17)):

$$J = \frac{\omega^2 T}{2\lambda}\left(1 + \frac{\omega^2}{2\lambda^2} - \frac{\omega}{\lambda}\sqrt{\frac{\omega^2}{4\lambda^2} + 1.}\right). \tag{3.19}$$

As we can see, the heat flux is proportional to the difference of the temperatures of the baths ΔT and not to the gradient $\Delta T/N$. This means that the thermal conductivity, defined according to Fourier law:

$$J = -\kappa\frac{\Delta T}{N}, \tag{3.20}$$

diverges in the thermodynamic limit as $\kappa \sim N$. This is a consequence of the fact that, being the system quadratic, transport is ballistic and is mediated by phonons that propagate unperturbed along the chain. In the thermodynamic limit, the heat-flux is a non-monotonous function of ω/λ (see the left panel of Figure 3.1) with a maximum at $\lambda_{max} = \sqrt{3}\omega/2$.
The temperature profile can also be expressed in terms of the function φ:

$$\begin{cases} T_1 = T_L - \frac{\omega^2}{2\lambda^2}\varphi_1\Delta T, \\ T_i = T - \frac{\omega^2}{2\lambda^2}\varphi_{2j-1}\Delta T, \quad 1 < j < N/2 \\ T_i = T + \frac{\omega^2}{2\lambda^2}\varphi_{2N-2j-1}\Delta T, \quad N/2 < j \leq j < N \\ T_N = T_R + \frac{\omega^2}{2\lambda^2}\varphi_1\Delta T. \end{cases} \tag{3.21}$$

The plot of (3.21) is reported in the right-hand panel in figure 3.1. The first thing that we notice is that the profile is flat in the bulk, in stark difference with the linear ramp predicted by Fourier law. Indeed, as we already mentioned, transport in this quadratic system is ballistic and not diffusive. Furthermore, we notice the curious fact that the temperature of the second site goes below the bulk value and then

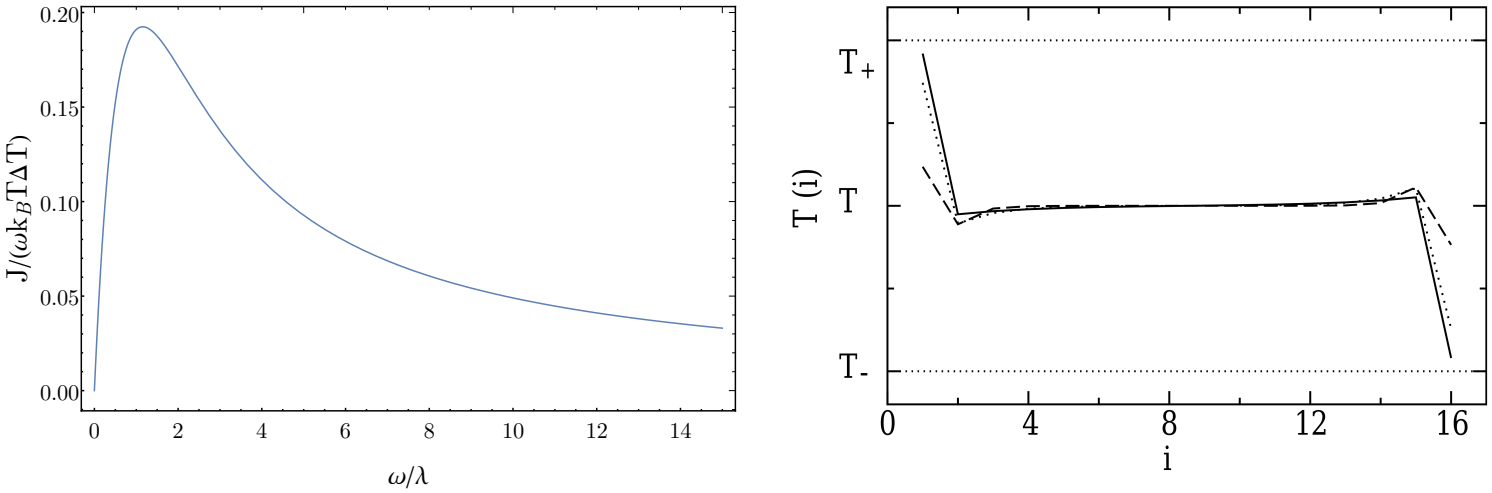

Figure 3.1: In the left panel we report the plot of the adimensional heat flux $J/(\omega k_B T)$ as a function of the a-dimensional ratio ω/λ. In the right panel we report the plot of the temperature profile (3.21) for $N = 16$ for $\omega^2/\lambda^2 = 0.05, 0.2, 1$ as the solid, dotted and dashed lines, respectively. The picture on the right is taken from [1].

relaxes exponentially fast to the bulk value (this can be seen from equations (3.17) and (3.21)).
Analytical solutions to the Lyapunov equation (3.10) have been found also for other systems, in particular Nazakawa extended [43] the solution for the nearest-neighbours harmonic chain to the case of free boundary conditions and to the case in which each particle moves in a pinning potential.

3.2 Green function method

In this section we are going to describe another method to study heat transport in quadratic systems, the so-called Langevin equation and Green function (LEGF) method [2, 44]. The philosophy behind this method is reminiscent of the one behind the celebrated Caldeira-Legget mechanism to induce dissipation in quantum systems and indeed the LEGF method itself can be used to tackle both quantum and classical problems.
The main difference with respect to the RLL method described in section 3.1 is that the baths are modeled as two one-dimensional chains of (quantum) harmonic

oscillators with $\mathcal{N}_L$ and $\mathcal{N}_R$ sites, respectively. At the initial time t_0 we switch on a linear interaction between the oscillators (that we assume to be at thermal equilibrium at temperatures T_L and T_R) and the system. The Hamiltonian for this extended system can thus be written as:

$$H = H_{sys} + H_L + H_R + H_{int}. \tag{3.22}$$

H_{sys} is the Hamiltonian of the chain (3.1), H_L and H_R are the Hamiltonians for the baths:

$$H_L = \sum_i \frac{p_{L,i}^2}{2m_{L,i}} + \frac{1}{2}\sum_i \omega_{L,i}^2 x_{L,i}^2, \quad H_R = \sum_i \frac{p_i^2}{2m_{R,i}} + \frac{1}{2}\sum_i \omega_{R,i}^2 x_{R,i}^2, \tag{3.23}$$

where $\{\omega_{L,R}\}$ are the frequencies of the harmonic oscillators of the baths and H_{int} is the linear interaction Hamiltonian:

$$H_{int} = \sum_{ij} V_{L,ij} x_i x_{L,j} + \sum_{ij} V_{R,ij} x_i x_{R,j}, \tag{3.24}$$

where the matrices V_L and V_R encode the couplings between the sites of the system and the ones of the baths. The equations of motion of the full Hamiltonian (3.22) are:

$$m_i \ddot{x}_i = \sum_j \left(\Phi_{ij} x_j + V_{R,ij} x_{R,j} + V_{L,ij} x_{L,j}\right) \tag{3.25}$$

$$m_{L,i}\ddot{x}_{L,i} = -\omega_{L,i}^2 x_{L,i} + \sum_j V_{L,ji} x_j, \quad m_{R,i}\ddot{x}_{R,i} = -\omega_{R,i}^2 x_{R,i} + \sum_j V_{R,ji} x_j. \tag{3.26}$$

The idea is now to solve the equations of motion for the baths (3.26) treating the system as a source and plug this solution into (3.25) to obtain an equation containing only the degrees of freedom of the system. The details of this calculation are reported in section C.1 in Appendix 3. The final result is:

$$m_i \ddot{x}_i(t) = -\sum_{ij} \Phi_{ij} x_j(t) + \xi_{L,i}(t) + \int_{t_0}^{t} d\tau \sum_{jl} V_{L,ij} g_{L,j}(t-\tau) m_{L,j}^{-1} V_{L,lj} x_l(\tau) + (L \to R), \tag{3.27}$$

where we defined:

$$\xi_{a,i}(t) = -\sum_j V_{a,ij} f_{a,j}(t-t_0) x_{L,j}(t_0) + g_{a,j}(t-t_0)\dot{x}_{L,j}(t_0), \tag{3.28}$$

and functions f and g are defined by:

$$f_{a,i}(s) = \cos(\omega_{a,i}s)\theta(s), \quad g_{a,i}(s) = \frac{\sin(\omega_{a,i}s)}{\omega_{a,i}}\theta(s), \quad a = L, R, \tag{3.29}$$

Looking at equation (3.27), we see that the only contribution of the initial conditions of the baths is in the ξ terms. Furthermore, these terms are linear combinations of an extensive number of periodic functions ($\mathcal{N}_{L,R}$ are supposed to be large) with random coefficients extracted from the distribution describing the thermal equilibrium of the baths. It follows that the ξ functions behave effectively as a noise and we can replace the average over the initial conditions of the baths with an average over the realization of $\boldsymbol{\xi}$: equation (3.27) is thus called a quantum Langevin equation. The convolution term in equation (3.27) encodes the dissipation and memory effects in the dynamics induced by the baths, in particular it is convenient to introduce the memory kernel:

$$\Sigma_{a,ij}(s) = V_{a,ij}g_{a,j}(s)m_{a,j}^{-1}V_{a,lj}, \quad a = L, R. \tag{3.30}$$

Assuming the oscillators in the bath are described by a Bose-Einstein distribution at time t_0, the correlation of the noise is given by[2]:

$$\begin{aligned}\langle \xi_{a,i}(t)\xi_{a,j}(\tau)\rangle = -\sum_l V_{a,il}V_{a,lj}\Bigg[&\frac{\hbar}{2m_{a,l}\omega_{a,l}}\cos(\omega_{a,l}(t-\tau))\coth\left(\frac{\hbar\omega_{a,i}}{2k_BT_a}\right)\\ &- i\frac{\hbar}{2m_{a,i}\omega_{a,i}}\sin(\omega_{a,i}(t-\tau))\Bigg], \quad a = L, R.\end{aligned} \tag{3.31}$$

For what follows, it will be useful to write (3.27) and (3.31) using a vector notation:

$$M\ddot{\boldsymbol{x}}(t) = -\Phi\boldsymbol{x}(t) + \boldsymbol{\xi}_L(t) + \int_{t_0}^{t} d\tau\Sigma_L(t-\tau)\boldsymbol{x}(\tau) + (L \to R), \tag{3.32}$$

$$\begin{aligned}\langle \boldsymbol{\xi}_a(t)\boldsymbol{\xi}_a(\tau)\rangle = -V_a\Bigg[&\frac{\hbar}{2M_a\Omega_a}\cos(\Omega_a(t-\tau))\coth\left(\frac{\hbar\Omega_a}{2k_BT_a}\right)\\ &- i\frac{\hbar}{2M_a\Omega_a}\sin(\Omega_a(t-\tau))\Bigg]V_a^T, \quad a = L, R.\end{aligned} \tag{3.33}$$

where we introduced:

$$\boldsymbol{x}^T = (x_1, ..., x_N), \quad \boldsymbol{\xi}_a^T = (\xi_1, ..., \xi_N) \quad \boldsymbol{x}_a^T = (x_{a,1}, ..., x_{a,N_a}), \quad M_{ij} = m_i\delta_{ij}, \tag{3.34}$$

$$\Omega_a = \omega_{a,i}\delta_{ij}, \quad f_{a,ij}(s) = f_{a,i}(s)\delta_{ij}, \quad g_{a,ij}(s) = g_{a,i}(s)\delta_{ij}, \tag{3.35}$$

$$\Sigma_a(s) = V_a g_a(t-\tau)M_a^{-1}V_a^T, \quad a = L, R \tag{3.36}$$

[2]The proof is reported in section C.2 of Appendix 3.

We now recall that we are interested in the properties of the stationary state that the system will reach after a transient. Therefore, we can take $t_0 \to -\infty$ and move to Fourier space with the following convention for the Fourier transforms:

$$\tilde{x}_i(\omega) = \int_{-\infty}^{\infty} \frac{dt}{2\pi} x_i(t) e^{i\omega t}, \tag{3.37}$$

$$\tilde{\xi}_{a,i}(\omega) = \int_{-\infty}^{\infty} \frac{dt}{2\pi} \xi_{a,i}(t) e^{i\omega t}, \tag{3.38}$$

$$\tilde{g}_{a,i}(\omega) = \int_{-\infty}^{\infty} dt g_{a,i}(t) e^{i\omega t}, \qquad \tilde{f}_{a,i}(\omega) = \int_{-\infty}^{\infty} dt f_{a,i}(t) e^{i\omega t} \tag{3.39}$$

The Langevin equation (3.32) trivially becomes:

$$-\omega^2 M \tilde{\boldsymbol{x}} = -\Phi \tilde{\boldsymbol{x}} + \Sigma_L(\omega)\tilde{\boldsymbol{x}} + \tilde{\boldsymbol{\xi}}_L + (L \to R). \tag{3.40}$$

This equation can be solved in terms of the Green function $G(\omega)$:

$$\tilde{\boldsymbol{x}}(\omega) = G(\omega)(\tilde{\boldsymbol{\xi}}_L(\omega) + \tilde{\boldsymbol{\xi}}_R(\omega)), \quad G(\omega) = [-\omega^2 M + \Phi - \Sigma_L(\omega) - \Sigma_R(\omega)]^{-1}. \tag{3.41}$$

By computing the Fourier transform of the noise-noise correlator[3] we find:

$$\langle \boldsymbol{\xi}_a(\omega) \boldsymbol{\xi}_a(\omega')^T \rangle = \frac{\hbar}{\pi} \delta(\omega + \omega') \Gamma_a(\omega)(1 + f(\Omega_a, T_a)), \quad \Gamma_a(\omega) = Im[\Sigma_a(\omega)] \tag{3.42}$$

which is a form of the fluctuation-dissipation relation.

3.2.1 Heat flux and temperature profile in the stationary state

The heat flux in the stationary state is given by the rate of work done by one of the baths, say the left-hand one, on the system. Since the force exerted by the bath on a the i-th particle in the chain is $-(V_L \boldsymbol{x}_L)_i$, the total rate of work is:

$$J = -\left\langle \dot{\boldsymbol{x}}^T V_L \boldsymbol{x}_L \right\rangle. \tag{3.43}$$

As explained in section C.4 of Appendix 3, this expression depends only on the Green function (3.41) and the imaginary part of the Fourier transform of the memory kernel $\Gamma_a(\omega)$ defined in (C.23):

$$J = \frac{1}{\pi} \int_{-\infty}^{\infty} d\omega Tr[G(\omega)\Gamma_L(\omega)G(\omega)^\dagger \Gamma_R(\omega)] \hbar\omega [f(\omega, T_L) - f(\omega, T_R)], \tag{3.44}$$

[3]The details of the calculation are reported in section (C.3) of Appendix 3.

notice that it correctly vanishes if the temperature of the baths are equal, $T_L = T_R$ In a similar fashion, it can be proved that the temperature T_i, i.e. the velocity-velocity correlator, can be expressed as:

$$T_i = k_B^{-1} m \langle x_i^2 \rangle = \frac{T_L}{\pi} \int_{-\infty}^{\infty} d\omega (G(\omega)\Gamma_L(\omega)G^\dagger(\omega))_{ii} \frac{\hbar\omega^3}{2} \coth\left(\frac{\hbar\omega}{2k_B T_L}\right) + (L \to R) \tag{3.45}$$

In the classical limit $\hbar\omega/k_B T_{L,R} \ll 1$, equations (3.44) and (3.45) become:

$$J = J = \frac{\Delta T}{\pi} \int_{-\infty}^{\infty} d\omega Tr[G(\omega)\Gamma_L(\omega)G(\omega)^\dagger\Gamma_R(\omega)] \tag{3.46}$$

$$T_i = \frac{T_L}{\pi} \int_{-\infty}^{\infty} d\omega (G(\omega)\Gamma_L(\omega)G^\dagger(\omega))_{ii} + (L \to R). \tag{3.47}$$

The integrand in the expression of the heat flux (3.46) is called transmission coefficient $\mathcal{T}(\omega)$:

$$\mathcal{T}(\omega) = \frac{1}{4\pi} Tr[G(\omega)\Gamma_L(\omega)G(\omega)^\dagger\Gamma_R(\omega)]. \tag{3.48}$$

Notice that we did not specify the form of $\Gamma_a(\omega)$, which encodes the properties of the bath. The most common choice is the so-called Ohmic bath, which corresponds to a purely imaginary $\Sigma_a(\omega) = i\Gamma_a(\omega)$ with:

$$\Gamma_{a,ij} = \lambda\omega R_{ij}, \tag{3.49}$$

where the matrix R_{ij} is the coupling matrix (3.15). If the baths are only coupled to the first and last site, the R matrix is given by the one in (3.4) and the Langevin equation of motion for the system becomes:

$$m_i\ddot{x}_i = -\sum_{ij} \Phi_{ij}x_j - \lambda\dot{x}_1 - \lambda\dot{x}_N + \xi_{L,1} + \xi_{R,N}. \tag{3.50}$$

The noise-noise correlation (3.42) also reduces to the Gaussian one in the classical limit. Notice that this choice in the classical limit reproduces the dynamics studied using the RLL method in section 3.1. Indeed, in [44] the LEGF method has been applied to a nearest-neighbours chain (which corresponds to a Φ matrix given by (3.16)) with pinning potentials. The full analytical computation of the heat flux and temperature profile were performed and the results of Lebowitz [9] and Nazakawa [43] were recovered in the relevant limiting cases. A closed expression for the heat flux in the quantum case was also obtained.
The Green function method has been applied to a variety of systems, ranging from

chains subject to magnetic fields [45, 46], disordered systems [47], and also purely quantum systems such as fermionic chains [48]. More recently it has been applied to a chain coupled to active baths [49].

3.3 Generalized eigenvalue method

In this section we describe a method to study transport which is closely-related to the Green function method described in section 3.2, which was introduced in [50] to study heat transport in quantum crystals. As we saw, the method relies on the inversion of the matrix $G^{-1}(\omega) = -\omega^2\mathbb{I} + \Phi - \Sigma_L(\omega) - \Sigma_R$ to compute the Green function (3.41). However, this operation can be sometimes difficult to perform analytically. From the numerical point of the view, since we are interested in the thermodynamic limit, we need to invert a very large matrix, which is computationally expensive. The method that we describe in this section essentially replaces the inversion of the $N \times N$ matrix with the solution of a $2N \times 2N$ eigenvalue problem.

We now consider the Green function (3.41), but for convenience we take the Laplace transform and not the Fourier one[4] :

$$G(s) = [s^2 + \Phi + s\lambda R]^{-1}, \tag{3.51}$$

where for simplicity we take all the masses equal to one. To compute the inverse of a matrix polynomial of degree two (such as the one in (3.51)), we can refer to the theory of the so-called generalized quadratic eigenvalue problem. We remind that the standard generalized eigenvalue problem consists in finding the zeroes of a matrix $T(s) = A + sB$, where A and B are matrices. The generalized quadratic eigenvalue problem consists in finding the zeroes of a quadratic matrix polynomial $P(s) = As^2 + Bs + C$: we see from (3.51) that $G^{-1}(s)$ has precisely this form. As we show in Appendix 4 the Green function $G(s)$ can be expressed as:

$$G(s) = \sum_{i=1}^{2N} \frac{s_i}{s - s_i} \boldsymbol{x}^{(i)} \boldsymbol{x}^{(i)T}, \quad G^{-1}(s_i)\boldsymbol{x}^{(i)} = 0, \quad \forall i = 1...2N, \tag{3.52}$$

where the poles s_i and the vectors $\boldsymbol{x}^{(i)}$ can be obtained by solving the $2N \times 2N$ eigenvalue problem [51](D.10). Equation (3.52) has several consequences. First of

[4]We remind that, since we are considering the stationary state we neglect the initial conditions, and thus the relation between the Fourier transform $\tilde{f}(\omega)$ and the Laplace one $\bar{f}(s)$ is simply $\tilde{f}(i\omega) = \bar{f}(s)$.

all, it gives a way to easily access the poles of the Green function, which, as we are going to see in Chapter 4, are sometimes crucial to understand the properties of the system. Furthermore, we can plug (3.52) into the integrals (3.44), (3.45), (3.46) and (3.47) to obtain an alternative expression for the heat flux and temperature profile that involves only sums over the $\{s_i\}_{i=1}^{2N}$. For example we consider the classical flux (3.46) with baths coupled only to the first and last site (so that the matrix R is given by (3.4) and the memory kernel is given by (3.49). Then, if we plug (3.52) into (3.46) we obtain:

$$J = \frac{\gamma^2 k_B \Delta T}{\pi} \int_{-\infty}^{\infty} G_{1N}(\omega) G_{N1}^{\dagger}(\omega) d\omega \tag{3.53}$$

$$= 2k_B \Delta T \gamma^2 \sum_{ij=1}^{2N} \frac{s_i^2 s_j}{s_i + s_j} x_1^{(i)} x_N^{(i)*} x_1^{(i)*} x_N^{(i)}. \tag{3.54}$$

This method has also been generalized to Ohmic baths with a soft cut-off [10], in which case the inverse of the Green function is a cubic matrix polynomial and thus one needs to consider the cubic eigenvalue problem.

3.4 Stochastic exchanges

In the previous sections of this chapter, we considered the dynamics of an otherwise deterministic system and then introduced a stochastic component to this dynamics by coupling the system to two heat reservoirs. In this section we consider a different class of quadratic models where the stochastic part of the dynamics comes from a momentum-exchange mechanism. In particular we will consider models described by Hamiltonian (3.1) (where we put $m_i = 1\ \forall i$ for simplicity) and at random times we exchange the momenta of two randomly-selected particles. We call this process a collision, as we can imagine it as a collision between the particles the outcome of which is the momentum exchange. More specifically, let us call $\{p_l\}_{l=1}^{N}$ the set of the momenta of all the particles at time t. Then, assuming there is a collision at time $t + \tau$, we randomly pick two particles with a probability $W_{n,m}$ and exchange their momenta:

$$(p_n, p_m) \to (p_m, p_n) \equiv (p_n^{'}, p_m^{'}), \tag{3.55}$$

where the prime denotes a quantity immediately after the collision. The inter-collision times τ are sampled randomly from a given distribution with a finite mean τ.

This momentum exchange mechanism was introduced as a way to mimic the effect

of nonlinear interactions, while keeping the model solvable as the quadratic one [52]. Heat transport in the nearest-neighbours chain with nearest-neighbours momentum exchange (i.e. only the momenta of adjacent particles are exchanged) was studied by coupling the chain to external baths in [53, 11] and it was found that the heat flux scales as $J \sim N^{-1/2}$ at stark variance with the deterministic system studied in 3.1. This scaling of the heat flux corresponds to a divergence of the heat conductivity $\kappa \sim N^{1/2}$ and in this case the transport is called anomalous [1].
More recently Tamaki and Saito [12] computed the thermal conductivity in a long-range harmonic chain with stochastic collisions between nearest neighbours particles using the Green-Kubo formula. In Chapter 5 we will apply the methods presented in this section to recover their result and to extend the computation to the thermal conductivity in the case of long-range collisions. In this section we recap the analysis presented in [54]: we study the dynamics of the uncoupled system and we will later obtain the thermal conductivity via the Green-Kubo formula. In particular, we want to obtain an equation for the time evolution of the "energy modes" of the system.
The main ingredients of this discussion will be the normal modes of the matrix Φ and since we will consider only traslational-invariant lattices, these are given by the standard Fourier modes:

$$\Phi\chi^\nu = \omega_\nu^2\chi^\nu, \chi_l^\nu = \frac{e^{-ik_\nu l}}{\sqrt{N}}, \quad k_\nu = \frac{2\pi\nu}{N}, \nu = -\frac{N}{2}+1, ..., \frac{N}{2}. \tag{3.56}$$

We now expand both positions and momenta on the eigenbasis of Φ:

$$\begin{cases} q_i = \sum_\nu Q_\nu \chi_i^{\nu *}, \quad p_i = \sum_\nu P_\nu \chi_i^{\nu *}, \\ P_\nu = \sum_i p_i \chi_i^\nu, \quad Q_\nu = \sum_i q_i \chi_i^\nu, \quad P_\nu^* = P_{-\nu}, \quad Q_\nu^* = Q_{-\nu} \end{cases} \tag{3.57}$$

so that the Hamiltonian (3.1) becomes:

$$H = \frac{1}{2}\sum_\nu (|P_\nu|^2 + \omega_\nu^2 |Q_\nu|^2). \tag{3.58}$$

After a collision which exchanges the momenta of particles n and m the change in P_ν is given by:

$$\Delta P_\nu = \sum_l (p_l^{'} - p_l)\chi_l^\nu = (p_n - p_m)(\chi_n^\nu - \chi_m^\nu) = (\chi_n^\nu - \chi_m^\nu)\sum_\mu (\chi_m^{\mu *} - \chi_n^\mu) P_{\mu *} \tag{3.59}$$

$$= -2\sum_\mu V_\nu V_\mu^* P_\mu. \tag{3.60}$$

where we introduced the vector $V_\mu^{(n,m)}$:

$$V_\mu^{(n,m)} = \frac{\chi_n^\mu - \chi_m^\mu}{\sqrt{2}} = \frac{e^{ik_\mu n} - e^{ik_\mu m}}{\sqrt{2N}}. \tag{3.61}$$

Note that the entries of this vector are random variables that depend on which particle we select for the exchange of momenta. We now switch to a vector notation by collecting the P_ν in a vector $\boldsymbol{P}$, so that equation (3.59) becomes:

$$\Delta \boldsymbol{P} = -2VV^\dagger \boldsymbol{P}, \tag{3.62}$$

and we thus see that there are two contributions to the dynamics of $\boldsymbol{P}$: the deterministic one regulated by the Hamiltonian (3.58) and the stochastic one (3.62).

3.4.1 Action-angle variables

It is convenient to switch to the classical counterparts of the creation-annihilation operators:

$$\boldsymbol{A} = i(2\Omega)^{1/2}\boldsymbol{Q} + (2\Omega)^{-1/2}\boldsymbol{P}, \quad \tilde{\boldsymbol{A}}^* = -i(2\Omega)^{1/2}\boldsymbol{Q} + (2\Omega)^{-1/2}\boldsymbol{P}, \tag{3.63}$$

where $\tilde{A}_\nu = A_{-\nu}$. The inverse of (3.63) is given by:

$$\boldsymbol{P} = \frac{1}{2}(2\Omega)^{1/2}(\boldsymbol{A} + \tilde{\boldsymbol{A}}^*), \quad \boldsymbol{Q} = \frac{1}{2i}(2\Omega)^{-1/2}(\boldsymbol{A} - \tilde{\boldsymbol{A}}). \tag{3.64}$$

Using (3.62) we find that after a collision $\boldsymbol{A}$ is given by:

$$\boldsymbol{A}' = (1 - M)\boldsymbol{A} - M\tilde{\boldsymbol{A}}^*, \quad M = \Omega^{-1/2}\boldsymbol{V}\boldsymbol{V}^\dagger\Omega^{1/2}, \tag{3.65}$$

which can also be written as an expression containing only $\boldsymbol{A}$:

$$\boldsymbol{A}' = \boldsymbol{A} - \boldsymbol{U}(\boldsymbol{W}^\dagger\boldsymbol{A} + \boldsymbol{W}^T\boldsymbol{A}^*), \quad U_\mu = V_\mu\sqrt{\frac{2}{\omega_\mu}}, \quad W_\mu = V_\mu\sqrt{2\omega_\mu}. \tag{3.66}$$

Equation (3.66) is the one that we use in the numerical implementation of this scheme: it is particularly convenient since it allows to reduce the effect of collisions to a matrix multiplication.
In order to get the full time evolution we also need to take into account the deterministic dynamics between times t and $t + \tau$. It can be easily proven using (3.58) and (3.63) that:

$$\boldsymbol{A}(t + \tau) = e^{i\omega\tau}\boldsymbol{A}(t). \tag{3.67}$$

Combining equations (3.67) and (3.65) we get time full evolution of $\boldsymbol{A}$ between time t and immediately after the first collision at time $t+\tau$:

$$\boldsymbol{A}^{'}(t+\tau) = (1-M)e^{i\omega\tau}\boldsymbol{A}(t) - Me^{-i\omega\tau}\tilde{\boldsymbol{A}}^{*}(t). \tag{3.68}$$

Now we switch to the action and angle variables I_ν, θ_ν defined as $A_\nu = \sqrt{I_v}e^{i\theta_\nu}$. The variation of these variables following a collision is:

$$I_\nu^{'} = I_\nu\left|1 - \frac{2V_\nu e^{-i\theta_\nu}}{\sqrt{I_\nu}}Z\right|^2, \tag{3.69}$$

$$\sin\theta_\nu^{'} = \sqrt{\frac{I-\nu}{I_\nu^{'}}}\sin\theta_\nu - 2\frac{Im(V_\nu)}{\sqrt{I_\nu^{'}\omega_\nu}}, \tag{3.70}$$

$$Z = Re(\sum_\mu \sqrt{I_\mu\omega_\mu}(V_\mu e^{-i\theta_\mu}). \tag{3.71}$$

Taking into account also the deterministic part of the dynamics (3.67) we get:

$$I_\nu^{'}(t+\tau) = I_\nu(t) + \Delta I_\nu(\{I\},\{\theta\}), \tag{3.72}$$

$$\theta_\nu^{'}(t+\tau) = \theta_\nu(t) + \omega_\nu\tau\theta_\nu(t) + \Delta\theta_\nu(\{I\},\{\theta\}), \tag{3.73}$$

where ΔI and $\Delta\theta$ can be read off (3.69) and (3.70). We thus see that the action variable change only due to the stochastic collisions and are conserved by the deterministic quadratic dynamics. We now consider the so-called kinetic limit:

$$N\to\infty, \quad \langle\tau\rangle\to 0, \quad \gamma = \frac{1}{N\langle\tau\rangle}, \tag{3.74}$$

with γ finite. This limit corresponds to a finite probability of having a collision per site and thus on the time-scale $T = 1/\gamma$ the total number of collisions becomes macroscopic. As we can see from (3.73) for a large number of collisions the phases θ_ν are randomized much faster than the action variables thanks to the presence of the $\omega_\nu\tau$ term. We therefore take the average of (3.72) over a uniform distribution of the angles. The result is:

$$\bar{I}_\nu^{'} = (1-2|V_\nu|^2)\bar{I}_\nu + 2\frac{|V_\nu|^2}{\omega_\nu}\sum_\mu \bar{I}_\mu\omega_\mu|V_{\mu|^2}. \tag{3.75}$$

This equation can be converted into an equation for the energy modes E_ν:

$$E_\nu = I_\nu\omega_\nu = \omega_\nu|A_\nu|^2, \tag{3.76}$$

by inserting (3.76) into (3.75):

$$E_\nu^{'} = E_\nu + \sum_\mu K_{\nu\mu} E_\mu, \quad K_{\mu\nu}^{(n,m)} = -2|V_\nu^{(n,m)}|^2 \delta_{\mu\nu} + 2|V_\nu^{(n,m)}|^2 |V_\mu|^2, \tag{3.77}$$

where we wrote explicitly the dependence of V on the choice of the colliding particles n, m. From the definition of K (3.77) we see that the constant vector $E_v = E_{eq}$ is an eigenvector of K with zero eigenvalue: this vector does not evolve and corresponds to the equilibrium state.
Note that the matrix K has random entries that depend on the choice of the particles $(n.m)$ that take part in the collision: we therefore need to compute the average of E_ν over the collisions occurring between a given time t and $t+T$, where $T = 1/\gamma$ is the time scale after which we expect the number of collision to be macroscopic. To begin with, from equation (3.77) we get:

$$E_\nu(t+T) = \sum_\mu \Bigg(\prod_{\{(n,m)\}} (\mathbb{I} + K^{(n,m)}) \Bigg)_{\nu\mu} E_\mu(t), \tag{3.78}$$

where the product runs over all the collision between t and $t+T$. Now we make the assumption that a single collision only alters the energies E_μ by a small amount[5]. We can then linearize equation (3.78):

$$E_\nu(t+T) - E_\nu(t) = \sum_\mu \sum_{\{(n,m)\}} K_{\nu\mu}^{(n,m)} E_\mu(t). \tag{3.79}$$

The sum over the collisions in the left-hand side of (3.79) is given by the average over the stochastic process $W_{n,m}$:

$$\frac{1}{N} \sum_{\{(n,m)\}} K^{(n,m)} = \sum_{n,m} W_{n,m} K^{(n,m)} \equiv \bar{K}, \tag{3.80}$$

while the right-hand side of (3.79) can be written as a time-derivative:

$$E_\nu(t+T) - E_\nu(t) \sim \dot{E}_\nu(t)/\gamma. \tag{3.81}$$

[5]This condition is satisfied when the normal modes χ^ν are given by the Fourier modes or are otherwise extended, in which case their components scale as $N^{-1/2}$ due to the normalization condition. If the eigenmodes are localized this condition might not be true, but we will not deal with such cases.

Inserting (3.80) and (3.81) into (3.79) we finally get an equation for the time evolution of the energy modes E_ν which can be written as a master equation:

$$\dot{E}_\nu = \sum_\mu (R_{\nu\mu}E_\mu - R_{\mu\nu}E_\nu), \quad R_{\mu\nu} = 2\gamma N \overline{|V_\nu|^2}\ \overline{|V_\mu|^2}. \tag{3.82}$$

The properties of the time evolution of the energy modes are thus given by the eigenvalues of the matrix R. We already saw that one of them is zero and corresponds to the equipartition state. The non-vanishing eigenvalues represent the relaxation rates of the various energy modes to this state:

$$E_\nu(t) - E_{eq} = E_{eq} e^{-|\mu_\nu| t}. \tag{3.83}$$

We will consider only cases where $W_{n,m} = W_{|n-m|}$. Then, using the definition of V_μ (3.61) we get:

$$R_{\mu\nu} = \gamma \sum_{l>0} W_l \Big[-4 \sin^2 \frac{k_\mu l}{2} \delta_{\mu\nu} + \frac{8}{N} \sin^2 \frac{k_\mu l}{2} \sin^2 \frac{k_\nu l}{2} \Big]. \tag{3.84}$$

In the large N limit the off-diagonal entries of $R_{\mu\nu}$ are small with respect to the diagonal ones and we thus neglect them (this also means to neglect the coupling between the various energy modes). In this approximation the $R_{\mu\nu}$ matrix is diagonal, and its eigenvalues μ_ν are trivially given by:

$$\mu_\nu = -4\gamma \sum_{l>0} W_l \sin^2 \frac{k_\mu l}{2}. \tag{3.85}$$

In [54] the exponential relaxation of the energy modes (3.83) is tested numerically for a series of clean and disordered systems finding a good agreement. Furthermore, this method is numerically very convenient since all the interesting quantities can be expressed in terms of the A_ν (e.g. the energy modes (3.76)) whose time evolution is implemented by a matrix multiplication (3.68).
In chapter 5 we will use (3.83) to compute the current-current correlation and extract the thermal conductivity via the Green-Kubo formula.

3.4.2 Thermal conductivity for short-range chains

In this subsection we recover the results of [11] for the thermal conductivity in a nearest-neighbours quadratic chain with nearest-neighbours collisions. This model

corresponds to a matrix Φ given by (3.16), the eigenfrequencies ω_ν, the probabilities $W_{n,m}$ and the rates $\mu(k)$ are given by:

$$\omega_\nu = 4\sin^2(k_\nu/2), \quad W_{n,m} = \delta_{|n-m|,1}, \quad \mu(k_\mu) = -4\gamma \sin^2 \frac{k_\mu}{2}. \tag{3.86}$$

In order to compute the thermal conductivity we use the Green-Kubo formula:

$$\kappa = \int_0^{t^*} dt C_N(t), \quad C_N(t) = \frac{J(t)J(0)}{N}, \quad N \gg 1, \quad t^* = N/v^* \tag{3.87}$$

where we introduced a cut-off time t^* and v^* is the typical velocity of propagation of energy excitations [1]. Basically, we are integrating only up to the time in which energy has propagated through the linear dimension of the system. The reason we introduce this cut-off is that in anomalous transport the thermal conductivity would, strictly speaking, diverge for $N = \infty$ due to the fact that the self-correlation of the current has long-living power-law tails. Integrating up to time t^* allows us to convert this diverge in time into a divergence with the system's size. Note also that the average in (3.87) is a micro-canonical average, but since we are considering a local system there is ensemble equivalence and we can replace it with a canonical average.

We now turn to the computation of the current-current correlations. Let us begin by introducing the Hamiltonian density h_l:

$$H = \sum_l h_l, \quad h_l = \frac{1}{2}\left(p_l^2 + \frac{1}{2}(x_{l+1} - x_l)^2 + \frac{1}{2}(x_{l-1} - x_l)^2\right), \tag{3.88}$$

where we symmetrized the potential energy following a common convention in the literature [1] The variation of h_l in an infinitesimal time dt defines the energy current through the continuity equation:

$$dh_l = -dj_l + dj_{l-1}, \tag{3.89}$$

where the d stands for the variation of a quantity in an infinitesimal time dt. The infinitesimal time evolution of the canonical coordinates is given by:

$$dx_l = \frac{\partial H}{\partial p_l} dt = p_l dt, \tag{3.90}$$

$$\begin{aligned} dp_l &= -\frac{\partial H}{\partial x_l} + dn_l(p_{l+1} - p_l) + dn_{l-1}(p_{l-1} - p_l) \\ &= -2x_l + x_{l-1} + x_{l+1} + dn_l(p_{l+1} - p_l) + dn_{l-1}(p_{l-1} - p_l), \end{aligned} \tag{3.91}$$

where we introduced the Poisson variable dn_l which can be either 0 or 1 with average [12]:

$$\langle dn_l \rangle = \gamma dt \tag{3.92}$$

Using equations (3.90) and (3.91) to compute the differential of (3.88) and comparing it to (3.89) we get:

$$dj_l = \frac{1}{2}(p_{l+1} + p_l)(x_{l+1} - x_l)dt + dn_l \frac{1}{2}(p_{l+1}^2 - p_l^2) \equiv j_l^{(det)} dt + dj_l^{(sto)}. \tag{3.93}$$

Notice that the current (3.93) is composed of two terms. The first one represents the rate of work done by a particle on the adjacent ones: we will call this term "deterministic". The second one stems from the stochastic collisions due to the fact that colliding particles trade their kinetic energy with each other and this exchange contributes to energy transport: we will call this second term "stochastic". We can further split the stochastic term by writing the Poisson process dn_l in terms of its fluctuation around the average value:

$$dj_l^{(sto)} = \frac{1}{2}(p_{l+1}^2 - p_l^2)\gamma dt + \frac{1}{2}(p_{l+1}^2 - p_l^2)(dn_l - \gamma dt) \equiv j_l^s dt + d\mathfrak{j}_l. \tag{3.94}$$

When we sum over l to compute the total current, the j_l^s term stems a telescopic sum that sums to zero so it does not contribute to the total current which reads:

$$J = J^{(det)} + d\mathfrak{J}, J^{(det)} = \sum_l j_l^{(det)}, \quad d\mathfrak{J} = \sum_l d\mathfrak{j}_l \tag{3.95}$$

In [55] it has been rigorously proved that, when integrated over time to get the thermal conductivity (3.87), the mixed correlation $\langle J^{(det)}(t) d\mathfrak{J}(0) \rangle$ vanishes and the auto-correlation of $d\mathfrak{J}$ yields a constant contribution to κ. Thus we only need to compute the correlation $\langle J^{(det)}(t) J^{(det)}(0) \rangle$: in order to do so, we write $J^{(det)}$ in terms of the normal modes variables introduced in section 3.4 by using the definitions of the normal modes (3.57) and (3.63) into (3.95) we get:

$$J^{(det)} = \sum_\mu \sin(k_\mu) |A_\nu|^2 = \sum_\mu v_\mu E_\mu, \tag{3.96}$$

where we used (3.76) and $v_\mu = \partial_{k_\mu} \omega_\mu$ with ω_ν given by (3.86). Notice that the formula on the left of the second equality in (3.96) is actually well-known in the

literature [1]. Now we can compute the correlator:

$$C_N(t) = N^{-1} \langle \sum_\mu v_\mu (E_\mu(t) - \langle E_\nu \rangle) \sum_\nu v_\nu E_\nu(0) \rangle \tag{3.97}$$

$$= N^{-1} \sum_{\mu\nu} v_\nu v_\mu \langle E_\mu(0) E_\nu(0) \rangle e^{\mu(k_\mu)t} \tag{3.98}$$

$$= N^{-1} (k_B T)^2 \sum_\mu v_\mu^2 e^{\mu(k_\mu)t}, \tag{3.99}$$

where in the first step we subtracted the value of the current at equilibrium (which is zero), in the second one we used (3.83) and in the final one we used $\langle E_\mu(0) E_\nu(0) \rangle = (k_B T)^2 \delta_{\mu\nu}$. Now we take the continuum limit and find:

$$C_N(t) \to C(t) = \frac{4(k_B T)^2}{\pi} \int_{2\pi/N}^{\pi} dk v(k)^2 e^{\mu(k)t}. \tag{3.100}$$

Since we are interested in the late-time power-law tails we also take the large-t limit. In this limit the integral in (3.100) is dominated by the low-k region and we can send the upper extremum to ∞ with exponentially small error:

$$C(t) = \frac{4(k_B T)^2}{\pi} \int_{2\pi/N}^{\pi} dk v(k)^2 e^{\mu(k)t} \sim t^{-1/2}. \tag{3.101}$$

Finally, we insert (3.101) into (3.87) and we recover the scaling $\kappa \sim N^{1/2}$ in the large N limit i.e. the result of [11]. In Chapter 6 we will extend this analysis to a long-range harmonic chain with long-range stochastic collisions.

Chapter 4

Heat transport in a fully-connected chain

In this chapter we apply the Green function method of section 3.2 to study heat transport in a fully-connected harmonic network. This model provides an example of long-range system in which transport properties can be computed analytically both in the classical and quantum regime with different configurations of coupling with the baths. This chapter is based on the paper [13].
The Hamiltonian of the system is given by:

$$H = \frac{1}{2m}\sum_{i=1}^{N} p_i^2 + \frac{k}{2N}\sum_{ij}(x_i - x_j)^2 = \frac{1}{2m}\sum_{i=1}^{N} p_i^2 + \frac{1}{2}\sum_{i,j=1}^{N}\Phi_{ij}x_i x_j, \tag{4.1}$$

where k is the coupling constant, N is the Kac factor (2.21) in the fully connected limit $\sigma = -1$ and Φ is given by:

$$\Phi_{ij} = 2k\left(\delta_{ij} - \frac{1}{N}\right). \tag{4.2}$$

We immediately remark that since the system is fully connected there is no notion of spatial ordering: despite this we will continue to refer to the "left-hand" bath and "right-hand" bath to fix the notation. Furthermore, since we are considering a long-range system it seems appropriate to consider both the case in which the baths are coupled only to sites 1 and N (that we will call intensive coupling) and the case where the baths are coupled to an extensive fraction of the system (that we will call extensive coupling). Furthermore, we will only consider the case where a site can be coupled at most with one bath, i.e. $N_L + N_R \leq N$. The matrices $\Gamma_L(\omega)$ and $\Gamma_R(\omega)$

introduced in section 3.2 are given by:

$$\Gamma_{L,ij}(\omega) = \lambda\omega\delta_{ij}\delta_{i1}, \qquad \Gamma_{R,ij} = \lambda\omega\delta_{ij}\delta_{1N}, \tag{4.3}$$

$$\Gamma_{L,ij}(\omega) = \lambda\omega\delta_{ij}\sum_{k=1}^{N_L}\delta_{jk}, \qquad \Gamma_{R,ij} = \lambda\omega\delta_{ij}\sum_{k=N-N_R+1}^{N}\delta_{jk}, \tag{4.4}$$

where (4.3) and (4.4) refer to the intensive coupling and extensive coupling, respectively. In both cases the Green function can be computed exactly. These calculations are performed in sections E.1 and E.2 of appendix 5 for the intensive and extensive case, respectively. In conclusion we have four cases to consider: classical and quantum regimes with intensive and extensive coupling. In particular, in the quantum regime we will always work in the linear response approximation $\Delta T \ll T$ and the heat flux (3.44) reduces to:

$$J_q = \frac{\Delta T}{\pi}\int_{-\infty}^{\infty} d\omega Tr[G(\omega)\Gamma_L(\omega)G^{\dagger}(\omega)\Gamma_R(\omega)]\frac{\partial f(\omega,T)}{\partial T}. \tag{4.5}$$

We organize the chapter in the following way: in sections 4.1 and 4.3 we consider the classical case with intensive and extensive couplings respectively. Sections 4.2 and 4.4 are devoted to the intensive and extensive coupling in the quantum regime, respectively. In all of these cases we will be able to analytically extract the scaling of all quantities with the system's size N for large N. Throughout the chapter, we will denote classical and quantum quantities with the subscript cl and q, respectively. Furthermore we will denote with the superscript int and ext quantities related to the intensive and extensive coupling case, respectively.

4.1 Intensive coupling, classical case

Inserting (4.3) into formulae (3.46) and (3.47) we get:

$$J_{cl}^{int} = \frac{k_B\Delta T}{\pi}\lambda^2\int_{-\infty}^{\infty} d\omega\,\omega^2|G_{1N}(\omega)|^2, \tag{4.6}$$

$$T_{cl,i}^{int} = \frac{\lambda m T_L}{\pi}\int_{-\infty}^{\infty} d\omega\omega^2|G_{i1}(\omega)|^2 + \frac{\lambda m T_R}{\pi}\int_{-\infty}^{\infty} d\omega\omega^2|G_{iN}(\omega)|^2.. \tag{4.7}$$

The Green function $G(\omega)$ (3.41) for the intensive coupling case is computed in section E.1.

4.1.1 Heat flux

Inserting the expression for G_{1N} (E.10) into (4.6) we get:

$$J_{cl}^{int} = \frac{k_B \Delta T \sqrt{2k/m}}{2\pi} I_1(k_1, N), \tag{4.8}$$

where the function I_1 is given by the following integral ($y = \omega\sqrt{2k/m}$):

$$I_1(k_1, N) = \frac{2k_1^2}{N^2} \int_{-\infty}^{\infty} \frac{(y^2-1)^2}{(y^2-1)^2 + k_1^2 y^2} \frac{dy}{y^2(y^2-1)^2 + k_1^2(y^2 - \frac{2}{N})^2}, \tag{4.9}$$

where the dimensionless coupling constant k_1 is given by:

$$k_1^2 = \frac{\lambda^2}{2mk}. \tag{4.10}$$

Integral (4.9) is plotted as a function of k_1 in figure 4.1a: its dependence on the coupling is qualitatively the same of the short-range one reported in figure 3.1. However the heat flux now depends on the system's size N in the thermodynamic limit: in order to prove this, we compute the integral (4.9) in the large N limit. Consider the second factor of the denominator of the integrand in (4.9), as a polynomial in $s = y^2$:

$$s(s-1)^2 + k_1^2(s - 2/N)^2, \tag{4.11}$$

as $N \to \infty$, (4.11) has a vanishing root which for large N is given by:

$$s_0(k_1, N) = -4k_1^2/N^2. \tag{4.12}$$

By decomposing the integrand in (4.9) in partial fractions, it is easy to see that the dominant contribution for large N is the one coming from (4.12):

$$I_1 = \frac{2k_1^2}{N^2} \int_{-\infty}^{\infty} \frac{dy}{y^2 + 4k_1^2/N^2} = \frac{\pi k_1}{N}, \tag{4.13}$$

and so the heat flux at leading order in N^{-1} reads as:

$$J_{cl}^{int} = k_B \Delta T \sqrt{2k/m} \frac{k_1}{2N}. \tag{4.14}$$

Notice that this result does not agree with the numerical one plotted in figure (4.1)a. To understand the problem, we also plot $NI_1(k_1, N)$ as a function of k_1 in figures 4.1a and 4.1b for different values of N: as N grows, the region of agreement between

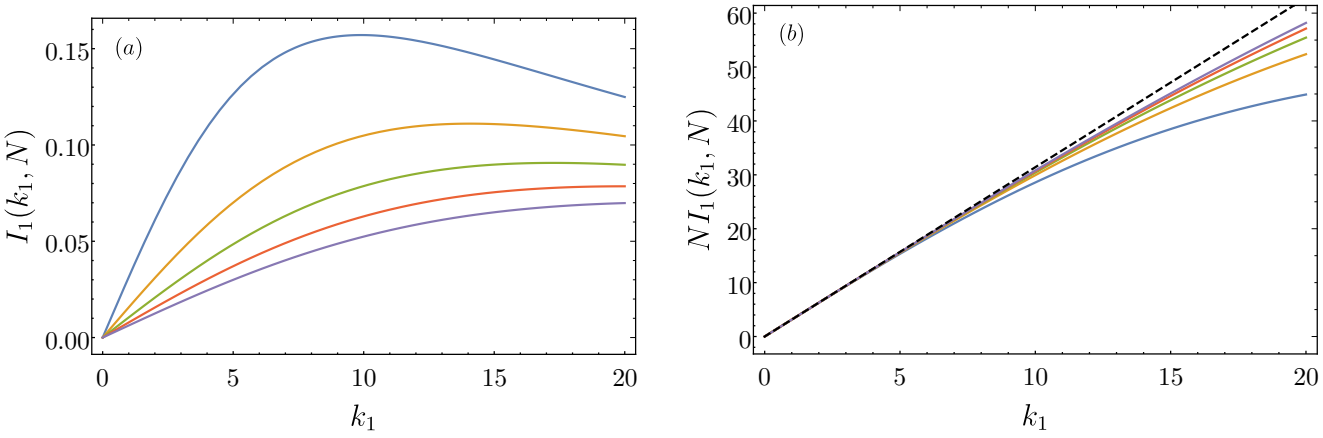

Figure 4.1: In panel (a) we report the plot of $I_1(k_1, N)$ for $N = 100, 200, 300, 400, 500$ from top to bottom, respectively. Notice how the flux reaches a maximum value and then decreases. In panel (b) we report the plot of $NI_1(k_1, N)$ for $N = 1000, 2000, 3000, 4000, 5000$, respectively. Note how the agreement with the analytical prediction (represented by the dashed black line) gets better and better as N grows.

the predicted scaling with N and dependence on k_1 4.13 grows as well. This fact can be understood in the following way: as N grows the maximum of I_1 moves to the right on the k_1 axis, as can be seen from figure 4.1 so when $N \to \infty$ the maximum is virtually at $k_1 = \infty$ so that only the linear region of $I_1(k_1, N)$ is visible.
We also remark that, even if the heat flux scales as N^{-1}, the system does not follow Fourier law: since the model is quadratic there can't be any diffusion mechanism. Indeed, as we are going to see in section 4.1.2, the temperature profile is flat in the bulk.

4.1.2 Temperature profile

Inserting the relevant Green function elements in (4.7) we derive an integral expression for temperature profile analogous to the one that we obtained for the heat flux (4.8), however we need to distinguish between the sites coupled to the baths and the uncoupled ones. For the first site, $i = 1$, using the expression for G_{11} (E.10)in the

large N limit we get:

$$T_1 = \frac{\lambda m T_L}{\pi} \int_{-\infty}^{\infty} \frac{\omega^2}{(m\omega^2 - 2k)^2 + \lambda^2\omega^2} + O(N^{-1}) = T_L + O(N^{-1}).$$

The same formula also holds for the last site $i = N$, with $L \to R$. For all the other uncoupled sites, $i \neq 1, N$, the temperature profile is given by (using (E.11)):

$$T_i = \frac{T_L + T_R}{2\pi} I_2(k_1, k_2, N), \tag{4.15}$$

where the integral I_2 is given by:

$$I_2(k_1, N) = \frac{4k_1}{N^2} \int_0^{+\infty} \frac{dy}{y^2(y^2-1)^2 + k_1^2(y^2 - \frac{2}{N})^2}. \tag{4.16}$$

Note that the temperature profile (4.15) is flat, confirming the fact that Fourier law is violated. The integral (4.16) can be decomposed in partial fractions and dealt with in the same way as I_1: the result is that at leading order for large N we have:

$$I_2 = I_1/k_1. \tag{4.17}$$

It follows that the temperature of the generic i-th site is given by:

$$T_{cl,i}^{int} = \frac{T_L + T_R}{2\pi} \frac{I_1}{k_1} = \frac{T_L + T_R}{2N}. \tag{4.18}$$

According to the result (4.18) the temperature of bulk oscillators does not equilibrate to the average of the temperatures of the baths, but vanishes in the thermodynamic limit. As we are going to see in the next paragraph, this behaviour is a peculiarity of the model and depends on the choice of the initial conditions.

4.1.3 Analysis of the equations of motion in the stationary regime

As we saw in Chapter 2 the equations of motion of the system coupled to Ohmic baths are given by (3.50) :

$$\ddot{x}_i = -\sum_j \Phi_{ij} x_j + \delta_{i1}(\xi_L - \lambda \dot{x}_i) + \delta_{i1}(\xi_L - \lambda \dot{x}_i), \tag{4.19}$$

where now Φ is given by (4.2) and we set all the masses $m = 1$. If we now introduce the center-of-mass coordinate $M(t) = \sum_i x_i/N$, and $S = x_1 + x_N$ the equations of motions can be cast in the following form:

$$\ddot{S} = -\lambda S - 2kS + 4kM + \xi, \tag{4.20}$$

$$\ddot{M} = (\xi - \lambda \dot{S})/N, \tag{4.21}$$

$$\ddot{x}_i = -2kx_i + 2kM, \quad i = 2, ..., N-1. \tag{4.22}$$

Switching to Fourier space, we find the following solution for $\tilde{M}(\omega)$ and the position $\tilde{x}_i(\omega)$ of the uncoupled sites:

$$\tilde{M}(\omega) = \frac{2k - \omega^2}{N\omega^2(\omega^2 + i\lambda\omega - 2k) - 4ik\lambda\omega}\tilde{\xi}(\omega), \tag{4.23}$$

$$\tilde{x}_i(\omega) = \frac{2k\tilde{M}(\omega)}{2k - \omega^2}. \tag{4.24}$$

Note that the pole on the proper frequency of the system $\omega^2 = 2k$ does not give any contribution, as if the baths were unable to properly interact with the system. It is convenient to recast equation (4.24) as:

$$\tilde{x}_i(\omega) = \frac{Q(\omega)}{\omega}\tilde{\xi}(\omega), \quad Q(\omega) \equiv \frac{-2k}{N}\frac{1}{\omega(\omega^2 - 2k) + i\lambda(\omega^2 - 4k/N)}, \tag{4.25}$$

so that it is evident that there is no pole on the dispersion law $\omega^2 = 2k$. Considering now the mean square velocity $\langle x_i^2 \rangle$, we can write the temperature of the i^{th} site as:

$$T_i = \lambda\frac{T_L + T_R}{\pi}\int d\omega |Q(\omega)|^2, \tag{4.26}$$

which reproduces exactly formula (4.15).
To get a better understanding of the physics of the model, let us introduce the relative coordinates $z_i = x_{i+1} - x_i$. Then, equation (4.22) entails that:

$$\ddot{z}_i = -2kz_i, \quad i = 2, ..., N-2. \tag{4.27}$$

So the relative coordinates of the uncoupled particles describe an harmonic motion without being influenced by the baths. This, in turn, means that the initial conditions of the system are essential to determine the properties of the stationary state at long times. Indeed, to solve the equations of motion we should use the Laplace, and not the Fourier, transform. When we used the Fourier transform in section 3.2 we

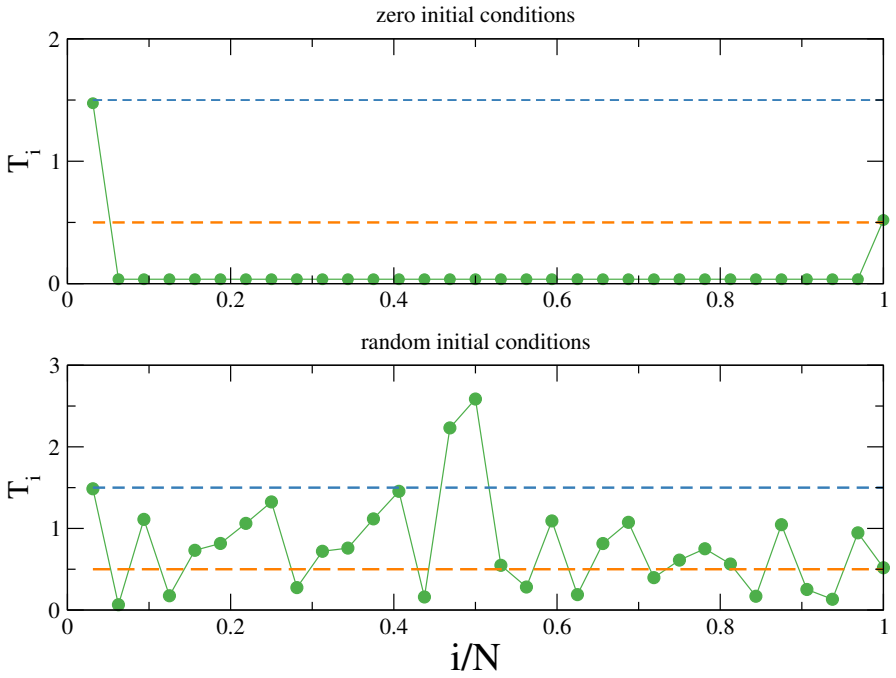

Figure 4.2: Temperature temperature obtained from simulations of the Langevin equation of motion for $N = 32$, intensive baths with $T_L = 1.5, T_R = 0.5$, $\lambda = 0.5$. Upper panel: zero initial conditions $x_i(0) = \dot{x}_i(0) = 0$ corresponding to the choice adopted in the analytical calculations. Lower panels: random initial conditions where $x_i(0)$ and $\dot{x}_i(0)$ are drawn from a Gaussian distribution with zero average and variance $(T_L + T_R)/2$. Averages are over trajectories of 10^5 time units.

assumed that the value of the initial condition would be irrelevant in the stationary state. Quantitatively we implicitly assumed $x_i(0) = \dot{x}_i(0) = 0$ for $i = 2, ..., N-2$: all our results presented in this chapter are thus valid provided we make this assumption on the initial conditions. To support the above considerations in figure 4.2 we report the kinetic temperatures measured in a Langevin simulation of the equation of motion for two different initial conditions. In the case $x_i(0) = \dot{x}_i(0) = 0$ the results coincide with the result (4.18). On the other hand, for random initial data the temperatures of the particles not coupled with the baths remain at their starting value and do not thermalize at all.

We remark that the crucial point is the cancellation of the pole in the dispersion relation of the system, which stems from two properties of the model. The first one is the linearity of the system, that allows the equations of motion to be solved exactly,

in terms of the Green's function, which in this analysis is given by $Q(\omega)/\omega$.
The second one is the conservation of the total magnetization M in absence of external baths, which originates from the mean-field nature of the system: from a mathematical point of view, this is related to the $(N-1)$-fold degeneracy of the spectrum of the matrix Φ. The second ingredient is the linearity of the system, that allows the equations of motion to be solved exactly in terms of the Green's function, which in this analysis is given by $Q(\omega)/\omega$. By lifting either of these properties, the temperature profile flattens on the average of the temperatures of the baths.
In order to demonstrate that the breaking of the matrix Φ may suffice to restore thermalization, we considered the following quadratic models:

$$H_1 = \sum_i \frac{p_i^2}{2} + \frac{k}{2N_\sigma} \sum_{ij=1}^{N} \frac{(x_i - x_j)^2}{|i-j|^{1+\sigma}}, \quad N_\sigma = \sum_{l=1}^{N} l^{-1-\sigma} \tag{4.28}$$

$$H_2 = \sum_i \frac{p_i^2}{2} + \frac{k}{2N} \sum_{ij=1}^{N} (x_i - x_j)^2 + \frac{g}{2} \sum_i (x_{i+1} - x_i)^2. \tag{4.29}$$

The first one (4.28) corresponds to a long-range power-law chain and will be the focus of chapter 4 while in the second one (4.29) we added a nearest-neighbours coupling to the fully-connected model (4.2). In both cases, we can apply the method described in section 3.1 and solve numerically the Lyapunov equation (3.10). The results for the temperature profile are plotted in figure 4.3: in both cases the profile is flat and given by the average temperature of the baths.
In [56] the authors computed numerically the temperature profile for random, graded and identical masses: in the first two cases the degeneracy is broken and indeed they find that the uncoupled particles thermalize to the average temperature of the baths. The result of this section is that heat flows directly between the sites coupled with the baths, completely bypassing the others, at least at leading order in N. This also explains why the temperature of the uncoupled sites vanishes, since they do not exchange energy with the baths. We also remark that in numerical analysis performed on interacting long-range chains, the temperature profile flattens to the average temperature of the baths in the fully-connected limit [3, 8].

Finally, we note that one can repeat the analysis presented in this subsection even if the baths induce a coloured noise: the result is once again that the residue related to the pole on the proper frequency of the system vanishes.

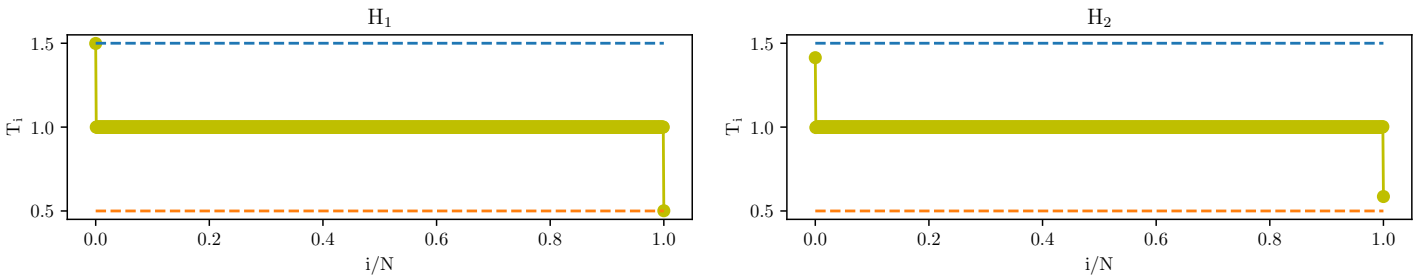

Figure 4.3: Numerical result for the temperature profile $T^{int}_{cl,i}$ for the Hamiltonians (4.28) and (4.29) on the left and on the right, respectively. We used the following values for the parameters:$T_L = 1.5$, $T_R = 0.5$ $k = g = 1$, $\sigma = -0.5$.

4.2 Intensive coupling, quantum case

The heat flux and temperature profile in the quantum regime for intensive couplings can be obtained by inserting (4.3) into (4.5):

$$J^{int}_q = \frac{\hbar\lambda^2\Delta T}{\pi}\int_{-\infty}^{+\infty} d\omega\,\omega^3|G_{1N}(\omega)|^2\frac{\partial f(\omega,T)}{\partial T}, \tag{4.30}$$

$$T^{int}_{q,i} = \frac{m\lambda}{k_B\pi}\int_{-\infty}^{\infty} d\omega\left[|G_{i1}|^2\frac{\hbar\omega^3}{2}\coth\left(\frac{\hbar\omega}{2k_BT_L}\right) + |G_{iN}|^2\frac{\hbar\omega^3}{2}\coth\left(\frac{\hbar\omega}{2k_BT_L}\right)\right]. \tag{4.31}$$

Note that the temperature profile is not yet expressed the linear response regime: we will perform the relevant expansion after having substituted in (4.31) the explicit expression of the Green function.

4.2.1 Heat flux

We insert the expression for G_{1N} (E.10) into (4.30) and we find:

$$J^{int}_q = \frac{k_B\Delta T\sqrt{2k/m}}{4}I_3(k_1,\theta;N), \tag{4.32}$$

where we introduced a dimensionless temperature θ as:

$$\theta = \frac{2k_BT}{\hbar}\sqrt{m/2k}, \tag{4.33}$$

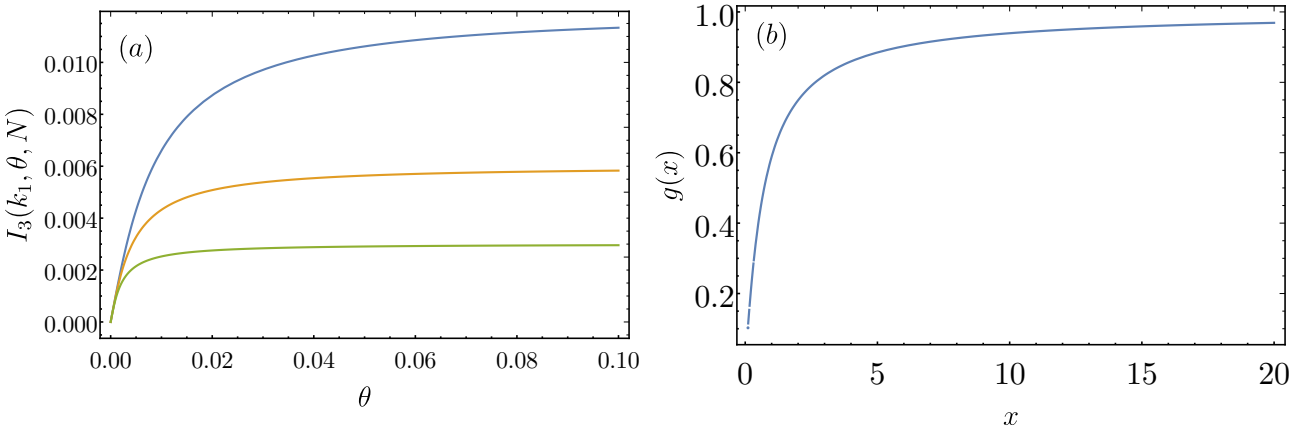

Figure 4.4: In panel (a) we report I_3 as a function of θ with $k_1 = 3$ and $N = 500, 1000, 2000$ from top to bottom, respectively. In panel (b) we plot the function $g(x)$ defined in (4.36).

and the the function $I_3(k_1, \theta, N)$ is given by:

$$I_3 = \frac{4}{\pi}\frac{k_1^2}{\theta^2 N^2}\int_{-\infty}^{\infty} dy\, \frac{(y^2-1)^2}{(y^2-1)^2 + k_1^2 y^2}\frac{y^2/\sinh^2(y/\theta)}{y^2(y^2-1)^2 + k_1^2(y^2-2/N)^2} \tag{4.34}$$

The integral I_3 (4.34) is plotted as a function of θ in figure 4.4: as expected, the heat flux vanishes in the low temperature region and saturates in the high temperature region. In appendix 6 we compute I_3 in the large N limit, and the final result is:

$$J_q^{int} = \frac{k_B \Delta T}{2N} k_1 \sqrt{\frac{2k}{m}}\, g\left(\frac{T_N(k_1)}{T}\right), \tag{4.35}$$

where the function $g(x)$ is given by:

$$g(x) = \frac{x^2}{\pi^2}\left[\psi^{(1)}\left(1+\frac{x}{\pi}\right) - \psi^{(1)}\left(1-\frac{x}{\pi}\right)\right] + \frac{x^2}{\sin^2(x)} - 2x, \tag{4.36}$$
$$\psi^{(1)}(z) = \frac{d^2}{dz^2}\log\Gamma(z),$$

being $\Gamma(z)$ the Euler Gamma function. The temperature $T_N(k_1)$ is the intrinsic temperature scale of the system, below which quantum effects are important. It is given by:

$$T_N(k_1) = \frac{k_1}{N}\frac{\hbar}{k_B}\sqrt{\frac{2k}{m}}. \tag{4.37}$$

To compare the quantum heat flux (4.32) and the classical one (4.8) we consider their ratio $r = J_q^{int}/J_{cl}^{int}$. For large N, this ratio is given by the function $g(x)$ (4.36). Its low and high temperature asymptotics are given by:

$$g\left(\frac{T_N}{T}\right) = \begin{cases} 1, & T \gg T_N, \\ \\ \dfrac{\pi}{3}\dfrac{T}{T_N} \sim TN, & T \ll T_N, \end{cases}$$

where we used the asymptotic formulas for the digamma function. We can see that at high temperature the quantum flux correctly converges to the classical one, while at low temperature it vanishes linearly with T. In figure 4.5 we plot the aforementioned ratio as a function of θ for several values of N: as N increases, the saturation to the classical value takes place at lower values of T. Finally, note that the flux (4.35) at low temperature does not depend on the coupling k_1:

$$J_q^{int} = \left(\frac{\pi^2 k_B^2 T}{3h}\right)\Delta T. \tag{4.38}$$

Furthermore, the quantity in parentheses depends only on universal constants and corresponds to the quantum of thermal conductance introduced in the context of transport in quantum harmonic wires in [57]

4.2.2 Temperature profile

As we did in the classical case we need to distinguish between the temperature of the sites coupled to the baths and the one of uncoupled ones. For site 1 in the large N limit we substitute (E.10) into (4.31):

$$T_1 = \frac{m\hbar\lambda}{2k_B\pi}\int_{-\infty}^{\infty}\frac{d\omega}{(m\omega^2 - 2k)^2 + \lambda^2\omega^2}\omega^3 \coth\left(\frac{\hbar\omega}{2k_B T_L}\right), \tag{4.39}$$

and the same expression also holds for site N with $L \to R$. The integral (4.39) is logarithmically divergent at large frequencies. This problem is unrelated with the long-range properties of the interaction and it is present even if we couple a single oscillator to two ohmic baths (see for example [58]). The divergence stems from the implicit hypothesis that the bath is able to excite arbitrarily high frequencies, which hidden in the choice $\Gamma \sim \lambda\omega$. If we consider a cut-off at high frequencies the divergence vanishes. To compute the temperature of the sites not coupled with the baths we need to insert (E.11) into (4.31) and then expand up to the first order in

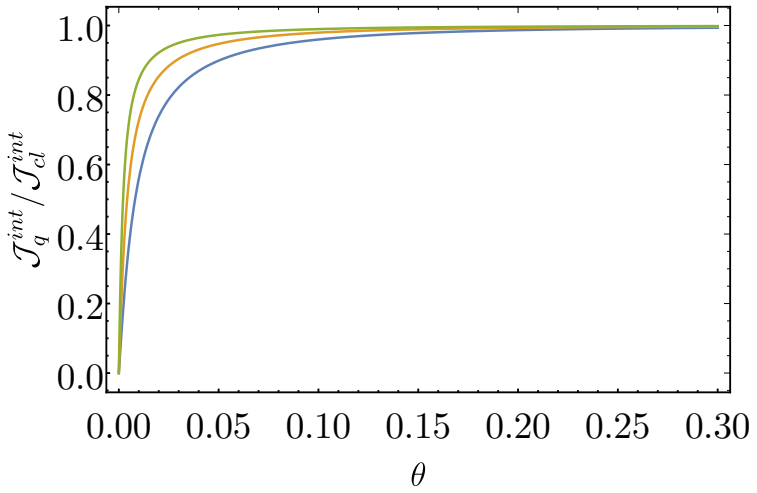

Figure 4.5: We report the plot of the ratio J_q^{int}/J_{cl}^{int} as a function of θ for $k_1 = 3$ and $N = 500, 1000, 2000$ from bottom to top, respectively.

ΔT. Note that since the square modulus of the Green function entries is an even function of ω the first-order term vanishes and thus in the linear response regime the bulk temperature profile is given by:

$$T_i = \frac{\hbar\lambda}{2mk_B} I_4, \tag{4.40}$$

where I_4 is given by:

$$I_4 = \frac{1}{N^2}\int_0^\infty dy \frac{y\coth(y/\theta)}{y^2(y^2-1)^2 + k_1^2(y^2-2/N)^2}. \tag{4.41}$$

The integral I_4 cannot be computed exactly, however we can compute its asymptotic behaviour at low temperature and we do it in section F.2 of appendix F. The result is:

$$T_{q,i}^{int} = \frac{\hbar\lambda k_B}{2m}\left[I_4(\theta=0) + \frac{\pi^2}{48}\frac{\theta^2}{k_1^2}\right], \tag{4.42}$$

where zero-temperature value of I_4 is given by:

$$I_4(\theta=0) = \frac{1}{2N^2}\left[2\ln\left(\frac{N}{2k_1}\right) + \frac{R}{\sqrt{1-R^2}}\left(\frac{\pi}{2} + \arctan\left(\frac{R}{\sqrt{1-R^2}}\right)\right)\right], \tag{4.43}$$

being R the real part of the non-vanishing roots of (4.11). The $I_4(\theta=0)$ term, which is non-vanishing even at zero temperature, can be interpreted as the contribution to the temperature of the zero-point energy of the system.

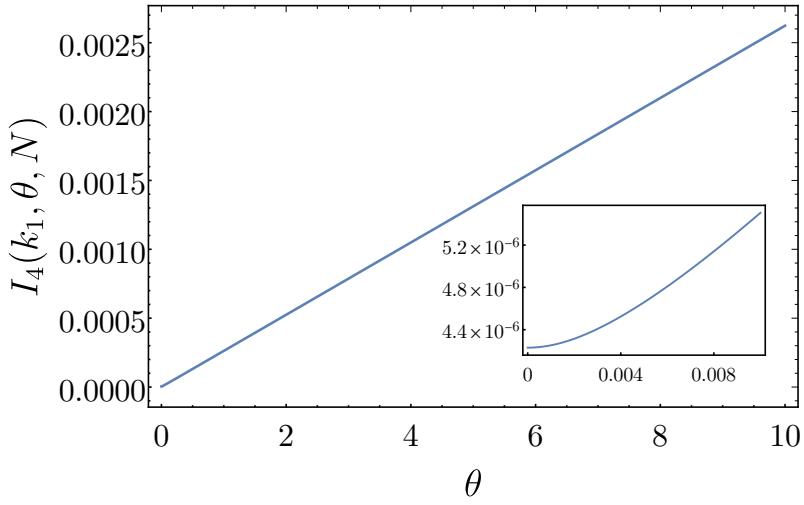

Figure 4.6: Plot of I_4 as a function of θ for $k_1 = 3$ and $N = 1000$. In the inset we plot I_4 at low temperatures.

4.3 Extensive coupling, classical case

The classical heat flux and temperature profile in the extensive case are found by inserting (4.4) into (3.46) and (3.47):

$$J_{cl}^{ext} = \frac{k_B \Delta T}{\pi} \int_{-\infty}^{+\infty} d\omega (\lambda\omega)^2 \sum_{i=N-N_R+1}^{N} \sum_{l=1}^{N_L} |G_{il}|^2 \tag{4.44}$$

$$T_{cl,i}^{ext} = \frac{m\lambda T_L}{\pi} \int_{-\infty}^{\infty} d\omega\omega \sum_{i=1}^{N_L} |G_{ik}(\omega)|^2 + \frac{m\lambda T_R}{\pi} \int_{-\infty}^{\infty} d\omega\omega \sum_{i=N-N_R+1}^{N} |G_{ik}(\omega)|^2. \tag{4.45}$$

The main difference between the intensive case formulae (4.6) and (4.7) is that now we need to sum over the Green function elements related to the sites coupled with the baths.

4.3.1 Heat flux

In order to compute the heat flux (4.44) we need to sum over all the Green function entries connecting two sites coupled to the baths. Inserting the result for the entries

of the Green function (E.20) into (4.44) we get:

$$J_{cl}^{ext} = \frac{k_B \Delta T \sqrt{2k/m}}{2\pi} I_5(k_1, \alpha_L, \alpha_R), \tag{4.46}$$

where we defined I_5 as:

$$I_5 = k_1^2 (2\alpha_L \alpha_R) \int_{-\infty}^{\infty} dy \frac{(y^2-1)^2}{[(y^2-1)^2 + k_1^2 y^2]\,[y^2(y^2-1)^2 + k_1^2(y^2 - (\alpha_R + \alpha_L))^2]}, \tag{4.47}$$

where we introduced the fraction of coupled sites $N_{L,R} = \alpha_{L,R} N$. In the derivation of (4.46) it is useful to note that the sum over the coupled sites collapses to $N_R N_L |G_{il}|^2$ since due to the symmetry of the model all of these entries are equal (see (E.20). As a check of (4.46), the heat flux reduces to the flux(4.8) of the intensive case if we set $\alpha_R = \alpha_L = 1/N$ in (4.47).
In figure 4.7 we report the plot of I_5 as a function of k_1 for some fixed values of α_L and α_R: its qualitative behaviour is the same as in the intensive case, the heat flux vanishes for both small and strong coupling. It is also interesting to note that in the extensive case the flux does not depend on N (although it decreases if we decrease the fractions of coupled sites), in contrast with the N^{-1} scaling of the intensive flux (4.14). This difference in scaling can be explained with the fact that, by coupling an extensive number of sites to the baths, we are increasing the energy pumped into the system by a factor N.

4.3.2 Temperature profile

As in the intensive case, we get different results if we consider the temperature T_i of a site which is directly coupled to a bath or not. If i is coupled to the left/right bath we insert (E.20) into (4.45) and we get at leading order $T_{cl,i}^{ext} = T_{L/R}$, as in the intensive case. If i is not coupled to any bath, we insert (E.20) into (4.45) and we get:

$$T_{cl,i}^{ext} = \frac{\alpha_L T_L + \alpha_R T_R}{\pi N} I_6(k_1, \alpha_L, \alpha_R), \tag{4.48}$$

where we introduced the integral I_6:

$$I_6 = k_1 \int_{-\infty}^{\infty} dy \frac{1}{[(y^2-1)^2 + k_1^2 y^2]\,[y^2(y^2-1)^2 + k_1^2(y^2 - \alpha_L - \alpha_R)^2]}. \tag{4.49}$$

If we set $\alpha_L = \alpha_R = 1/N$ we recover the result of intensive case (4.15). Note that even in this case the temperature of the uncoupled sites scales as N^{-1}: indeed, the

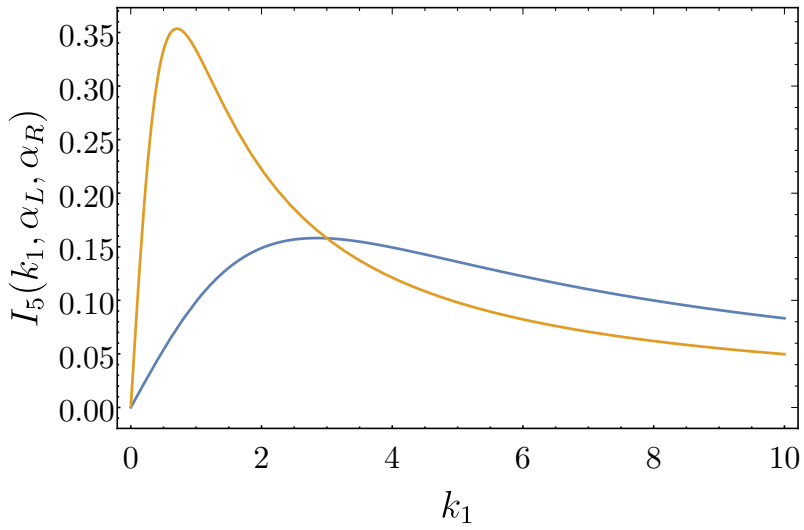

Figure 4.7: Plot of I_5 as a function of k_1 with $\alpha_L = 1/6, \alpha_R = 1/10$ and $\alpha_L = \alpha_R = 1/2$. The first choice of parameters corresponds to the curve with larger maximum.

same argument used in section 4.1.2 for the intensive coupling case holds also in the extensive case as can be seen by replacing S with the sum of the positions of the sites coupled to the baths.

4.4 Extensive coupling, quantum case

The quantum heat flux and temperature profile in the extensive coupling case are obtained by inserting (4.4) into (4.5) and (3.45):

$$J_q^{ext} = \frac{k_B \Delta T}{\pi} \int_{-\infty}^{+\infty} d\omega (\lambda\omega)^2 \sum_{i=N-N_R+1}^{N} \sum_{l=1}^{N_L} |G_{il}|^2 \frac{\partial f}{\partial T}, \tag{4.50}$$

$$T_{q,i}^{ext} = \frac{m\lambda}{k_B} \left[\int_{-\infty}^{\infty} d\omega\omega \sum_{i=k}^{N_L} |G_{ik}(\omega)|^2 \frac{\hbar\omega}{\pi} \coth\left(\frac{\hbar\omega}{2k_B T_L}\right) + \int_{-\infty}^{\infty} d\omega\omega \sum_{i=N-N_R+1}^{N} |G_{ik}(\omega)|^2 \frac{\hbar\omega}{\pi} \coth\left(\frac{\hbar\omega}{2k_B T_R}\right) \right]. \tag{4.51}$$

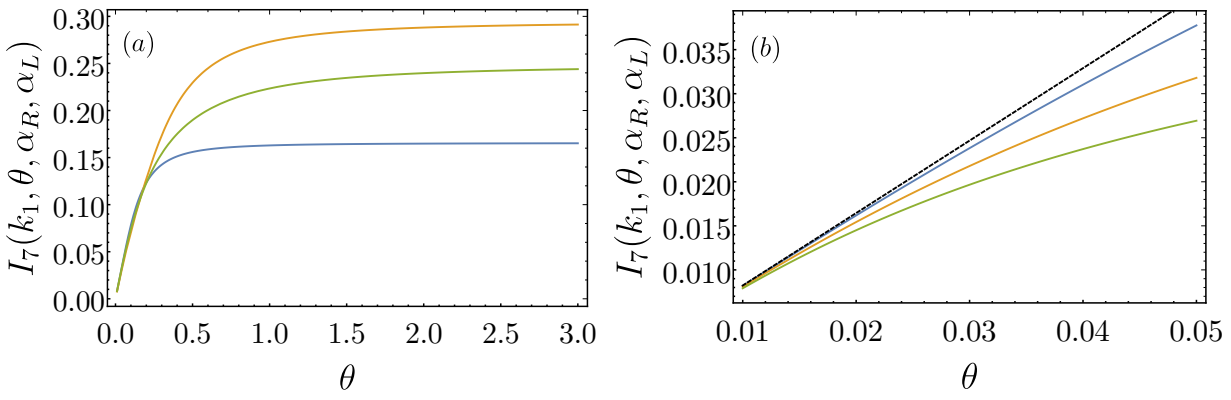

Figure 4.8: In panel (a) we plot I_7 (4.53) as a function of θ for $k_1 = 3$, $\alpha_L = 1/20, 1/3, 1/2$ and $\alpha_R = 1/20, 1/5, 1/2$ from bottom to top, respectively. In panel (b) we plot I_7 for low θ with $\alpha_L = \alpha_R = 1/3$ and $k_1 = 5, 10, 15$ from bottom to top, respectively. The black dashed line is the linear approximation (4.55).

4.4.1 Heat flux

Inserting the Green function elements (E.20) into (4.50) we get:

$$J_q^{ext} = \frac{k_B \Delta T \sqrt{2k/m}}{\pi} I_7(k_1, \theta, \alpha_L, \alpha_R), \tag{4.52}$$

where the integral I_7 is given by:

$$I_7 = \alpha_L \alpha_R \frac{k_1^2}{\theta^2} \int_{-\infty}^{\infty} dy \frac{(y^2-1)^2}{(y^2-1)^2 + k_1^2 y^2} \frac{y^2/\sinh(y/\theta)}{y^2 (y^2-1)^2 + k_1^2 (y^2 - (\alpha_L + \alpha_R))^2}. \tag{4.53}$$

In figure 4.8a we plot I_7 as a function of θ with fixed $\alpha_L + \alpha_R$: as expected, the heat flux vanishes at low temperature, while it saturates at high temperature.While it is not possible to compute I_7 (at variance with the intensive case I_3 (4.34)), we can obtain an estimate for the low-temperature behaviour using the following representation of the delta function:

$$\lim_{\theta \to 0} \frac{3}{\pi^2 \theta^3} \frac{y^2}{\sinh^2(y/\theta)} = \delta(y), \tag{4.54}$$

so that I_7 for small θ is given by:

$$I_7 = \frac{\pi^2}{3} \frac{\alpha_R \alpha_L}{(\alpha_R + \alpha_L)^2} \theta. \tag{4.55}$$

The heat flux thus vanishes linearly with the temperature, like in the intensive case (4.35). In figure 4.8*b*, we report the numerical plot of I_7 and its low-temperature approximation (4.55) for several values of k_1. Looking at 4.8*b* we see that the value of θ below which the linear approximation is valid decreases as a function of k_1. Since we are not able to solve (4.53) exactly we cannot provide an expression for this temperature scale in the extensive case. As in the intensive case (4.2.1), at low temperature the flux can be expressed in terms of the quantum of thermal conductance:

$$J_q^{ext} = \left(\frac{\pi^2 k_B^2 T}{3h}\right) \frac{4\alpha_R \alpha_L}{(\alpha_R + \alpha_L)^2} \Delta T, \tag{4.56}$$

where now we also have a "geometrical factor" that depends on the fraction of coupled sites. Note that for $\alpha_L = \alpha_R$ we recover the intensive result (4.2.1).

4.4.2 Temperature profile

The temperature of the sites directly coupled to the baths (i.e. $i = 1, ..., N_L$ and $i = N - N_R + 1, ..., N$) diverges as in the intensive case due to the non-physical contribution of high frequencies. The temperature of the uncoupled sites(i.e. $i = N_L + 1, ...N - N_R$) is obtained by inserting (E.21) into (4.51):

$$T_{q,i}^{ext} = \frac{\hbar\lambda}{2\pi N m k_B} \left[\alpha_L I_8(\theta^L, k_1, \alpha_{L,R}) + \alpha_R I_8(\theta^R, k_1, \alpha_L, \alpha_R)\right], \tag{4.57}$$

where $\theta^{L,R} = 2k_B T_{L,R}/\hbar\sqrt{2k/m}$ the integral $I_8(\theta, k_1, \alpha_L, \alpha_R)$ as:

$$I_8 = \int_{-\infty}^{\infty} dy \frac{y \coth(y/\theta)}{y^2(y^2-1)^2 + k_1^2(y^2 - \alpha_L - \alpha_R)^2}. \tag{4.58}$$

In the linear response regime we must Taylor expand (4.57) around $\Delta T = 0$ for $T_{L,R} = T \pm \Delta T/2$:

$$T_{q,i}^{ext} = \frac{\hbar\lambda}{2\pi N m k_B} \left[(\alpha_L + \alpha_R) I_8^{(0)} + \frac{k_B \Delta T}{\hbar\sqrt{2k/m}} (\alpha_L - \alpha_R) I_8^{(1)}\right], \tag{4.59}$$

where:

$$I_8^{(0)} = \int_{-\infty}^{\infty} dy \frac{(y^2-1)^2 y \coth(y/\theta)}{[y^2(y^2-1)^2 + k_1^2(y^2 - \alpha_R - \alpha_L)^2]}, \tag{4.60}$$

$$I_8^{(1)} = \theta^{-2} \int_{-\infty}^{\infty} dy \frac{y^2/\sinh^2(y/\theta)}{[y^2(y^2-1)^2 + k_1^2(y^2 - \alpha_R - \alpha_L)^2]}. \tag{4.61}$$

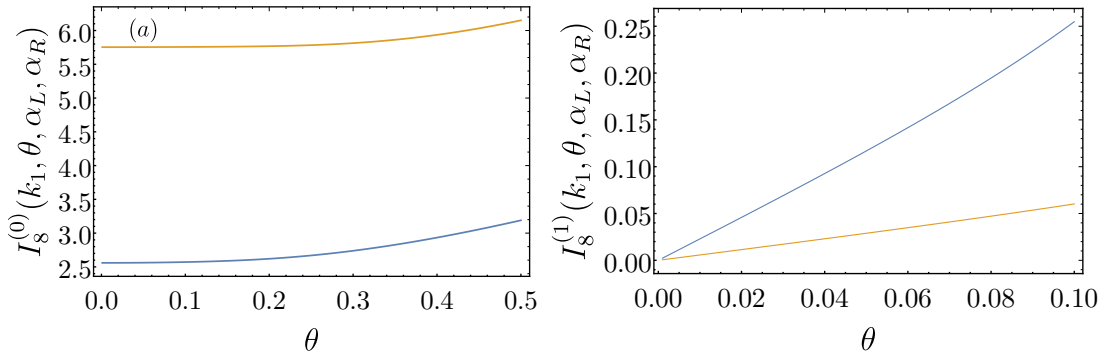

Figure 4.9: In panel (a) we report the plot of I_8 as a function of θ with $k_1 = 3$ and $\alpha_L + \alpha_R = 0.4, 0.8$ respectively. In panel (b) we report the plot of I_8 as a function of θ with $k_1 = 3$ and $\alpha_L + \alpha_R = 0.4$.

In figure 4.9a we report the plot of $I_8^{(0)}$: note that it does not vanish as the temperature goes to zero. Indeed, $I_8^{(0)}(k2 = 0)$ can be interpreted as the contribution to the temperature of the zero-point energy of the system. We can compute the low-temperature of $I_8^{(1)}$ by using once again (4.54):

$$I_8^{(1)} = \frac{\pi^2}{3k_1^2(\alpha_L + \alpha_R)^2}\theta. \tag{4.62}$$

In figure 4.9b we report the plot of $I_8^{(1)}$ and (4.62) and we see that there is good agreement between the exact plot of I_8 and the approximation (4.62). Expression (4.59) entails that, if we couple the same fraction of sites to the left and to the right bath, the term proportional to ΔT vanishes. This explains why in the intensive case $\alpha_L = \alpha_R = 1/N$ the term proportional to ΔT vanishes. Finally one can check numerically that $I_8^{(0)}$ goes as θ^2 for small θ and thus the temperature profile for small T (4.59) behaves as :

$$T_{q,i}^{ext} = \frac{\hbar\lambda}{2\pi N m k_B}\left[(\alpha_L + \alpha_R)I_8^{(0)}(\theta = 0) + \frac{k_B\Delta T}{\hbar\sqrt{2k/m}}\frac{\pi^2}{3k_1^2}\frac{(\alpha_L - \alpha_R)}{(\alpha_L + \alpha_R)^2}\theta\right]. \tag{4.63}$$

In this chapter we studied heat transport in a fully-coupled harmonic network by computing the heat flux and the temperature profile both in the intensive and extensive coupling cases. Since we studied several cases, we recapitulate for convenience our results in table 4.1

Coupling	Quantity	Classical	Quantum
Intensive	J^{int}	$J^{int}_{cl} \sim \Delta T/N$	$J^{int}_{q} \sim T\Delta T$
	T^{int}_{i}	$T^{int}_{cl,i} \sim T/N$	$T^{int}_{q,i} \sim T^2 + O(\ln N/N^2)$
Extensive	J^{ext}	$J^{ext}_{cl} \sim \Delta T N^0$	$J^{ext}_{q} \sim T\Delta T$
	T^{ext}_{i}	$T^{ext}_{cl,i} \sim N^{-1}$	$T^{ext}_{q,i} \sim const/N + T/N$

Table 4.1: Summary of main results about thermal transport in the fully-connected harmonic network (4.2). We report the low-temperature behaviour of the quantum results.

Chapter 5

Heat flux in a power-law long-range chain

In this chapter we study the heat flux in the stationary state of a power-law long-range chain which is coupled on site 1 and N to two ohmic heat baths. The Hamiltonian of the system is given by:

$$H = \frac{1}{2}\sum_i p_i^2 + \frac{1}{2}\sum_{ij} x_i \Phi_{ij} x_j, \tag{5.1}$$

where the interaction matrix Φ is given by:

$$\Phi_{ij} = \left(2\delta_{ij} - \frac{1}{N_\sigma}\frac{1}{|i-j|^{1+\sigma}}\right), \quad N_\sigma = \sum_{l=1}^{N} l^{-\sigma}, \tag{5.2}$$

and N_σ is the Kac factor defined in (2.21).
In order to compute the heat flux we are going to use both the RLL method, the LEGF method and the generalized eigenvalues method, described in sections 3.1, 3.2 and 3.3, respectively. We remark that, at variance with the nearest-neighbours chain or the fully connected network, the analytical implementation of the aforementioned methods presents significant challenges. The main problem is that the matrix Φ is neither tridiagonal (as in the nearest-neighbours case (3.16)) nor has a structure which allows us to easily invert (3.52) using a known formula, such as in the fully-coupled case (4.2). We also remark that not even the spectrum of (5.2) is exactly known in the literature: in the continuum limit it would correspond to the spectrum of the fractional Laplacian with open boundary condition, which is not known in general and does not correspond to the usual sinusoidal waves [59]. For all these

reasons, our analysis will be purely numerical: the main result of this chapter is that heat transport is super-diffusive and the heat flux scales as a power of the system's size N. The determination of the scaling exponent, however, is hindered by the presence of strong finite-size effects.
In section 5.1 we will report the results for the heat flux obtained with the RLL method for small coupling λ and we compare them with known perturbative results valid for generic quadratic systems. In section 5.2 we report our results for generic values of the coupling. The main conclusion is that the heat flux scales as a power law of the system size $J \sim N^{-\gamma}$, however the determination of the exponent γ is hindered by the presence of strong finite-size effects. Finally, in section 5.3 we study the structure of the transmission coefficient (i.e. the integrand of the heat flux) and we see how its properties can be used to infer the scaling of the heat flux with the size of the system.

5.1 Heat flux for small coupling

For small values of the chain-bath coupling λ it is possible to perform a power-series expansion of the heat flux J. Retaining only the leading term yields so-called Matsuda-Ishii's formula, $J = J_{MI}$ [60, 1]:

$$J_{MI} = \lambda \Delta T \sum_k \frac{\psi_{k,1}^2 \psi_{k,N}^2}{\psi_{k,1}^2 + \psi_{k,N}^2}, \tag{5.3}$$

where $\psi_{k,,n}$ denotes the n component of the kth eigenvector of the matrix Φ defined in (5.2). For an homogeneous and mirror-symmetric model, as the one we are considering $\psi_{k,1} = \psi_{k,N}$ for $k = 1...N$ and the above expression simplifies to

$$J_{MI} = \frac{\lambda \Delta T}{2}. \tag{5.4}$$

We thus see that for small λ heat transport is ballistic.

In the short-range case $\sigma \to \infty$, this result applies for $\lambda \ll \lambda_0 \approx O(1)$. In the long-range case, however, the situation is more complicated. In figure 5.1, we compare formula (5.4) and the numerical solution of the Lyapunov equation (3.10) with the ϕ matrix given by (5.2). As we can see, (5.4) holds for λ smaller than a certain threshold $\lambda_0(\sigma, N)$, that depends both on N and on σ. More specifically, λ_0 decreases with σ and with N. On the other hand, for $\sigma > 0$ the perturbative approximation holds well in the considered range of λ.

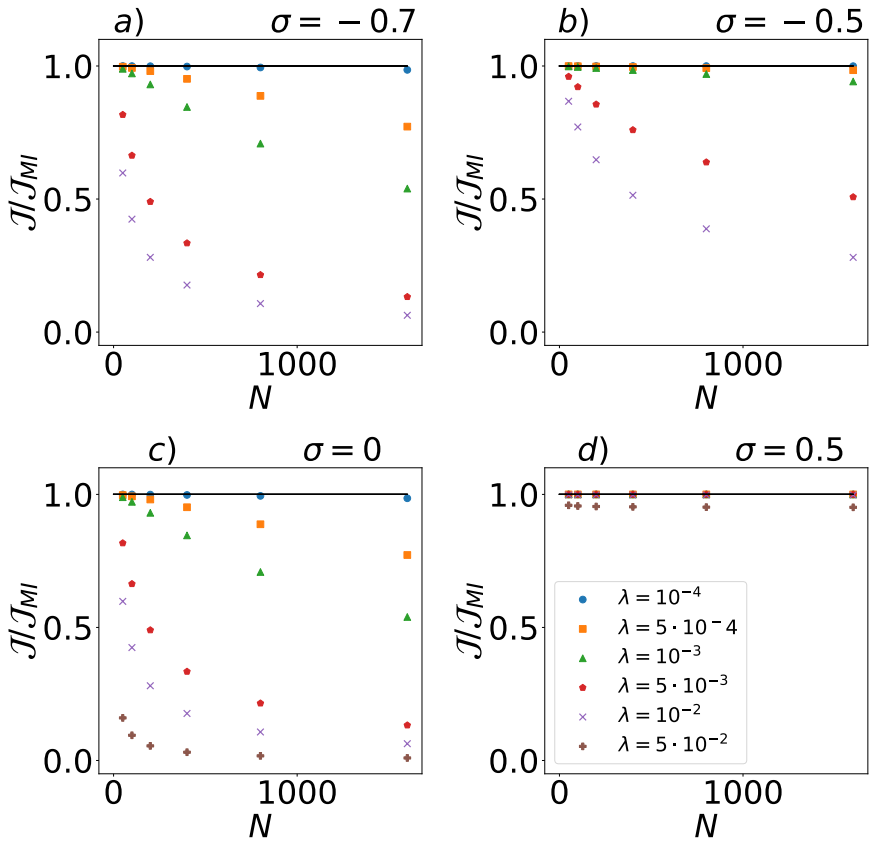

Figure 5.1: Plots of the ratio between the heat flux J, computed numerically with the RLL method, and the Matsuuda-Ishii heat flux (5.4) versus the system size N for several values of σ and λ in the weak coupling regime.

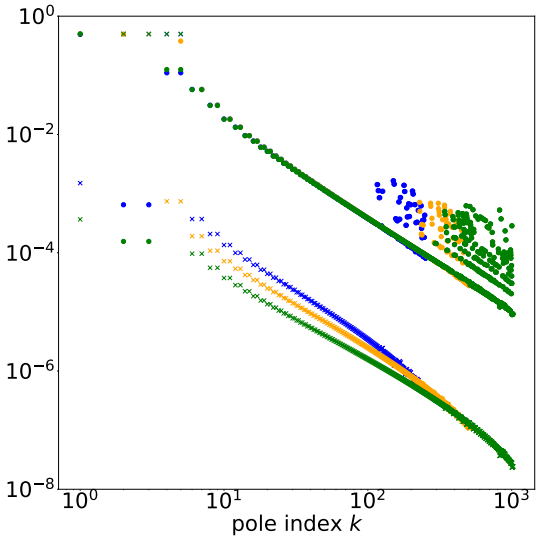

Figure 5.2: Plots of the spacing between the imaginary parts of the poles of the Green's function $Im(s_{k+1}) - Im(s_k)$ (circles) and the real parts of the poles $Re(s_k)$ (crosses) for $\sigma = -0.5$. Different colors correspond to different system's size: $N = 256, 512, 1024$ in blue, orange, green, respectively.

We remark that usually the perturbative approach is justified assuming that the separation of the unperturbed normal mode frequencies is smaller than the typical dissipation caused by the coupling with the baths [61]. This assumption can be checked by examining the poles of the Green function s_a, which we will analyze in detail in section 5.3. In particular, we compare the spacings between the position of consecutive poles, given by $Im(s_{a+1} - s_a)$ and the real parts of the poles $Re(s_a)$, which encode the strength of dissipation[1]. As we can see from figure 5.2, the former is always much larger than the latter: the perturbative expansion is thus justified in the small λ limit.

[1]Note that, since we are working using Laplace transform and with the Fourier one, the usual role of the imaginary and real part of the poles of the Green function is reversed.

5.2 Heat flux for generic value of the coupling

We now want to understand how the flux scales with the system size N for larger coupling. In order to so, we computed the heat flux using the RLL method for several values of N and σ for $\lambda = 1$. As shown in figure 5.3 the data can be fitted with a power law $J \propto N^{-\gamma}$. The result of this fit is reported in figure 5.4*a*
The application of the Green function method is more problematic. Indeed, in order to compute the heat flux using (3.46) we need to numerically invert the matrix (3.41) to obtain the Green function $G(\omega)$. This operation is computationally heavy for a dense matrix such as (5.2). Furthermore, in order to compute the integral over the frequency we need the Green function $G(\omega)$ for several value of ω: this sampling has to be fine, especially if the transmission coefficient is rapidly oscillating (as is our case, as we will see). For all these reasons with this method we can study system's sizes at most of order $N \sim 10^2$.
Even if the direct computation of the Green function is computationally heavy, we can easily compute its poles solving the $2N \times 2N$ eigenvalue problem (D.10), compute the heat flux using formula (3.54) and fit a power law. In figure 5.4*b* we report both the exponents fitted with the generalized eigenvalues method and with the RLL method. As we can see, they are qualitatively in agreement.
Looking at the fitted exponents in figure 5.4, we can identify three regions. The region close to the mean-field case $\sigma = -1$ and the one close to the short-range case $\sigma > 1$, where finite-size effects are almost absent, and an intermediate region in which finite-size effects are quite strong. We also note that γ seems to be converging to the short-range value $\gamma = 0$ while σ goes to 1. In conclusion, even if we are not able to extract the exact values of the exponents, it is clear that the flux scales with some nontrivial power of the system's size N.

5.2.1 Transmission coefficient

In this section we compute the quantity $(\lambda\omega)^2|G_{1N}(\omega)|^2$, which is basically the transmission coefficient (3.48), for the power-law chain (5.2): as we are going to see its properties are crucial to understand the scaling of the heat flux.
In figure 5.5 we report our results for several values of σ. We can see that the transmission coefficient is characterized by a rather complicated peak structure which consists of $N - 2$ peaks (as can be checked numerically). Notice $G(-\omega) = G(\omega)^*$, as can be seen from (3.41). Thus, since the transmission coefficient depends on the square modulus of $G(\omega)$, we will consider only the case $\omega > 0$. Let us denote by ω_k,

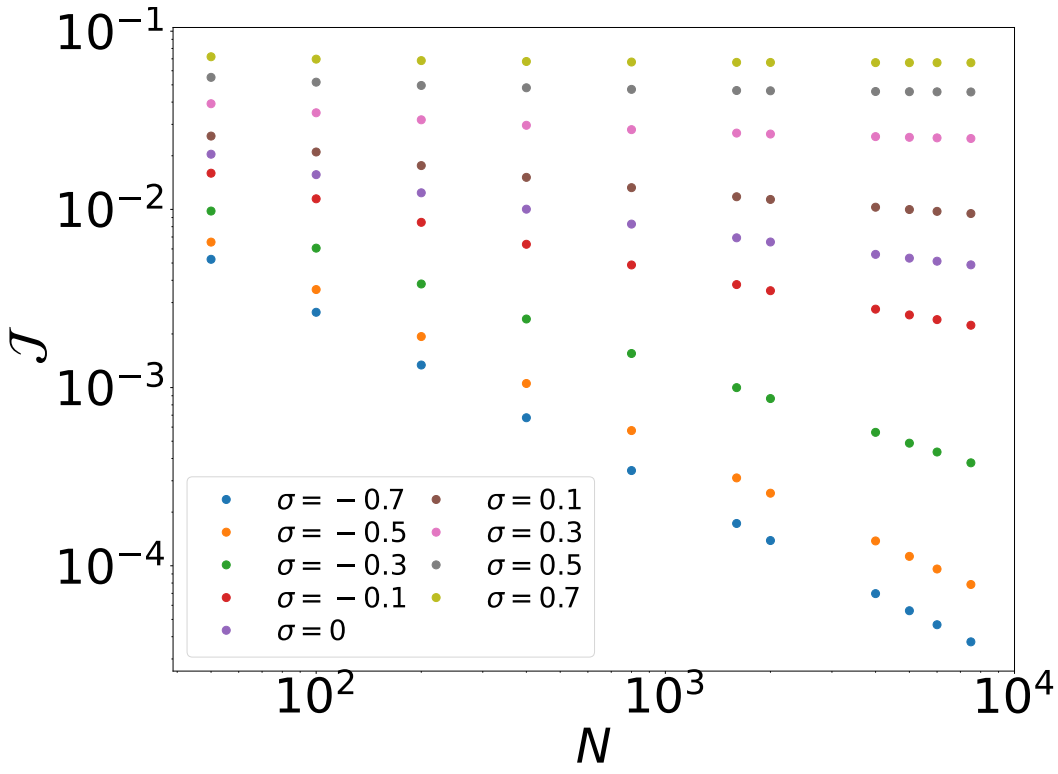

Figure 5.3: Log-log plot of the heat flux J versus the system's size N for $\lambda = 1$ and different values of the long-range exponent σ. The flux is computed using the RLL method as described in the text.

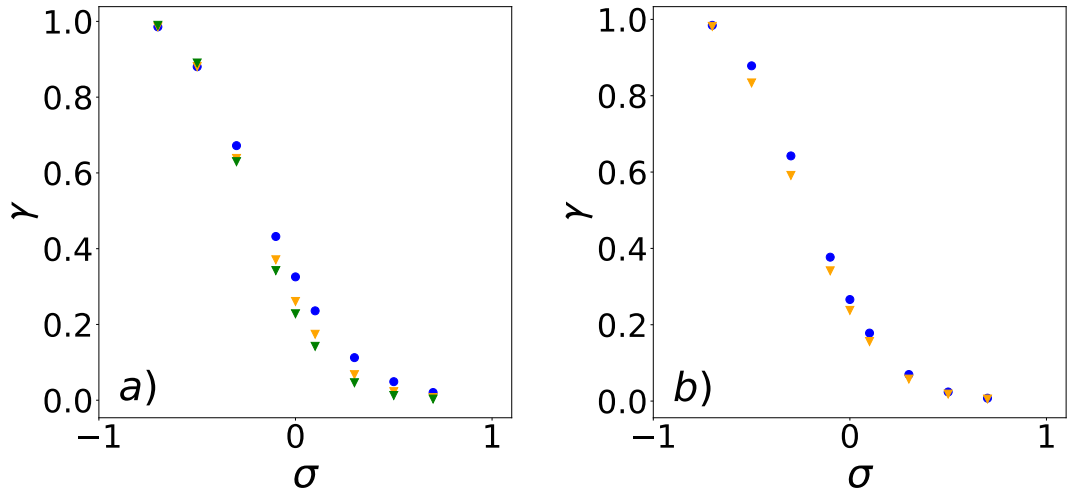

Figure 5.4: Plot of the scaling exponent of the flux γ, defined as $J \propto N^{-\gamma}$, (a), we report the exponents obtained by fitting a power law on the heat flux obtained with the RLL method. To check the finite-size effects, each data set corresponds to a fit over different length ranges, $50 \leq N \leq 1600$ (circles), $500 \leq N \leq 2000$ (squares), $1500 \leq N \leq 7500$ (triangles). Panel (b), comparison between the exponents obtained by the RLL method (circles) and the generalized eigenvalue method (triangles).

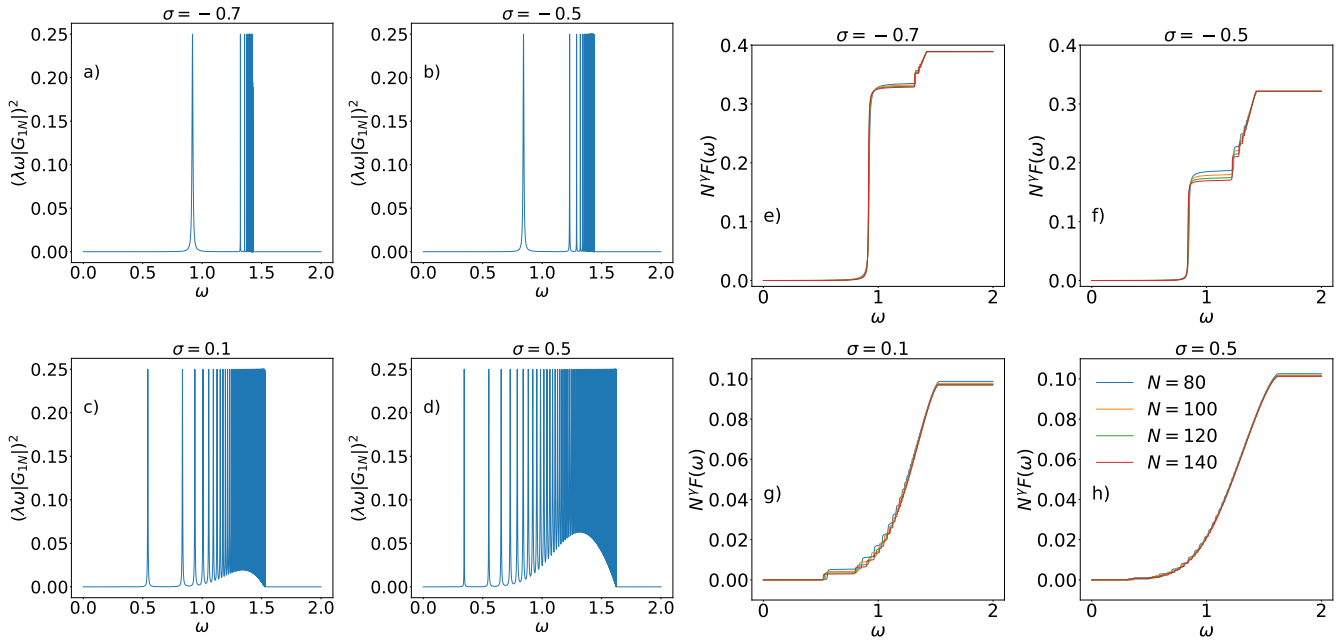

Figure 5.5: Panels a), b), c), d) : transmission coefficient $\lambda^2\omega^2|G_{1N}(\omega)^2$ for different values of the range exponent $\sigma = -0.7, 0.5, 0.1, 0.5$ and for a chain with $N = 100$. Only positive frequencies are reported. Panels e), f), g), h): rescaled cumulative function $N^\gamma F(\omega)$, for $N = 80, 100, 120, 140$ and $\sigma = -0.7, -0.5, -0.1, 0.5$ in panels a), b), c), d) respectively. The values of γ are taken from the blue points in figure 5.4a. The abrupt increase of the cumulative function in panels e) and f) at $\omega \approx 1.3$ is due to the dominant contribution of the first peak in panels a) and b. The subsequent, smaller, jumps are due to the contributions of the other peaks.

$k = 1, 2 \ldots$ the location of the peak frequencies for positive ω. As it is evident from 5.5, the peaks accumulate at a band-edge frequency $\omega_B < 2$. Furthermore, upon approaching ω_B, the width of the peaks decreases. This is the reason why it is important to finely sample the Green's function in ω, especially in the proximity of the band edge: we used a logarithmic sampling in order to increase the sampling points near ω_B. It can be checked numerically that the first few peaks are Lorentzian with amplitude $\Delta_k \approx N^{-1}$, exactly like the only peak present in the in the fully-connected case (4.13). The subsequent peaks are too narrow to be resolved. For positive values of σ the situation becomes even more complicated, as a curve emerges below the peaks, as we can see in figure 5.5d) for $\sigma = 0.5$.

For the reasons outlined above, it seems more convenient to consider the cumulative function $F(\omega)$, that is, the integral in (4.6), performed up to frequency ω. In figures 5.5 from e) to h) we report the function $F(\omega)$, for several values of N of order 10^2 and σ, rescaled by N^γ, where γ is the exponent obtained with the RLL method for values of N of order $10^2 : 10^3$. As we can see, the curves nicely collapse for $\sigma = -0.7, -0.5$, but for higher values of σ, such as $\sigma = -0.3$, the collapse is not as good due to the finite-size effects, as expected.

5.3 Poles of the Green's function

To get a better understanding of the peak structure we compute the poles of the Green function using the generalized eigenvalue method: As we already mentioned, the positions ω_k of the peaks in figure 5.5 are given by the absolute value of the imaginary part of s_a, while the absolute value of the imaginary part should be proportional to their widths Δ_k.

In particular, we consider all the peaks as Lorentzian – for simplicity, but also because all the peaks that we were able to resolve are actually very well approximated by a Lorentzian – with width given by $\Delta_k(N) = Re(s_k)$. In this approximation, as far as scaling with the size is concerned, the heat flux can be estimated as the sum of the widths of the peaks $\Delta_k(N)$. Furthermore, from the numerics the height of each peak results to be $\lambda^2/4$ (indeed, note that in figure 5.5, in which $\lambda = 1$, the heights of the peaks are all the same and equal to $1/4$). Thus, we replace the transmission coefficient with a sum of normalized Lorentzian peaks, and we get:

$$\frac{J}{\Delta T} \approx \int_{-\infty}^{\infty} \frac{d\omega}{\pi} \sum_{k=1}^{N-2} \frac{\lambda^2 \Delta_k(N)^2/4}{(\omega - \omega_k)^2 + \Delta_k(N)^2} = \frac{\lambda^2}{4} \sum_{k=1}^{N-2} \Delta_k(N). \tag{5.5}$$

The relevant information should thus be contained in the dependence of the Δ_k on k and N. Physically, this is the effective damping of plane waves due to the coupling with the thermal reservoirs.

The dependence of Δ_k on N is reported in figure 5.6, where we plot the real parts of the poles as a function of the imaginary ones, for negative and positive values of σ, respectively. Since the resonances accumulates at the band-edges, it is convenient to report the frequencies as a function of their relative distance from ω_B. Let us focus on the case of negative σ, to begin with. From the leftmost panels of figure 5.6, it is seen that the poles can be grouped in two sets, each having different dependencies

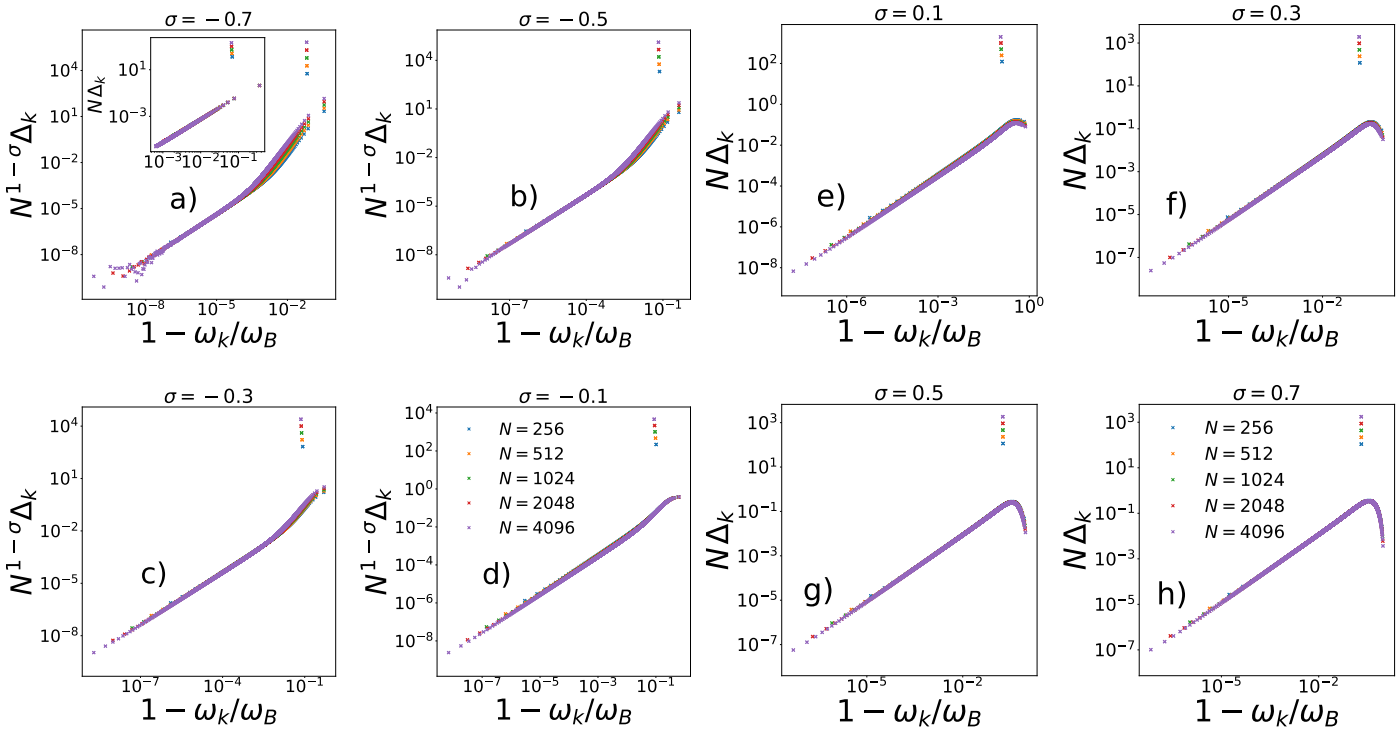

Figure 5.6: Real parts of the poles of the Green's functions s_a versus the distance of their imaginary parts from the band-edge. Leftmost panel: $\sigma < 0$, vertical axis rescaled by N^{ϕ} with $\phi \approx 1 - \sigma$. The inset in panel (a) demonstrates the different scaling the collapse for the widths of the first peaks (the first $80, 160, 320, 640, 1280$ for $N = 256, 512, 1024, 2048, 4096$, respectively) rescaled by N. For the other values of σ, we get the same scaling for the first peaks. Rightmost panel: same for $\sigma > 0$, with vertical axis rescaled by N. Note that such scaling works for the whole spectrum in this case.

on ω_k and N. Empirically, this is accounted for by the following scaling:

$$\Delta_k(N) \approx \begin{cases} d_k/N, & k < k_o \\ d_k/N^{\phi}, & k > k_o, \end{cases} \tag{5.6}$$

where $k_o << N$ and d_k do not depend N. We do not have a theoretical estimate of ϕ, but we find that there is a good collapse upon choosing $\phi \approx 1 + |\sigma|$.
Furthermore, as we can see from 5.6 there are a few poles whose widths do not follow this scaling and fall consistently well outside the collapsed curve. It actually turns out that there are two degenerate eigenvalues between the s_as that do not follow the scaling law. However this is inconsequential, as one can check that the contribution of the these eigenvalues to the heat flux (3.54) vanishes. Heuristically, this is because the eigenvectors related to these eigenvalues are localized at the endpoints of the chain and therefore do not contribute to transport. This also explains why the peaks in figure 5.5 are $N-2$ instead of N. We can therefore infer the following scaling law for the heat flux plugging (5.6) into (5.5):

$$J \approx \frac{\sum_{k=1}^{k_o} d_k}{N} + \frac{\sum_{k=k_o}^{N} d_k}{N^{\phi}} \propto N^{1-\phi}. \tag{5.7}$$

The first term scales as N^{-1}, since k_o does not scale with N (as can be inferred from figure 5.6). On the other hand, the second term scale as $N^{1-\phi}$ since each d_k is of order 1 and thus their sum scales as N. Finally, since $\phi > 0$, we get the reported scaling for the heat flux. For positive σ, the scaling of Δ_k is reported in the right-most panels of figure 5.6: as we can see in this case $\Delta_k \approx N^{-1}$, over the entire spectrum. Therefore, the estimate the heat flux yields

$$J \approx \frac{\sum_{k=1}^{N} d_k}{N} \approx \mathcal{O}(1). \tag{5.8}$$

So the heat flux for positive σ behaves as the heat flux for $\sigma = \infty$ (the nearest-neighbours case), that is, it does not scale with N.

To summarize, according to approximation (5.5) and the numerical estimate of ϕ extracted from the data, we find that the heat flux scales as:

$$J \propto N^{-\tilde{\gamma}}, \qquad \tilde{\gamma} \approx \begin{cases} 1-\phi, & \sigma < 0, \\ 0, & \sigma > 0. \end{cases} \tag{5.9}$$

As we already mentioned, see figure 5.6, we found a good collapse of the imaginary part of the poles of the Green's functions for $\phi \approx 1 - |\sigma|$. So this yields

$$\tilde{\gamma} \approx -\sigma \tag{5.10}$$

for negative σ. Admittedly, this estimate accounts only qualitatively for the behavior of the exponents as given in figure 5.4. The deviations are sizeable and the dependence of γ on σ appears to be non-linear. While this could be due to the aforementioned finite-size effects, the discrepancy is present even for values of σ for which the exponent γ has basically converged (for example $\sigma = -0.7, -0.5$). A more likely possibility is that, while the widths of the peaks of figure 5.5 are indeed related to the real parts of s_a on general grounds, they are not exactly equal. On the other hand, we point out that, since the s_a are related to the widths of the peaks, the transition in the scaling of the Δ_ks at $\sigma = 0$ suggests that the scaling of the heat-flux between the short-range and the long-range behaviour has to occur at $\sigma = 0$.

Chapter 6

Long-range stochastic collisions

In this chapter we consider a power-law long-range harmonic chain with stochastic collisions and we compute the thermal conductivity using the Green-Kubo formula as described in section 3.4. The case of nearest-neighbours collision was studied in [12]: we will consider the more general case of long-range collisions. This model is interesting because it provides an example of analytically solvable long-range model which is not fully-connected, at variance with the open-boundary condition power-law chain that we studied in Chapter 5. Furthermore, as we already said in section 3.4, the quadratic chains with stochastic collision are believed to share some properties with anharmonic chains and thus this model could provide some insight on the behaviour of interacting long-range systems.
In section 6.1 we introduce the model making contact with the formalism described in section 3.4, in section 6.2 we describe the splitting of the current in a deterministic and a stochastic term like we did in section 3.4.2, and in section 6.3 we compute the correlation of the deterministic current and the scaling with the system's size of the thermal current.

6.1 The model

The deterministic part of the dynamics is generated by the Hamiltonian:

$$H = \sum_{l=1}^{N} \frac{p_l^2}{2} + \frac{1}{N_\delta} \sum_{l=1}^{N} \sum_{r=1}^{N/2} \frac{(x_l - x_{l+r})^2}{r^\delta} = \sum_{l=1}^{N} \frac{p_l^2}{2} + \frac{1}{2} \sum_{ij} \Phi_{ij} x_i x_j, \qquad (6.1)$$

where (in this chapter the long-range exponent in the Hamiltonian is denoted by δ and not by $1+\sigma$):

$$\Phi_{ij} = 2\delta_{ij} - \frac{1}{N_\delta} \frac{1}{(min(|i-j|, N-|i-j|))^\delta} \tag{6.2}$$

and N_δ is the Kac factor (2.21). Note the difference between the $\mathbf{\Phi}$ matrix (6.2) and the one corresponding to the chain with open boundary conditions (5.2). Since (6.2) is circulant it can be diagonalized using Fourier modes (3.56) and the frequencies and velocities of the excitations are given by:

$$\omega_\mu^2 = \frac{1}{N_\delta} \sum_{r=1}^{N/2} \frac{4\sin^2(k_\mu r/2)}{r^\delta}, \quad v_\mu = \frac{1}{N_\delta \omega_\mu} \sum_{r=1}^{N/2} \frac{\sin(k_\mu r)}{r^{\delta-1}}, \tag{6.3}$$

where we remind that the Fourier wave-numbers k_ν assume the values (3.56):

$$k_\nu = \frac{2\pi\nu}{N}, \quad \nu = -\frac{N}{2}+1, ..., \frac{N}{2}. \tag{6.4}$$

At variance with the short-ranged stochastic collisions examined in section 3.4.2, we now consider long-range collisions, i.e., using the notation introduced in section 3.4,the probability of having a collision between the particle on site i and the one on site j is given by:

$$W_{ij} = \frac{1}{N_\alpha |i-j|^\alpha}, \quad N_\alpha^{-1} = \sum_{r=1}^{N/2} r^{-\alpha}. \tag{6.5}$$

Using (6.5) and (3.85) we see that the decay ratio μ_ν of the energy mode E_ν is given by:

$$\mu_\nu = \frac{4\gamma}{N_\alpha} \sum_{l=1}^{N} \frac{\sin^2(k_\nu l/2)}{l^\alpha}. \tag{6.6}$$

We will consider the range of values of α and δ which lead to a well-definite large-N limit, namely $\delta > 2$ and $\alpha > 1$. The second of these conditions is the usual condition for having additive interactions, while the first is required to have a finite current correlation function, as we see below. For these values of δ and α we can express ω_ν, v_ν and μ_ν as functions $\omega(k)$, $v(k)$, $\mu(k)$ of the momentum k in the thermodynamic limit by sending $N \to \infty$ in (6.3) and (6.6). The resulting series can be computed

in terms of polylogarithm functions [1]:

$$\omega^2(k) = \frac{2}{\zeta(\delta)}\left[2\zeta(\delta) - Li_\delta(e^{ik}) - Li_\delta(e^{-ik})\right], \tag{6.8}$$

$$v(k) = \frac{1}{\zeta(\delta)\omega_k}\frac{1}{2i}\left[Li_{\delta-1}(e^{ik}) - Li_{\delta-1}(e^{-ik})\right], \tag{6.9}$$

$$|\mu(k)| = \frac{2\gamma}{\zeta(\alpha)}\left[2\zeta(\alpha) - Li_\alpha(e^{ik}) - Li_\alpha(e^{-ik})\right], \tag{6.10}$$

Since we are considering the large time limit, the integral in (3.100) will be dominated by the low-k region: it is thus useful to extract the low-momentum behaviours of (6.8), (6.9) and (6.10). In order to do that we use the following formula:

$$Li_s(e^z) = \Gamma(1-s)(-z)^{s-1} + \sum_{m=0}^{\infty}\frac{\zeta(s-m)}{m!}z^m, \quad s \notin \mathbb{N} \tag{6.11}$$

$$Li_n(e^z) = \frac{z^{n-1}}{(n-1)!}(H_{n-1} - ln(-z)) + \sum_{k=0,\neq n-1}^{\infty}\frac{\zeta(k-n)}{k!}z^k, \quad n \in \mathbb{N}, \tag{6.12}$$

which are valid for $|z| < 2\pi$.[2] The results for non-integer values of δ, are:

$$\omega^2(k) \approx \begin{cases} a_\delta|k|^{\delta-1}, & 1 < \delta < 3, \\ b_\delta k^2, & \delta > 3, \end{cases} \qquad v(k) \approx \begin{cases} \sqrt{a_\delta}\left(\frac{\delta-1}{2}\right)|k|^{(\delta-3)/2}sign(k), & 1 < \delta < 3, \\ 2\sqrt{b_\delta}sign(k), & \delta > 3. \end{cases} \tag{6.14}$$

and

$$\mu(k) \approx \begin{cases} a_\alpha\gamma|k|^{\alpha-1}, & 1 < \alpha < 3, \\ b_\alpha\gamma k^2, & \alpha > 3. \end{cases} \tag{6.15}$$

[1] The polylogarithm $Li_a(z)$ is defined as:

$$Li_a(z) = \sum_{n=1}^{\infty}\frac{z^n}{n^a}. \tag{6.7}$$

[2] Here H_n is the nth harmonic number, defined as:

$$H_n = \sum_{k=1}^{n}\frac{1}{k}. \tag{6.13}$$

where we defined:

$$a_s = \frac{-2}{\zeta(s)}\Gamma(1-s)\sin\left(\frac{\pi s}{2}\right) \qquad\qquad b_s = \frac{\zeta(s-2)}{\zeta(s)}. \tag{6.16}$$

We also recall that for purely nearest-neighbours collisions the decay rate of the energy modes are given by (3.86), which for low-momentum behaves as:

$$\mu(k) \sim -\gamma k^2 \tag{6.17}$$

6.2 Expression of the heat current

As we did in section 3.4.2 we want to define the energy current, starting from the continuity equation (3.89). The Hamiltonian density h_l related to (6.1) is given by:

$$h_l = \frac{p_l^2}{2} + \frac{1}{2N_\delta}\sum_{r=1}^{N/2}\left[\frac{(x_{l+r}-x_l)^2}{2r^\delta} + \frac{(x_{l-r}-x_l)^2}{2r^\delta}\right]. \tag{6.18}$$

The stochastic infinitesimal evolution of the canonical coordinates is instead given by:

$$dx_l = p_l dt, \tag{6.19}$$

$$dp_l = \frac{1}{N_\delta}\sum_{r=1}^{N/2}\frac{x_{l+r}+x_{l-r}-2x_l}{r^\delta}dt + \sum_{r=1}^{N/2}\Big[dn_{l,l+r}(p_{l+r}-p_l) + dn_{l,l-r}(p_{l-r}-p_l)\Big], \tag{6.20}$$

where $dn_{l,l'}$ are random Poisson variables which can be either 0 or 1 with average:

$$\langle dn_{l,l'}\rangle = \gamma|l-l'|^{-\alpha}dt. \tag{6.21}$$

The limit $\alpha \to \infty$ corresponds to the nearest-neighbours collisions described in section 3.4.2 and indeed in this limit equations (6.18), (6.20) and (6.21) reduce to their counterparts (3.88), (3.91) and (3.92), respectively. The heat current is defined in terms of the continuity equation (3.89), and it can be decomposed in a deterministic and a stochastic term, as in section 3.4.2:

$$dj_l = j_l^{det}dt + dj_l^{sto}, \quad dj_l^{sto} = j_l^S\gamma dt + d\mathfrak{j}_l. \tag{6.22}$$

The deterministic current j_l^{det} is given by:

$$j_l^{(det)} = -\frac{1}{N_\delta} \sum_{m=l+1}^{l+N/2} \sum_{r=l-m}^{N/2} \frac{1}{2r^\delta}(x_m - x_{m-r})(p_m + p_{m-r}), \tag{6.23}$$

while the stochastic terms are given by:

$$j_l^s = -\frac{1}{N_\alpha} \sum_{r=1}^{N/2} \left(\frac{p_{l+r}^2 - p_l^2}{2} \right), d\mathfrak{j}_l = -\frac{1}{N_\alpha} \sum_{r=1}^{N/2} d\mathfrak{m}_{l,l+r} \left(\frac{p_{l+r}^2 - p_l^2}{2} \right), \tag{6.24}$$

where $d\mathfrak{m}$ represent the fluctuation of the process dn around its average:

$$d\mathfrak{m}_{l,l+r} = dn_{l,l+r} - \langle dn_{l,l+r} \rangle . \tag{6.25}$$

The limit $\delta \to \infty$, $\alpha \to \infty$ corresponds to the nearest-neighbours chain with nearest-neighbours collisions studied in section 3.4.2, while the limit $\alpha \to \infty$ corresponds to the long-range chain with nearest-neighbours collisions studied by Saito in [12]. Notice that in the $\alpha \to \infty$ limit, $b_\alpha = 1$. As in the nearest-neighbours collisions case, the sum $\sum_l j_l^s$ is telescopic and sums to zero, therefore the total current is once again given by (3.95) with $j_l^{(det)}$ and $d\mathfrak{j}_l$ given by (6.23) and (6.24) respectively. Furthermore, the argument used in [55] to prove the vanishing of the contribution of the cross correlation $\left\langle J^{(det)} d\mathfrak{J} \right\rangle$ to the thermal conductivity relies only on the oddness of the current under time-reversal, which holds also in our model. In conclusion, the only contributions to the thermal conductivity are given once again only by the auto-correlations of $J^{(det)}$ and $d\mathfrak{J}$: the former will be computed in next section. For what concerns the latter, it is known [55] that in the case of nearest-neighbours momentum exchanges it gives a constant contribution in N to thermal conductivity. In the long-range case one could argue that, since the probability that two particles collide decreases with their distance r as $r^{-\alpha}$ with $\alpha > 1$, the contribution to the total energy current coming from this process should be small. On the other hand, no matter how far the colliding particles, the exchange of their momenta induces a finite energy transfer. The analysis of the autocorrelation of the stochastic current is postponed to a future development of this manuscript.

6.3 Correlation of $J^{(det)}$

In this section we compute the correlation of the deterministic current $J^{(det)}$ using formula (3.100). We remind that the validity of such formula rests on the assumption

of equivalence between microcanonical and canonical ensemble, which holds for the values of δ and α we are considering. Will consider two different cases: long-range dynamics and short-range collisions (which corresponds to $\alpha > 3$) and long-range dynamics and long-range collisions. In the first case we expect to recover the same scalings obtained in [12], while the latter contains new results.

6.3.1 $2 < \delta < 3$, $\alpha = \infty$

This case corresponds to a long-range deterministic dynamics with nearest-neighbours collisions. The auto-correlation of the deterministic current $J^{(det)}$ is obtained by inserting (6.9) and (6.17) into (3.100):

$$C_N(t) \approx \frac{2}{\pi} \int_{2\pi/N}^{\infty} dk a_\delta \left(\frac{\delta-1}{2}\right)^2 k^{\delta-3} e^{-\gamma k^2 t} \tag{6.26}$$

$$= \frac{a_\delta}{4\pi}(\delta-1)^2(\gamma t)^{1-\delta/2}\Gamma\left(\frac{\delta}{2}-1, 4\pi^2\frac{\gamma t}{N^2}\right), \tag{6.27}$$

where we used the expression for the incomplete Gamma function:

$$\Gamma(s,x) = \int_x^{\infty} du u^{s-1} e^{-u}. \tag{6.28}$$

We kept the N dependence in the lower extremum to compute the corrections for large-but finite-N. Expanding (6.26) in the scaling variable t/N^2 we get:

$$C_N(t) \approx \frac{(\delta-1)\Gamma(2-\delta)\sin(\pi\delta/2)\Gamma(\delta/2-1)}{2\pi\zeta(\delta)}(\gamma t)^{1-\delta/2} + S_N(t) \tag{6.29}$$

$$S_N(t) = \frac{2(2\pi)^{\delta-3}(\delta-1)\Gamma(2-\delta)\sin(\pi\delta/2)}{\zeta(\delta)N^{\delta-2}} \sum_{m=0}^{\infty} \frac{(-1)^{m+1}(2\pi)^m}{\delta-2+2m}\left(\frac{\gamma t}{N^2}\right)^m. \tag{6.30}$$

It is important to note that there is time-independent term corresponding to $m = 0$ given by:

$$\Theta(\delta, N) \equiv c_0 = -\frac{2(2\pi)^{\delta-3}(\delta-1)\Gamma(2-\delta)\sin(\pi\delta/2)}{\zeta(\delta)(\delta-2)N^{\delta-2}}. \tag{6.31}$$

If we strictly take $N = \infty$ then this term has no influence on the result and we recover the results of [12]. However in numerical simulations one can never really consider infinite systems and furthermore the decay of c_0 with N is rather slow since $0 < \delta - 2 < 1$. Therefore one has to subtract c_0 from the result of the numerical

simulation in order to see a power law. The, significant, effect of this subtraction is reported in figure 6.1 where we compare the numerical results for the full correlation function $C_N(t)$ (panel a)) and $C_N(t) - \Theta(\delta, N)$ (panel (b)). As it is evident from the figure the result is that, in order to see the expected power-law tail, we need to subtract $\Theta(\delta, N)$ from $C_N(t)$.

6.3.2 $\delta > 3$, $\alpha = \infty$

This case corresponds to an effectively short-range dynamics with nearest-neighbours collisions. The group velocity is constant at low momenta (see (6.9)) and the correlation at large times is given by:

$$C_N(t) \approx \frac{2}{\pi} \int_{2\pi/N}^{\infty} dk b_\delta e^{-\gamma t k^2} = \frac{\mathrm{Erfc}(2\pi\sqrt{\gamma t}/N)}{\sqrt{\pi\gamma t}}, \tag{6.32}$$

where we introduced the complementary error function Erfc:

$$\mathrm{Erfc}(x) = 1 - \frac{2}{\sqrt{\pi}} \int_0^x ds\, e^{-s^2}. \tag{6.33}$$

Noting that once again the scaling variable is $\gamma t/N^2$, expanding in series we find:

$$C_N(t) = \frac{\zeta(\delta-2)}{\sqrt{\pi}\zeta(\delta)} \frac{1}{\sqrt{\gamma t}} + S_N(t) \tag{6.34}$$

$$S_N(t) = \frac{4\zeta(\delta-2)}{\zeta(\delta)N} \sum_{m=0}^{\infty} \frac{(-1)^{m+1}(2\pi)^{2m}}{2m+1} \left(\frac{\gamma t}{N^2}\right)^m. \tag{6.35}$$

Once again we have a constant term given by:

$$c_0 = -\frac{4\zeta(\delta-2)}{\zeta(\delta)N}. \tag{6.36}$$

Notice that the decay with N is much faster than the decay of the constant term with $2 < \delta < 3$, and we do not expect this term to affect the numerical data. In the $N = \infty$ limit we recover the results of [11, 12].

6.3.3 $2 < \delta < 3$, $1 < \alpha < 3$

This case corresponds to a long-range dynamics with long-range collisions. The correlation is given by:

$$C_N(t) \approx \frac{2}{\pi}\int_{2\pi/N}^{\infty} dk a_\delta \left(\frac{\delta-1}{2}\right)^2 k^{\delta-3} e^{-\gamma a_\alpha k^{\alpha-1} t} \tag{6.37}$$

$$= \frac{2a_\delta a_\alpha^{(2-\delta)/(\alpha-1)}}{\alpha-1}(\gamma t)^{(2-\delta)/(\alpha-1)}\Gamma\left(\frac{\delta-2}{\alpha-1}, a_\alpha(2\pi)^{\alpha-1}\frac{\gamma t}{N^{\alpha-1}}\right). \tag{6.38}$$

Now the scaling variable encoding the finite-size corrections is $\gamma t/N^{\alpha-1}$. Expanding in series we get:

$$C_N(t) = \frac{2}{\pi}\frac{a_\delta a_\alpha^{(2-\delta)/(\alpha-1)}}{\alpha-1}(\gamma t)^{(2-\delta)/(\alpha-1))}) + S_N \tag{6.39}$$

$$S_N = \frac{(\delta-1)\Gamma(2-\delta)(2\pi)^{\delta-2}}{\pi\zeta(\delta)}\sin\left(\frac{\pi\delta}{2}\right)N^{2-\delta}\sum_{m=0}^{\infty}\frac{(2\pi)^{m(\alpha-1)}(-1)^{m+1}}{m![\delta-2+m(\alpha-1)]}\left(\frac{\gamma t a_\alpha}{N^{\alpha-1}}\right)^m. \tag{6.40}$$

The constant term is thus given by:

$$c_0 = -\frac{2^{\delta-2}(\delta-1)\Gamma(2-\delta)(2\pi)^{\delta-2}}{\pi\zeta(\delta)(\delta-2)}\sin\left(\frac{\pi\delta}{2}\right)N^{2-\delta}. \tag{6.41}$$

Note that it does not depend on α: we do not yet have a heuristic explanation of this fact.

6.3.4 $\delta > 3$, $1 < \alpha < 3$

This case corresponds to a short-range dynamics with long-range collisions. The correlation is given by:

$$C_N(t) = \frac{2}{\pi}\int_{2\pi/N}^{\infty} dk b_\delta e^{-\gamma t a_\alpha k^{\alpha-1}} \tag{6.42}$$

$$= 4\mathrm{Ei}\left(\frac{\alpha-2}{\alpha-1}, \frac{-(2\pi)^\alpha}{\pi\zeta(\delta)}\Gamma(1-\alpha)\sin\left(\frac{\pi\alpha}{2}\right)\frac{\gamma t}{N^{\alpha-1}}\right)\frac{\zeta(\delta-2)}{(\alpha-1)\zeta(\delta)N}, \tag{6.43}$$

where we introduced the Integral Exponential $\mathrm{Ei}(a,x)$ as:

$$\mathrm{Ei}(a,x) = \int_1^\infty dt\frac{e^{t(-x)}}{t^a}. \tag{6.44}$$

The series expansion now reads as:

$$C_N(t) = 2^{\frac{\alpha-2}{\alpha-1}} \frac{\zeta(\delta-2)\Gamma(\frac{\alpha}{\alpha-1})}{\pi\zeta(\delta)} \left[\Gamma(1-\alpha)\sin\left(\frac{\pi\alpha}{2}\right)\right]^{1/(1-\alpha)} \left(\frac{\gamma t}{\zeta(\alpha)}\right)^{1/1-\alpha} + S_N \quad (6.45)$$

$$S_N = \frac{4\zeta(\delta-2)}{\zeta(\delta)} \sum_{m=0}^{\infty} \left[\frac{(2\pi)^\alpha \Gamma(1-\alpha)\sin(\pi\alpha/2)}{\pi\zeta(\alpha)}\right]^m \frac{(-1)^{m+1}}{m!(m\alpha-m+1)} \left(\frac{\gamma t}{N^{\alpha-1}}\right)^m. \quad (6.46)$$

Notice that the scaling correctly matches with the case $2 < \delta < 3$ putting $\delta = 3$. The constant term is the same as in the case of the short-range dynamics and nearest-neighbours collisions:

$$c_0 = -\frac{4\zeta(\delta-2)}{\zeta(\delta)N}. \quad (6.47)$$

We can obtain the scaling of the thermal conductivity κ with the system size in the thermodynamic limit as explained in section 3.4.2. The results are:

$$\kappa \sim \begin{cases} N^{2-\delta/2}, & 2 < \delta < 3, \quad \alpha = \infty, \\ N^{1/2}, & \delta > 3, \quad \alpha = \infty, \\ N^{(\alpha-\delta+1)/(\alpha-1)}, & 2 < \delta < 3, \ 1 < \alpha < 3, \\ N^{(\alpha-2)/(\alpha-1)}, & \delta > 3, \ 1 < \alpha < 3. \end{cases} \quad (6.48)$$

Note that the scaling exponent is negative in the last case in (6.48) if $1 < \alpha < 2$: this means that the integral over time in the Green-Kubo formula converges even if we send the upper extremum of the time integral to ∞ and thus the thermal conductivity does not scale with N in the thermodynamic limit and transport is qualitatively ballistic. The results for the case $\alpha > 3$ can be obtained from the ones of the case $\alpha = \infty$ by replacing $\gamma \to b_\alpha \gamma$ as can be seen by comparing (6.6) and (6.17):the scaling of the thermal conductivity is thus the same in both cases.
In figure 6.2 we report the comparisons between our analytical predictions and numerical simulations for the scaling exponent of the thermal conductivity β ($\kappa \sim N^\beta$). As we can see, the agreement is rather good, apart from the region near integer values of the exponents (where logarithmic corrections should be taken into account).

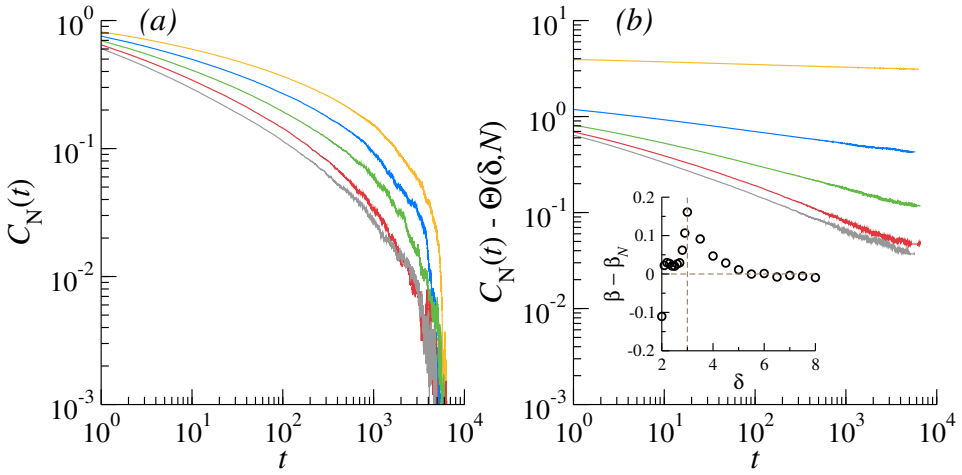

Figure 6.1: We report the results for the current-current correlation function $C_N(t)$ in the case of nearest-neighbours collisions analyzed by Saito to show the effect of the constant term (6.31). In panel a) we report the current-current correlation function $C_N(t)$ for a ring of $N = 512$ oscillators and for $\delta = 2.1$ (yellow), 2.3 (blues), 2.5 (green), 2.7 (red), and 2.9 (grey). On the the right-hand panel we report the same correlation functions as in panel a), shifted by the constant $\Theta(\delta, N)$. The inset shows the deviations of the numerically determined scaling exponent (β_N) of the correlations $C_N(t) \sim t^{-\beta}$, from the analytical solution $\beta = \delta/2 - 1$ first derived by Saito in [12]. Courtesy of Carlos Mejia- Monasterio [15].

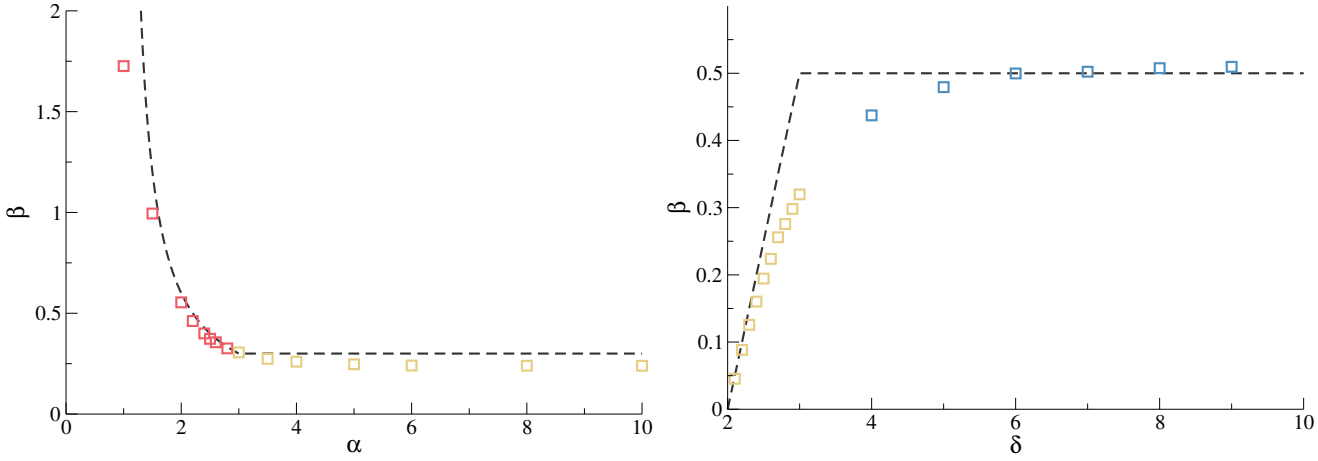

Figure 6.2: We report the values of the scaling exponent β of the current-current correlation function $C(t) \sim t^{-\beta}$. The values are obtained from numerical simulation of the stochastic dynamics (6.20) following the scheme described in section 3.4. Black dashed lines represent the analytical predictions while the points are the results of numerical simulations for a ring of $N = 512$ particles. The right-hand panel corresponds to the case of nearest-neighbours collisions and we report the behaviour of β as a function of δ. As we can see, the agreement is rather good for small and large values of δ. Near the transition point ($\delta = 2$) between the long-range and short-range phases of the Hamiltonian the the data are affected by strong finite-size corrections that cause a disagreement with the $N \to \infty$ analytical result. On the left-hand panel, we consider the case of long-range collisions and report the behaviour of β as a function of α for fixed $\delta = 2.6$. In this case the agreement between the numerical results and the analytical ones is good for all the non-integers values of α with the exception of a little overshoot for large values of α. Courtesy of Carlos Mejia- Monasterio [15].

Chapter 7

Conclusions

In this PhD thesis I have studied heat transport in harmonic long-range chains. As we are going to recap below, despite the linearity of the chains, we still find anomalous transport, a feature absent in short-range quadratic systems. The computation of transport quantities in long-range harmonic chains can be performed using techniques already present in the literature and applied, up to now, to short-range harmonic systems. In some cases, such as the fully connected chain, these techniques can be extended and fully applied to long-range systems. In other cases, such as the power-law harmonic chain, they can be applied but the long-range character of the model does not allow to reach a complete analytical solution. Despite this, we are still able to show that the heat flux in the power-law chain is anomalous, although the exact value of the scaling exponent is still to be determined. Finally, we extended Saito and Tamaki analysis of the power-law chain with stochastic momentum exchanges to the case of long-range exchanges (i.e. two particles at distance r can exchange their momenta at random times with probability $r^{-\alpha}$), finding an interesting interplay between the long-range exponent of the Hamiltonian dynamics of the system and the one of the probability of exchanging the momentum of two particles. We remark that this model allows for a complete analytical computation of the scaling exponent of the thermal conductivity, while not being fully connected, at variance with the power-law chains analyzed before.

In Chapter 4, we started from the apparently simple case of a fully-connected chain: we considered both the case in which only the two boundary sites are coupled to the baths and also the one in which an extensive portion of the system is coupled to the external reservoirs. In both cases we analytically computed the scaling of both the heat flux and the temperature profile with the system size N, in the classical and quantum cases. In the classical regime, the heat flux scales as N^{-1} in the

intensive case. On the other hand in the extensive coupling case the heat flux does not depend on N in the thermodynamic limit. Our physical explanation for this behaviour is that if we couple the baths extensively to the systems, we pump an extensive amount of energy in the latter. Thus the flux in the extensive case gets a factor of N with respect to the flux in the intensive coupling case. One peculiar result of our analysis is that the classical temperature profile in the bulk is flat and vanishes as N^{-1}, both in the intensive and in the extensive case. We find that the reason for this peculiar behaviour lies in the decoupling of the dynamics of the sites not connected to the baths which stems from the degeneracy of the model. Indeed, as we checked numerically, breaking the degeneracy of the model, e.g. by adding a pinning potential, makes the temperature profile flatten to the average temperature of the baths in the thermodynamic limit. For what concerns the quantum regime, in the intensive case we computed exactly the heat flux in the linear response regime. We found that it is given by a nontrivial function of the ratio between the average temperature of the baths and a characteristic temperature of the system T_N. The latter vanishes for large N as N^{-1}. For $T > T_N$ the heat flux scales as N^{-1} and thus the system qualitatively behaves as in the classical case. On the other hand for $T < T_N$ the heat flux does not depend on N and vanishes linearly with T. It should be noted that, since T_N vanishes as N grows, in the thermodynamic limit quantum effects are relevant only in a vanishing region of the temperature. We also computed the temperature profile for low T: the leading order is given by a constant term (which can be interpreted as a zero-point energy contribution to the temperature profile) and a term which vanishes as T^2.
In the extensive coupling case we were unable to analytically compute the heat flux, nonetheless we obtained an integral expression for it. By plotting the latter it is evident that, like in the intensive case, there is a proper temperature scale of the system which discriminates between a quantum and a classical region, although at this stage we are unable to compute it. The only information that we know about this temperature scale is that it does not vanish in the thermodynamic limit: this is an important difference with the intensive coupling case, since it means that quantum effects are important in a finite, non-vanishing, range of temperatures even when N is very large. Chapter 4 is based on the results obtain in the paper [13]. While the latter was in preparation, the manuscript [56] was published: here the authors study heat transport for the classical fully connected chain and their results agree with ours. They also consider the case of disordered and graded masses (which completely break the degeneracy of the model) and, in agreement with our conclusions, in these cases the temperature profile is finite and flattens to the average temperature of the baths.
In Chapter 5 we moved to the more complicated setting of a long-range chain with

power-law decaying coupling to understand whether in long-range systems it would be possible to have anomalous transport also in the case of linear systems (at variance with what happens in short-range chains [11]). We thus focused on the computation of the heat flux to understand it scaling with N. In this case we were not able to get any analytical results, despite the apparent simplicity of the model. The reason for this is that the quadratic form of the potential energy is given by a matrix which is dense and thus we cannot easily solve the Lyapunov equation as it can be done for the short-range chain. Similarly, the Green function associated to the chain cannot be analytically computed as we are unable to perform the required matrix inversion. We thus proceeded numerically: both the Lyapunov equation and the Green function method unequivocally show that the heat flux scales as a power law of the system size. However, both methods are hindered by strong finite-size effects and thus we cannot use them to extract the exact value of the scaling exponent.
We managed to get some insights on the value of the exponent by analyzing the spectral properties of the system via the numerical computation of the poles of the Green function. This computation was performed via the generalized eigenvalue method, which is seldom used in the literature. The main result of this analysis is the presence of a sharp transition in the behaviour of the system at $\sigma = 0$, $1+\sigma$ being the exponent of the power-law interaction. We also provided an estimate of the scaling exponent of the flux. Chapter 5 is based on the results obtained in the publication [14]. A further development of this analysis would be of course a more accurate analysis of the finite-size effects to be able to properly compare our estimate of the scaling exponent of the heat flux with the numerical results. On the analytical side, a computation of the Green function of the chain would be invaluable to compute the heat flux: as we mentioned in chapter 4, this problem could be related with the definition of the discrete fractional Laplacian with open boundary conditions [59].
In chapter 6 we considered a different setup to study heat transport: at variance with the preceding models, in which the chain was coupled to the heat baths, we considered again the power-law chain, but we added a stochastic dynamics via random collisions between the particles. The case of nearest-neighbours collisions was already solved by Saito: we extended the analysis to the case of long-range collisions computing thermal conductivity via the Green-Kubo formula obtaining an analytical prediction for its scaling with system size. In most cases this scaling leads to a divergence of thermal conductivity with N, a trait typical of anomalous transport. It should be noted that our results are obtained by considering only the deterministic part of the current, disregarding the contribution coming from the stochastic exchange of the kinetic energy between particles: the latter assumption could be checked via numerical simulations of the stochastic current which we plan to do in the future.

The results of this chapter will be contained in a future publication [15].

Appendices

Appendix A

Fourier transform of (2.10)

In this appendix we compute the Fourier transform of the Fourier interaction (2.10):

$$\omega(\boldsymbol{q}) = \int_{|\boldsymbol{r}|>a} d^d\boldsymbol{r}|\boldsymbol{r}|^{-\alpha} e^{i\boldsymbol{q}\cdot\boldsymbol{r}}. \tag{A.1}$$

To begin with, we switch to spherical coordinates and we orient the z-axis along the vector $\boldsymbol{q}$, so that the only angular dependence in the integrand is on the polar angle θ:

$$\omega(\boldsymbol{q}) = \Omega_{d-2} \int_{r>a} \int_0^\pi dr\, d\theta \sin\theta r^{d-1-\alpha} e^{iqr\cos\theta} = \frac{2\Omega_{d-2}}{q} \int_a^\infty r^{d-\alpha-2} \sin(qr) dr \tag{A.2}$$

The factor Ω_{d-2} is the volume of a $d-2$-dimensional hypersphere coming from the integration on the other angles. This integral can be computed exactly in terms of an hypergeometric function:

$$\begin{aligned}\omega(\boldsymbol{q}) = 2\Omega_{d-2}\Bigg[&- q^\sigma \cos(\frac{\pi\sigma}{2})\Gamma(-1-\sigma) \\ &+ \frac{a^{-\sigma}}{\sigma}\, {}_1F_2(-\frac{\sigma}{2}; \frac{3}{2}, 1-\frac{\sigma}{2}, -\frac{a^2q^2}{4})\Bigg].\end{aligned} \tag{A.3}$$

Since we are interested in the low-momentum regime, we can expand the hypergeometric function:

$${}_1F_2(-\frac{\sigma}{2}; \frac{3}{2}, 1-\frac{\sigma}{2}, -\frac{a^2q^2}{4}) \approx 1 - \frac{l^2\,(q^2 s)}{6(s-2)}, \tag{A.4}$$

and we get for $\omega(\boldsymbol{q})$:

$$\omega(\boldsymbol{q}) = c_1 q^\sigma + c_2 q^2 + c_3, \tag{A.5}$$

where a, b and c are constants that can be read off (A.3) and (A.4):

$$c_1 = -2\Omega_{d-2}\cos(\frac{\pi\sigma}{2})\Gamma(-1-\sigma),\ c_2 = \frac{a^{2-\sigma}\sigma}{6(\sigma-2)},\ c_3 = -1/\sigma. \tag{A.6}$$

The constant term c_3 can be reabsorbed in the value of the critical temperature. We note also that if $\sigma > 2$ the dominant behaviour is q^σ and the coefficient c_1 is positive, while for $\sigma > 2$ the dominant term is q^2 and $c_2 > 0$.

Appendix B

Solution of the Lyapunov equation (3.10)

In this appendix we outline the procedure used by Rieder, Lebowitz and Lieb [9] to obtain the solution to the Lyapunov equation (3.10) for the nearest-neighbours chain (3.16).
To begin with we express the matrices U, V, Z in terms of their deviations from the equilibrium solution (3.12), X, Y, W :

$$U = \frac{k_B T}{\omega^2}\left(G^{-1} + \frac{\Delta T}{T} X\right), \tag{B.1}$$

$$V = k_B T\left(\mathbb{I} + \frac{\Delta T}{T} Y\right), \tag{B.2}$$

$$Z = \frac{k_B \Delta T}{\lambda} W. \tag{B.3}$$

Inserting this ansatz into the Lyapunov equation (3.10) we get three equations for X, Y and W:

$$X^T = X, \quad Y^T = Y, \quad W^T = -W, \tag{B.4}$$

$$Y = XG + WR, \tag{B.5}$$

$$2S - YR - RY = (\omega/\lambda)^2 [G, W]. \tag{B.6}$$

We now consider equation (B.6). By inserting the explicit expressions for the matrices R and S(3.6) we notice that the left-hand side of equation (B.6) has non-zero entries only on the "border"[1], i.e. $2S_{ij} - (YR + RY)_{ij} \neq 0$ only if either $i, j = 1, N$. It

[1]Matrices with this property are called bordered matrices

follows that $[G, W]$ has the same property. In particular, writing the left-hand side of equation (3.10) we get (recall the definition of G (3.16)) :

$$W_{i,j+1} + W_{i,j-1} - W_{i+1,j} - W_{i-1,j} = 0, \quad \forall i, j \neq 1, N. \tag{B.7}$$

Taking into account also the anti-symmetry of W expressed by (B.4), the solution to (B.7) is given by:

$$W_{ij} = \varphi_{|i-j|} sign(j-i), \quad W_{ii} = 0, \tag{B.8}$$

where the function φ_k must be determined by the border components of (B.6):

$$(\omega^2/\lambda^2)\varphi_j = \delta_{j1} - Y_{1,j} = \delta_{j,1} + Y_{N,N-j+1}, \tag{B.9}$$

with the convention $\varphi_N = 0$. The other matrices $\boldsymbol{X}$ and $\boldsymbol{Y}$ can be expressed in terms of the function φ as well. In order to determine matrix $\boldsymbol{X}$ we anti-symmetrize equation (B.5):

$$[G, X] = WR + RW. \tag{B.10}$$

The right-hand side of (B.10) is non-zero only at the border, so the components of X satisfy the same equation as the components of W (B.7), with the difference that now the matrix X is symmetric. One possibility is to take $X_{ab} = f_{a+b}$, where f is an unknown function that must be determined by considering the border components of (B.10), which yield:

$$f_k = \varphi_{k-1}, \quad f_{N+k+1 = -\varphi_{N-k} = f_{N+1-k}}, \quad 1 < ks < N. \tag{B.11}$$

In particular, from equations (B.11) it follows that the matrix X is anti-symmetric with respect to the anti-diagonal:

$$X_{ij} = \begin{cases} \varphi_{i+j-1}, & i+j < N+1, \\ -\varphi_{2N+1-i-j}, & i+j > N+1. \end{cases} \tag{B.12}$$

We now turn to the matrix Y. If we plug the expressions for the components of Z (B.8) and X (B.12) into equation (B.5) we can express Y_{ij} in terms of the φ_j. This expression is not very illuminating, but if we insert it in equation (B.9) we get a recursive equation for φ_j:

$$(\omega/\lambda)^2 \varphi_j = -2\varphi_j - \varphi_{j-1} - \varphi_{j+1} + \delta_{1,j}, \tag{B.13}$$

with the boundary conditions $\varphi_0 = \varphi_N = 0$. If we now plug back this condition into the expression of Y_{ij} we mentioned above we can show that:

$$Y = S - (\omega/\lambda)^2 X. \tag{B.14}$$

The final step is to compute the solution of (B). The form of suggests a power-law ansatz $\varphi_j = a^j$, substituting in equation (B) we find two solutions $a_\pm$:

$$a_\pm = 1 + \frac{\omega^2}{2\lambda^2} \pm \frac{\omega^2}{2\lambda^2}\sqrt{1 + \frac{4\lambda^2}{\omega^2}}. \tag{B.15}$$

The solution to (B) is thus of the form $\varphi_j = c_1 a_+^j + c_2 a_-^j$, where c_1 and c_2 are constants constrained by the boundary conditions. The final result is:

$$\varphi_j = \frac{\sinh[(N-j)\alpha]}{\sinh(N\alpha)}, \quad e^\alpha = a_-, \tag{B.16}$$

eventually we will take the thermodynamic limit and (B.16) reduces to:

$$\varphi_j = e^{\alpha j}. \tag{B.17}$$

If we now plug (B.16) into the expression for $\boldsymbol{Y}$ (B.14) we can compute the heat flux and temperature profile using (3.14) and (3.13) obtaining the results (3.19) and (3.21) quoted in the main text.

Appendix C

Derivation of the results used in section 3.2

In this appendix we discuss several calculations related to the derivation of the formulas for the heat flux and temperature profile in the LEGF method described in section 3.2.

C.1 Derivation of equation (3.27)

In this section we provide the solution for the equation of motion for the baths (3.26): since both equations have the same form we will consider only the equation for the left-hand bath:

$$\ddot{x}_{L,i} = -\omega_{L,i}^2 x_{L,i} - m_{L,i}^{-1} \sum_j V_{L,ji} x_j, \tag{C.1}$$

which is a linear in-homogeneous equation. As is well known its solution is given by:

$$x_{L,i} = x_{L,i}^{(0)} + \bar{x}_{L,i}, \tag{C.2}$$

where $x_{L,i}^{(0)}$ is the general solution to the homogeneous equation (obtained from (C.1) by setting $V_L = 0$) and $\bar{x}_{L,i}$ is a solution of the full in-homogeneous equation. Since the homogeneous equation is just the standard harmonic oscillator equation, we have:

$$x_{L,i}^{(0)} = \cos(\omega_{L,i}(t - t_0)) x_{L,i}(t_0) + \frac{\sin(\omega_{L,i}(t - t_0))}{\omega_{L,i}} \dot{x}_{L,i}(t_0), \tag{C.3}$$

where we also imposed the initial conditions at time t_0. The particular solution of the in-homogeneous equation can be found with the method of variation of parameters

and the final result is:

$$\bar{x}_{L,i} = \int_{t_0}^{t} d\tau \frac{\sin(\omega_{L,i}(t-\tau)}{\omega_{L,i}} m_{L,i}^{-1} \sum_j V_{L,ji} x_j(\tau). \tag{C.4}$$

Summing (C.3) and (C.4) we get the full solution to (C.1):

$$x_{L,i} = f_{L,i}(t-t_0)x_{L,i}(t_0) + g_{L,i}(t-t_0)\dot{x}_{L,i}(t_0) + \int_{t_0}^{t} d\tau g_{L,i}(t-\tau) \sum_j m_{L,i} V_{L,ji} x_j(\tau), \tag{C.5}$$

where we defined the quantities:

$$f_{a,i}(s) = \cos(\omega_{a,i}s)\theta(s), \quad g_{a,i}(s) = \frac{\sin(\omega_{a,i}s)}{\omega_{a,i}}\theta(s), \quad a = L, R, \tag{C.6}$$

and $\theta(s)$ is the Heaviside theta function. The solution for the equation of motion for the right-hand bath has the same form as (C.5) with $L \to R$. Inserting the solutions $x_{L,i}(t)$ and $x_{R,i}(t)$ in the equation of motion for the system (3.25) we finally get equation (3.27).

C.2 Derivation of the noise correlators

We will derive the noise correlation for the left-hand bath: as usual, to get the corresponding expression for the right-hand bath we just need to replace L with R. The Hamiltonian of the baths (3.23) is given by:

$$H = \frac{1}{2} \sum_i p_i^2 + \omega_{x,i}^2 x_{a,i}^2, \quad a = L, R. \tag{C.7}$$

which can be expressed in terms of the usual creation/annihilation operators:

$$H = \sum_i \hbar\omega_{a,i}(b_{a,i}^\dagger b_{a,i} + 1/2), \quad b_{a,i} = \sqrt{\frac{m_{a,i}\omega_{a,i}}{\hbar}} x_{a,i} + \frac{i}{\sqrt{2\omega_{a,i}\hbar}}, \quad a = L, R. \tag{C.8}$$

Assuming the left-hand and right-hand bath are respectively described by a Bose-Einstein distribution at temperature T_L T_R we have the following thermal averages:

$$\langle b_{a,i}^\dagger b_{a,j} \rangle = f(\omega_{a,i}, T_a)\delta_{ij}, \quad f(\omega, T) = \frac{1}{e^{\beta\hbar\omega} - 1}, \quad \beta = 1/(k_B T), \tag{C.9}$$

from which, using definition given in (C.8) we get the correlators of the canonical coordinates (with $\dot{x} = p/m$):

$$\langle x_{a,i} x_{a,j} \rangle = \frac{\hbar}{2m_{a,i}\omega_{a,i}} \coth\left(\frac{\hbar\omega_{a,i}}{k_B T_a}\right), \tag{C.10}$$

$$\langle \dot{x}_{a,i} x_{a,j} \rangle = -i\frac{\hbar}{m_{a,i}}\delta_{ij}, \tag{C.11}$$

$$\langle \dot{x}_{a,i} \dot{x}_{a,j} \rangle = \frac{\hbar\omega_{a,i}}{2m_{a,i}} \coth\left(\frac{\hbar\omega_{a,i}}{k_B T_a}\right). \tag{C.12}$$

Since at time t_0 the baths are assumed to be a thermal equilibrium we can compute the correlators between the ξ functions defined in (3.28) and we get equation (3.31)

C.3 Fourier transform of the noise correlator (3.31)

The Fourier transform of the noise correlator

$$\langle \xi_{a,i}(t)\xi_{a,j}(\tau)\rangle$$

(3.31) is given by:

$$\langle \tilde{\xi}_{a,i}(\omega)\tilde{\xi}_{a,j}(\omega')\rangle = \int_{-\infty}^{\infty}\frac{dt}{2\pi}\int_{-\infty}^{\infty}\frac{d\tau}{2\pi}\langle \xi_{a,i}(t)\xi_{a,j}(\tau)\rangle \tag{C.13}$$

$$= \int_{-\infty}^{\infty}\frac{dt}{2\pi}\int_{-\infty}^{\infty}\frac{d\tau}{2\pi}\sum_l V_{a,il}V_{a,lj}\left[\frac{-\hbar}{2m_{a,l}\omega_{a,l}}\cos(\omega_{a,l}(t-\tau)) + i\frac{i\hbar}{m_{a,i}}\sin(\omega_{a,i}(t-\tau))\right]. \tag{C.14}$$

Using the following elementary integrals:

$$\int_{-\infty}^{\infty}\frac{dt}{2\pi}\int_{-\infty}^{\infty}\frac{d\tau}{2\pi}\cos(\omega_0(t-\tau))e^{i\omega t + i\omega'\tau} = \delta(\omega+\omega')\left[\delta(\omega+\omega_0)+\delta(\omega-\omega_0)\right], \tag{C.15}$$

$$\int_{-\infty}^{\infty}\frac{dt}{2\pi}\int_{-\infty}^{\infty}\frac{d\tau}{2\pi}\cos(\omega_0(t-\tau))e^{i\omega t + i\omega'\tau} = -i\delta(\omega+\omega')\left[\delta(\omega+\omega_0)-\delta(\omega-\omega_0)\right], \tag{C.16}$$

we get:

$$\langle \tilde{\xi}_{a,i}(\omega)\tilde{\xi}_{a,j}(\omega')\rangle = -\hbar\delta(\omega+\omega')(1+f(\omega,T_a)) \sum_l \left[V_{a,il}V_{a,lj}[\delta(\omega+\omega_{a,l})-\delta(\omega-\omega_{a,l})]\right]. \tag{C.17}$$

The factor $(1 + f(\omega, T_a))$ encodes thermal fluctuation: we thus expect the other factor in (C.17) to encode dissipative effects. Dissipation is typically expressed by the imaginary part of the Fourier transform of the memory kernel (3.30):

$$\Sigma_{a,ij(\omega)} = \int_{-\infty}^{\infty} dt \Sigma_{a,ij}(t) e^{i\omega t} = \sum_l \frac{V_{a,il} V_{a,lj}}{m_{a,l}} \int_{-\infty}^{\infty} dt g_{a,l}(t) e^{i\omega t}, \tag{C.18}$$

$$\tag{C.19}$$

where the $g_{a,l}$ function is defined in (C.6). Using the following integral[1] :

$$\int_{-\infty}^{\infty} dt \sin(\omega_0 t)\theta(t) e^{i\omega t} = \frac{\omega}{\omega^2 - \omega_0^2} - \frac{i\pi}{2}(\delta(\omega + \omega_0) - \delta(\omega - \omega_0), \tag{C.21}$$

we thus get:

$$\tilde{\Sigma}_{a,ij}(\omega) = \sum_l \frac{V_{a,il} V_{a,lj}}{m_{a,l}} \frac{1}{\omega^2 - \omega_{a,l}^2} - i\pi \sum_l \frac{V_{a,il} V_{a,lj}}{m_{a,l}\omega_{a,l}} (\delta(\omega + \omega_{a,l}) - \delta(\omega - \omega_{a,l}). \tag{C.22}$$

It is convenient to define the matrix $\Gamma_{a,ij}$ given by the imaginary part of $\tilde{\Sigma}_{a,ij}(\omega)$:

$$\Gamma_{a,ij}(\omega) = Im[\tilde{\Sigma}_{a,ij}(\omega)] = -\pi \sum_l \frac{V_{a,il} V_{a,lj}}{m_{a,l}\omega_{a,l}} (\delta(\omega + \omega_{a,l}) - \delta(\omega - \omega_{a,l})), \tag{C.23}$$

so that the noise-noise correlator (C.17) can be written as in equation (3.33).

C.4 Derivation of heat flux and temperature profile

In this appendix we report the steps to compute the heat flux (3.44) and the temperature profile (3.45). The first thing to do is to compute the correlator (3.43). We begin by taking the Fourier transform of the solution of the equation of motion of the baths (C.5) and multiplying it on the right by V_a:

$$V_a \tilde{\boldsymbol{x}}_a(\omega) = \boldsymbol{\xi}_a(\omega) + \Sigma_a(\omega)\tilde{\boldsymbol{x}}(\omega), \quad a = L, R, \tag{C.24}$$

[1]The integral can be computed by inserting a regulator $e^{-\epsilon t}$ in the integrand and the taking the $\epsilon \to 0$ limit using the Shotoski formulas:

$$\frac{1}{x + i\epsilon} = P.V.\frac{1}{x} - i\pi\delta(x), \tag{C.20}$$

where *P.V.* stands for "principal value" and is omitted in the main text.

where we used the definitions of $\boldsymbol{\xi}_{L,R}$ (3.28) and $\Sigma_{L,R}$ (3.30). Inserting this result into (3.43) we obtain, after some algebra and using the correlators (3.42), formula (3.44).
In order to obtain the temperature profile (3.45) we start from the velocity-velocity correlator:

$$\langle \dot{\boldsymbol{x}}(t)\dot{\boldsymbol{x}^T}(t)\rangle = -\int_{-\infty}^{\infty} d\omega \int_{-\infty}^{\infty} d\omega'\, \omega\omega' e^{-i(\omega+\omega')t} \langle \tilde{\boldsymbol{x}}(\omega)\tilde{\boldsymbol{x}}^T(\omega')\rangle \,. \tag{C.25}$$

Now insert the solution of the Langevin equation of motion for the system (3.41) and using the noise-noise correlator (3.31) we obtain (3.45).

Appendix D

Generalized eigenvalue method

D.1 Derivation of equation (3.52)

In this appendix we analyze the generalized eigenvalue problem following the review [51]. The generalized quadratic eigenvalue problem consists in finding the set of the complex number s_i such that:

$$\det(P(s_i)) = 0, \quad P(s) = As^2 + Bs + C = 0, \tag{D.1}$$

where A, B and C are $N \times N$ complex matrices and we will assume that the matrix P is non-singular, i.e. its determinant is not identically vanishing. Furthermore we assume that $\det A \neq 0$: in this case the determinant of P is a polynomial of degree $2N$, as can be seen by considering the limit of large s. The set of the s_i is called the spectrum of $P(s)$ and they are related to the eigenvectors of $P(s)$ $\boldsymbol{y}^{(i)}$[1] :

$$P(s_i)\boldsymbol{y}^{(i)} = 0. \tag{D.2}$$

Now the main idea is to linearize (D.1), that is, to reduce the quadratic problem to a linear one. The problem is similar to the reduction of a second-order differential equation to two first-order ones:

$$ay'' + by' + c = 0 \rightarrow \begin{cases} az' + bz + c = 0 \\ z = y'. \end{cases} \tag{D.3}$$

In our case, we want to find a $2N \times 2N$ matrix linear in s, $D + sE$, such that:

$$\begin{pmatrix} P(s) & \mathbb{O} \\ \mathbb{O} & \mathbb{I} \end{pmatrix} = F(s)(D - Es)G(s), \tag{D.4}$$

[1] we will assume that the right and left eigenvectors are equal: this hypothesis can be easily relaxed.

where $\det(F(S))$ and $\det(G(s))$ are non-zero constants. Taking the determinant of equation (D.4) it is easy to see the values s_i that satisfy (D.1) are those and only those that satisfy the condition $\det(D + Es_i) = 0$. This linearization is not unique, we are going to use the following one [51]:

$$\begin{cases} D = \begin{pmatrix} \mathbb{O} & N \\ -K & -C \end{pmatrix}, \\ E = \begin{pmatrix} N & \mathbb{O} \\ \mathbb{O} & M \end{pmatrix}, \end{cases} \quad \begin{cases} F(s) = \begin{pmatrix} -(C+sA)N^{-1} & -\mathbb{I} \\ N^{-1} & \mathbb{O} \end{pmatrix}, \\ G(s) = \begin{pmatrix} \mathbb{I} & \mathbb{O} \\ s\mathbb{I} & \mathbb{I} \end{pmatrix}. \end{cases} \tag{D.5}$$

Using this linearization $D - Es$ with some algebra one can prove that:

$$P(s)^{-1} = -(\mathbb{I}, \mathbb{O})(D - sE)(\mathbb{I}, \mathbb{O})^T. \tag{D.6}$$

Furthermore the eigenvectors of $D - s_i E$ are closely related to the ones of $P(s)$:

$$(D - s_i E)\boldsymbol{z}^{(i)} = 0, \boldsymbol{z}^{(i)} = \begin{pmatrix} \boldsymbol{y}^{(i)} \\ s_i \boldsymbol{y}^{(i)} \end{pmatrix}, \tag{D.7}$$

and is convenient to organize the eigenvectors in a matrix:

$$Z = \begin{pmatrix} X \\ SX \end{pmatrix}, \quad Y = [\boldsymbol{y}^{(1)}, ...\boldsymbol{y}^{(N)}], \quad S = diag(s_1, ..., s_N). \tag{D.8}$$

If $s \neq s_i \ \forall i = 1...N$ we have $(D - sE)^{-1} = Z(S - s\mathbb{I})Z^\dagger$ and finally we obtain a formula for $P(s)^{-1}$ in terms of the eigenvectors s_i and the eigenvectors $\boldsymbol{y}^{(i)}$:

$$\begin{aligned} P(s)^{-1} &= -(\mathbb{I}, \mathbb{O})(D - sE)(\mathbb{I}, \mathbb{O})^T \\ &= -(\mathbb{I}, \mathbb{O})Z(S - s\mathbb{I})Z^\dagger(\mathbb{I}, \mathbb{O})^T \\ &= -Y(S - s\mathbb{I})SY^\dagger = \sum_i \frac{s_i \boldsymbol{y}^{(i)} \boldsymbol{y}^{(i)T}}{s - s_i}. \end{aligned} \tag{D.9}$$

Taking $A = \mathbb{I}$, $B = R$ and $C = \Phi$ we can apply this obtain equation (3.52). Note that equation (D.7) becomes:

$$\left[\begin{pmatrix} \mathbb{O} & \mathbb{I} \\ -R & -\Phi \end{pmatrix} - s \begin{pmatrix} \mathbb{I} & \mathbb{O} \\ \mathbb{O} & \mathbb{I} \end{pmatrix} \right] \begin{pmatrix} \boldsymbol{y}^{(i)} \\ s_i \boldsymbol{y}^{(i)} \end{pmatrix} = 0, \tag{D.10}$$

so that the set of s_i and $\boldsymbol{y}^{(i)}$ can be obtained by solving a standard eigenvalue problem.

Appendix E

Green function for the fully-connected chain

E.1 Computation of the Green function for the fully-connected network: intensive coupling

In this section we compute the Green function (3.41) for the fully-connected harmonic network analyzed in Chapter 3 in the intensive coupling case. Inserting (4.2) and (4.3) into (3.41) we can write the Green function as $G = Z^{int\,-1}$ where:

$$Z_{ij}^{int} = \begin{cases} -m\omega^2 - i\lambda\omega + 2k(1-1/N), & i = j = 1, N \\ -m\omega^2 + 2k(1-1/N), & i = j \neq 1, N \\ -2k/N, & i \neq j \end{cases}, \tag{E.1}$$

which can be written as $-Z^{int} = D^{int} + \boldsymbol{u}\boldsymbol{u}^T$, with:

$$D_{ij}^{int} = \begin{cases} m\omega^2 + i\lambda\omega - 2k, & i = j = 1, N, \\ m\omega^2 - 2k, & i = j \neq 1, N, , \\ 0, & i \neq j, \end{cases} \quad u_i = \sqrt{2k/N}\ \forall i \tag{E.2}$$

(E.3)

We can now invert the matrix $-Z^{int}$ using the Sherman-Morrison formula [62]: given a matrix $A = M + \boldsymbol{u}\boldsymbol{v}^T$, the inverse A^{-1} is given by:

$$A^{-1} = M^{-1} + \frac{A^{-1}\boldsymbol{u}\boldsymbol{v}^{\,T}A^{-1}}{1 + \boldsymbol{v}^T A^{-1}\boldsymbol{u}}. \tag{E.4}$$

Using (E.4) we can write the Green function as:

$$G(\omega) = Z^{-1} = -\left(D^{-1} + \frac{D^{-1}uu^TD^{-1}}{1+u^TD^{-1}u}\right), \tag{E.5}$$

and using (E.2) we can compute:

$$1 + u^TD^{-1}u = 1 + (2k/N)\sum_i D_{ii}^{-1} \tag{E.6}$$

$$= \frac{N(m\omega^2 + i\lambda\omega - 2k)(m\omega^2 - 2k)}{N(m\omega^2 + i\lambda\omega - 2k)(m\omega^2 - 2k) - 4i\lambda k\omega}, \tag{E.7}$$

and

$$\left(D^{-1}uu^TD^{-1}\right) = \frac{2k}{N}\begin{pmatrix} d_1^2 & d_1d_2 & \cdots & d_1d_2 \\ d_1d_2 & d_2^2 & \cdots & d_1d_2 \\ \vdots & \vdots & \ddots & \vdots \\ d_1d_2 & d_1d_2 & \cdots & d_1^2 \end{pmatrix}, \tag{E.8}$$

$$d_1 = (m\omega^2 + i\lambda\omega - 2k)^{-1}, \quad d_2 = (m\omega^2 - 2k)^{-1}. \tag{E.9}$$

Finally we can write the various elements of the Green function:

$$G_{1N} = G_{11} = G_{NN} = \frac{m\omega^2 - 2k}{m\omega^2 - i\lambda\omega - 2k}\frac{-2k/\omega}{mN\omega\left(m\omega^2 + i\lambda\omega - 2k\right) - 4i\lambda k}, \tag{E.10}$$

$$G_{1j} = G_{Nj} = G_{i1} = G_{iN} = \frac{2k/\omega}{N(m\omega^2 + i\lambda\omega - 2k)m\omega - 4i\lambda k}, \quad i,j \neq 1,N, \tag{E.11}$$

$$G_{ij} = \frac{m\omega^2 + i\lambda\omega - 2k}{m\omega^2 - 2k}\frac{2k/\omega}{mN\omega\left(m\omega^2 + i\lambda\omega - 2k\right) - 4i\lambda k}, \quad i,j \neq 1,N. \tag{E.12}$$

E.2 Computation of the Green function for the fully-connected network: intensive coupling

To compute the Green function in the extensive coupling case we insert (4.2) and (4.4) into (3.41). We can then write the Green function as $G = Z^{ext-1}$ where:

$$Z_{ij}^{ext} = (-m\omega^2\mathbb{I} + \Phi - \Sigma_L - \Sigma_R)_{ij} \tag{E.13}$$

$$= \begin{cases} -m\omega^2 - i\lambda\omega + 2k(1-1/N), & i = j = 1...n_L, N - n_R + 1...N, \\ -m\omega^2 + 2k(1-1/N), & i = j, \text{ otherwise}, \\ -2k/N, & i \neq j. \end{cases} \tag{E.14}$$

Once again this matrix can be decomposed, in order to apply the Sherman-Morrison formula, as $-Z^{ext} = D^{ext} + \boldsymbol{u}\boldsymbol{u}^T$, where $\boldsymbol{u}$ is the same vector of (E.2) and:

$$D_{ij}^{ext} = \begin{cases} m\omega^2 + i\lambda\omega - 2k, \quad i = j = 1...n_L, N - n_R + 1...N, \\ m\omega^2 - 2k, \quad i = j, \text{otherwise}, \\ 0, \quad i \neq j. \end{cases} \tag{E.15}$$

The denominator of the fraction in Sherman Morrison formula is given by:

$$1 + \boldsymbol{u}^T D^{ext-1} \boldsymbol{u} = \frac{N(m\omega^2 + i\lambda\omega - 2k)(m\omega^2 - 2k)}{Nm\omega^2(m\omega^2 + i\lambda\omega - 2k) - 2k(N_L + N_R)i\lambda\omega}. \tag{E.16}$$

Notice that if $N_L = N_R = 1$ we recover the result of the intensive case (E.6). We now define the set of the sites coupled to the baths $\mathcal{I}_L$ and $\mathcal{I}_R$:

$$\mathcal{I}_L = (1, ..., N_L), \quad \mathcal{I}_R = (N - N_R + 1, ..., N_R), \quad \mathcal{I} = \mathcal{I}_L + \mathcal{I}_R. \tag{E.17}$$

With this notation, the numerator in the Sherman-Morrison formula is given by:

$$\left(D^{ext-1} u u^T D^{ext-1}\right)_{ij} = \frac{2k}{N} \begin{cases} d_1^2, \quad (i,j) \in (\mathcal{I}_a, \mathcal{I}_b), \quad a, b = L, R, \\ d_1 d_2, \quad i \neq \mathcal{I}_L, \mathcal{I}_R, j \in \mathcal{I}_a, \quad a = L, R, \\ d_1 d_2, \quad j \neq \mathcal{I}_L, \mathcal{I}_R, i \in \mathcal{I}_a, \quad a = L, R, \\ d_2^2, \quad (i,j) \neq (\mathcal{I}_a, \mathcal{I}_b), \end{cases} \tag{E.18}$$

where d_1 and d_2 are defined in (E.8). Note that the values of $\left(D^{ext-1} u u^T D^{ext-1}\right)_{ij}$ are the same of the intensive case (E.8), so the values of the entries of the Green function can be obtained simply by replacing

$$4i\lambda k\omega \to 2i(N_L + N_R)\lambda k\omega, \tag{E.19}$$

into (E.10), (E.11) and (E.12). We finally get:

$$\begin{cases} G_{ij} = \dfrac{m\omega^2 - 2k}{m\omega^2 - i\lambda\omega - 2k} \dfrac{-2k/\omega}{mN\omega\left(m\omega^2 + i\lambda\omega - 2k\right) - 2i(N_L + N_R)\lambda k}, \\ \\ (i,j) \in (\mathcal{I}_a, \mathcal{I}_b), \quad a, b = L, R, \end{cases} \tag{E.20}$$

$$\begin{cases} G_{ij} = \dfrac{2k/\omega}{N(m\omega^2 + i\lambda\omega - 2k)m\omega - 2i(N_L + N_R)\lambda k}, \\ \\ i \neq \mathcal{I}_L, \mathcal{I}_R, j \in \mathcal{I}_a, \quad a = L, R, \end{cases} \tag{E.21}$$

$$\begin{cases} G_{ij} = \dfrac{m\omega^2 + i\lambda\omega - 2k}{m\omega^2 - 2k} \dfrac{2k/\omega}{mN\omega(m\omega^2 + i\lambda\omega - 2k) - 2i(N_L + N_R)\lambda k}, \\ \\ (i,j) \neq (\mathcal{I}_a, \mathcal{I}_b), \quad a, b = L, R. \end{cases} \tag{E.22}$$

The Green function entries (E.20) connect two sites coupled with the baths, entries (E.21) connect one site coupled to the baths to an uncoupled one and finally entries (E.22) connect two sites which are not coupled to the baths.

Appendix F

Calculation of I_3 and I_4

F.1 Calculation of I_3

In this appendix we will compute the integral (4.34) in the large N limit. Since the denominator of the integrand in (4.34) is the same as the one in (4.9) we can once again exploit the presence of the vanishing root (4.12). In the large N limit, the dominant contribution to I_3 is:

$$I_3 = \frac{2}{\pi}\frac{k_1 a}{N}\int_{-\infty}^{\infty}\frac{dx}{x^2+a^2}\frac{x^2}{\sinh^2(x)}, \tag{F.1}$$

where we conveniently made the change of variable $x = y/k_2$ and a is given by:

$$a = \frac{2k_1}{k_2 N} = T_N/T, \quad T_N = \frac{\hbar k_1\sqrt{2k/m}}{k_B N}. \tag{F.2}$$

As in the classical case (4.9), we cannot directly take the limit $N \to \infty$, because in this limit $a = 0$ and (F.1) diverges. To compute (F.1) we employ contour integration and Cauchy's theorem. Let us introduce the following function of complex variable z:

$$f(z) = \frac{z^2}{z^2+a^2}\frac{1}{\sinh^2(z)}, \tag{F.3}$$

The poles of f are all located on the imaginary axis, at the following positions (with the corresponding residue):

$$z_n = in\pi, \quad n \in \mathbb{Z}\{0\}, \quad \text{Res}_n = \tfrac{2i\pi a^2 n}{(a^2-\pi^2 n^2)^2}, \tag{F.4}$$

$$z_{\pm a} = \pm ia, \qquad \text{Res}_{\pm a} = \mp\tfrac{ia}{2\sin^2(a)}. \tag{F.5}$$

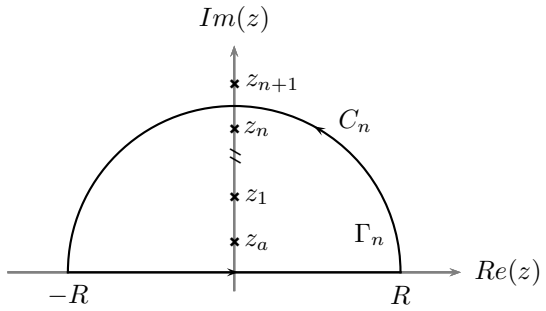

Figure F.1: The contour Γ_n used to compute the integral I_3

Consider now the contour Γ_n plotted in figure F.1: it is composed by a segment $[-R, R]$ and a semicircle $\mathcal{C}_n$ of radius R, which is such that Γ_n contains the first n z_k poles and the one in z_a. Let now be I_R the integral of $f(z)$ over the aforementioned segment. Then, by the residue theorem, we have:

$$I_R = \int_{-R}^{R} dx f(x) = -\int_{\mathcal{C}_n} dz f(z) + 2\pi i \left[\sum_{k}^{n} \mathrm{Res}_k + \mathrm{Res}_{+a} \right]. \tag{F.6}$$

I_3 can then be obtained by taking the limit $R \to \infty$ of I_R as follows:

$$I_3 = \frac{2}{\pi} \frac{k_1 a}{N} \lim_{R\to\infty} I_R. \tag{F.7}$$

We now have to compute the limit $R \to \infty$, which also entails the limit $n \to \infty$ of the right-hand side of (F.6). For large R the integral of f over $\mathcal{C}_n$ is:

$$\int_{\mathcal{C}_n} dz f(z) \approx iR \int_0^{\pi} \frac{e^{i\theta} d\theta}{\sinh^2(Re^{i\theta})} = iR(-2i \coth(R)/R) \to 2. \tag{F.8}$$

The sum over the residues becomes a series that can be resummed. We can thus finally express I_3 as:

$$I_3 = \frac{2k_1}{N} g(a), \tag{F.9}$$

where the function $g(x)$ is given by:

$$g(x) = \frac{x^2}{\pi^2}\left[\psi^{(1)}\left(1+\frac{x}{\pi}\right) - \psi^{(1)}\left(1-\frac{x}{\pi}\right)\right] + \frac{x^2}{\sin^2(x)} - 2x, \tag{F.10}$$

$$\psi^{(1)}(z) = \frac{d^2}{dz^2}\Gamma(z), \tag{F.11}$$

where $\Gamma(z)$ is the Euler Gamma function.

F.2 Low-temperature behaviour of I_4

In this section we compute the low-temperature of integral I_4 (4.41). We start by expanding the hyperbolic cotangent in (4.41) using the following series, valid for large x:

$$\coth(x) = 1 + 2\sum_{n=0}^{\infty} e^{-2(n+1)x}. \tag{F.12}$$

The integral of the first term is:

$$I_4(\theta=0) = \frac{1}{N^2}\int_0^\infty dy \frac{y}{y^2(y^2-1)^2 + k_1^2(y^2-2/N)^2}$$

$$= \frac{1}{2N^2}\int_0^\infty ds \frac{1}{s(s-1)^2 + k_1^2(s-2/N)^2}. \tag{F.13}$$

Note that the denominator in (F.13) is the polynomial (4.11). Let R be the real part of the non-vanishing roots which is the same for both of them since they are complex conjugate. Then, using standard partial fraction decomposition we get:

$$I_4(\theta=0) = \frac{1}{2N^2}\left[2\ln\left(\frac{N}{2k_1}\right) + \frac{R}{\sqrt{1-R^2}}\left(\frac{\pi}{2} + \arctan\left(\frac{R}{\sqrt{1-R^2}}\right)\right)\right]. \tag{F.14}$$

We now turn to the integral of the second term in (F.12):

$$\frac{2}{N^2}\int_0^\infty fy \sum_{n=0}^{\infty} \frac{ye^{-2(n+1)y}}{y^2+a^2}. \tag{F.15}$$

Consider the integral of the generic term of the series (F.12) which can be written as:

$$2\int_0^\infty dy \frac{ye^{-2(n+1)y}}{y^2+a^2} = \sin(2a(n+1))(\pi - 2Si(2a(n+1))) - 2\cos(2a(n+1))Ci(2a(n+1))$$

$$\approx \frac{1}{2n^2a^2}, \tag{F.16}$$

where a is given by (F.2), Si and Ci are the exponential sine and cosine. Expanding the result (F.16) for small a we get:

$$2N^{-2}\int_0^\infty dy\frac{ye^{-2(n+1)y}}{y^2+a^2}\approx\frac{1}{2n^2a^2}. \tag{F.17}$$

We can finally sum over n (F.17) and we get:

$$\int_0^\infty dy\sum_{n=0}^{\infty}\frac{2e^{-2(n+1)y}y}{y^2+a^2}\approx\frac{\pi^2}{12a^2}, \tag{F.18}$$

where we used $\sum_n(n+1)^2=\pi^2/6$. In conclusion by summing (F.14) and (F.18) we get (4.59).

Bibliography

[1] S. Lepri, R. Livi, and A. Politi. Thermal conduction in classical low-dimensional lattices. *Physics Reports*, 377:1–80, 2003.

[2] Abhishek Dhar. Heat transport in low-dimensional systems. *Advances in Physics*, 57(5):457–537, sep 2008.

[3] Carlos Olivares and Celia Anteneodo. Role of the range of the interactions in thermal conduction. *Phys. Rev. E*, 94:042117, 2016.

[4] Debarshee Bagchi. Energy transport in the presence of long-range interactions. *Phys. Rev. E*, 96(4):042121, 2017.

[5] Jianjin Wang, Sergey V Dmitriev, and Daxing Xiong. Thermal transport in long-range interacting fermi-pasta-ulam chains. *Physical Review Research*, 2(1):013179, 2020.

[6] Debarshee Bagchi. Heat transport in long-ranged fermi-pasta-ulam-tsingou-type models. *Physical Review E*, 104(5):054108, 2021.

[7] P Di Cintio, S Iubini, S Lepri, and R Livi. Equilibrium time-correlation functions of the long-range interacting fermi–pasta–ulam model. *Journal of Physics A: Mathematical and Theoretical*, 52(27):274001, 2019.

[8] Stefano Iubini, Pierfrancesco Di Cintio, Stefano Lepri, Roberto Livi, and Lapo Casetti. Heat transport in oscillator chains with long-range interactions coupled to thermal reservoirs. *Phys. Rev. E*, 97:032102, Mar 2018.

[9] Z. Rieder, J. L. Lebowitz, and E. Lieb. Properties of a harmonic crystal in a stationary nonequilibrium state. *Journal of Mathematical Physics*, 8(5):1073–1078, 1967.

[10] Nahuel Freitas and Juan Pablo Paz. Analytic solution for heat flow through a general harmonic network. *Phys. Rev. E*, 90:042128, Oct 2014.

[11] S Lepri, C Mejí a-Monasterio, and A Politi. A stochastic model of anomalous heat transport: analytical solution of the steady state. *Journal of Physics A: Mathematical and Theoretical*, 42(2):025001, nov 2008.

[12] Shuji Tamaki and Keiji Saito. Energy current correlation in solvable long-range interacting systems. *Phys. Rev. E*, 101:042118, Apr 2020.

[13] Francesco Andreucci, Stefano Lepri, Stefano Ruffo, and Andrea Trombettoni. Classical and quantum harmonic mean-field models coupled intensively and extensively with external baths. *SciPost Phys. Core*, 5:036, 2022.

[14] Francesco Andreucci, Stefano Lepri, Stefano Ruffo, and Andrea Trombettoni. Nonequilibrium steady states of long-range coupled harmonic chains. *Phys. Rev. E*, 108:024115, Aug 2023.

[15] Francesco Andreucci, Stefano Lepri, Stefano Ruffo, and Carlos Mejia-Monasterio. *to appear*.

[16] David Mukamel. Notes on the statistical mechanics of systems with long-range interactions, 2009.

[17] Shamik Gupta and Stefano Ruffo. The world of long-range interactions: A bird's eye view. *International Journal of Modern Physics A*, 32(09):1741018, mar 2017.

[18] Nicolò Defenu, Tobias Donner, Tommaso Macrì, Guido Pagano, Stefano Ruffo, and Andrea Trombettoni. Long-range interacting quantum systems, 2021.

[19] Nicolò Defenu, Alessio Lerose, and Silvia Pappalardi. Out-of-equilibrium dynamics of quantum many-body systems with long-range interactions, 2023.

[20] M. Kac, G. E. Uhlenbeck, and P. C. Hemmer. On the van der Waals Theory of the Vapor-Liquid Equilibrium. I. Discussion of a One-Dimensional Model. *Journal of Mathematical Physics*, 4(2):216–228, 12 2004.

[21] Mathias Van Regemortel, Dries Sels, and Michiel Wouters. Information propagation and equilibration in long-range kitaev chains. *Phys. Rev. A*, 93:032311, Mar 2016.

[22] Alessandro Campa, Thierry Dauxois, and Stefano Ruffo. Statistical mechanics and dynamics of solvable models with long-range interactions. *Physics Reports*, 480(3):57–159, 2009.

[23] Pierre de Buyl, Giovanni De Ninno, Duccio Fanelli, Cesare Nardini, Aurelio Patelli, Francesco Piazza, and Yoshiyuki Y Yamaguchi. Absence of thermalization for systems with long-range interactions coupled to a thermal bath. *Physical Review E*, 87(4):042110, 2013.

[24] Freeman J. Dyson. Existence of a phase-transition in a one-dimensional Ising ferromagnet. *Communications in Mathematical Physics*, 12(2):91 – 107, 1969.

[25] D. J. Thouless. Long-range order in one-dimensional ising systems. *Phys. Rev.*, 187:732–733, Nov 1969.

[26] Nicolò Defenu, Alessandro Codello, Stefano Ruffo, and Andrea Trombettoni. Criticality of spin systems with weak long-range interactions. *Journal of Physics A: Mathematical and Theoretical*, 53(14):143001, mar 2020.

[27] J. Sak. Recursion relations and fixed points for ferromagnets with long-range interactions. *Phys. Rev. B*, 8:281–285, Jul 1973.

[28] Maria Chiara Angelini, Giorgio Parisi, and Federico Ricci-Tersenghi. Relations between short-range and long-range ising models. *Physical Review E*, 89(6), jun 2014.

[29] G. Gori, M. Michelangeli, N. Defenu, and A. Trombettoni. One-dimensional long-range percolation: A numerical study. *Physical Review E*, 96(1), jul 2017.

[30] Erik Luijten and Henk W. J. Blöte. Boundary between long-range and short-range critical behavior in systems with algebraic interactions. *Physical Review Letters*, 89(2), jun 2002.

[31] T. Blanchard, M. Picco, and M. A. Rajabpour. Influence of long-range interactions on the critical behavior of the ising model. *EPL (Europhysics Letters)*, 101(5):56003, mar 2013.

[32] Nicolò Defenu. Metastability and discrete spectrum of long-range systems. *Proceedings of the National Academy of Sciences*, 118(30), jul 2021.

[33] X.-P. Huang and C. F. Driscoll. Relaxation of 2d turbulence to a metaequilibrium near the minimum enstrophy state. *Phys. Rev. Lett.*, 72:2187–2190, Apr 1994.

[34] P. H. Chavanis. Kinetic theory of point vortices: Diffusion coefficient and systematic drift. *Phys. Rev. E*, 64:026309, Jul 2001.

[35] N. I. Muskhelishvili. *Some Basic Problems of the Mathematical Theory of Elasticity*. Springer Dordrecht.

[36] D. Leibfried, R. Blatt, C. Monroe, and D. Wineland. Quantum dynamics of single trapped ions. *Rev. Mod. Phys.*, 75:281–324, Mar 2003.

[37] C. Monroe, W. C. Campbell, L.-M. Duan, Z.-X. Gong, A. V. Gorshkov, P. W. Hess, R. Islam, K. Kim, N. M. Linke, G. Pagano, P. Richerme, C. Senko, and N. Y. Yao. Programmable quantum simulations of spin systems with trapped ions. *Rev. Mod. Phys.*, 93:025001, Apr 2021.

[38] Joseph W. Britton, Brian C Sawyer, C.-C. Joseph Wang, James K. Freericks, Hermann Uys, Michael J. Biercuk, and John J. Bollinger. Engineered two-dimensional ising interactions in a trapped-ion quantum simulator with hundreds of spins. *Nature*, 2012.

[39] R. Mottl, F. Brennecke, K. Baumann, R. Landig, T. Donner, and T. Esslinger. Roton-type mode softening in a quantum gas with cavity-mediated long-range interactions. *Science*, 336(6088):1570–1573, 2012.

[40] Tim Keller, Simon B Jäger, and Giovanna Morigi. Phases of cold atoms interacting via photon-mediated long-range forces. *Journal of Statistical Mechanics: Theory and Experiment*, 2017(6):064002, jun 2017.

[41] Hannes Risken. *The Fokker-Planck Equation*. Springer Berlin, Heidelberg.

[42] P. Virtanen, R. Gommers, and T.E. et al. Oliphant. Scipy 1.0: fundamental algorithms for scientific computing in python. *Nature*, 2020.

[43] Hiroshi Nakazawa. On the Lattice Thermal Conduction. *Progress of Theoretical Physics Supplement*, 45:231–262, 05 1970.

[44] Abhishek Dhar and Dibyendu Roy. Heat transport in harmonic lattices. *Journal of Statistical Physics*, 125(4):801–820, dec 2006.

[45] Junaid Majeed Bhat, Gaëtan Cane, Cédric Bernardin, and Abhishek Dhar. Heat transport in an ordered harmonic chain in presence of a uniform magnetic field. *Journal of Statistical Physics*, 186(1), nov 2021.

[46] Gaëtan Cane, Junaid Majeed Bhat, Abhishek Dhar, and Cé dric Bernardin. Localization effects due to a random magnetic field on heat transport in a harmonic chain. *Journal of Statistical Mechanics: Theory and Experiment*, 2021(11):113204, nov 2021.

[47] Dibyendu Roy and Abhishek Dhar. Role of pinning potentials in heat transport through disordered harmonic chains. *Physical Review E*, 78(5), nov 2008.

[48] Dibyendu Roy and Abhishek Dhar. Electron transport in a one dimensional conductor with inelastic scattering by self-consistent reservoirs. *Phys. Rev. B*, 75:195110, May 2007.

[49] Ion Santra and Urna Basu. Activity driven transport in harmonic chains. *SciPost Phys.*, 13:041, 2022.

[50] Nahuel Freitas, Esteban A Martinez, and Juan Pablo Paz. Heat transport through ion crystals. *Physica Scripta*, 91(1):013007, dec 2015.

[51] Françoise Tisseur and Karl Meerbergen. The quadratic eigenvalue problem. *SIAM Review*, 43(2):235–286, 2001.

[52] Luca Delfini, Stefano Lepri, Roberto Livi, and Antonio Politi. Nonequilibrium invariant measure under heat flow. *Phys. Rev. Lett.*, 101:120604, Sep 2008.

[53] L Delfini, S Lepri, R Livi, C Mejí a-Monasterio, and A Politi. Nonequilibrium dynamics of a stochastic model of anomalous heat transport: numerical analysis. *Journal of Physics A: Mathematical and Theoretical*, 43(14):145001, mar 2010.

[54] Stefano Lepri. Thermalization of isolated harmonic networks under conservative noise. *Journal of Statistical Physics*, 190(1), nov 2022.

[55] Giada Basile, Cédric Bernardin, Milton Jara, Tomasz Komorowski, and Stefano Olla. Thermal conductivity in harmonic lattices with random collisions, 2015.

[56] Lucianno Defaveri, Carlos Olivares, and Celia Anteneodo. Heat flux in chains of nonlocally coupled harmonic oscillators: Mean-field limit. *Phys. Rev. E*, 105:054149, May 2022.

[57] Luis G. C. Rego and George Kirczenow. Quantized thermal conductance of dielectric quantum wires. *Phys. Rev. Lett.*, 81:232–235, Jul 1998.

[58] Dvira Segal, Abraham Nitzan, and Peter Hänggi. Thermal conductance through molecular wires. *The Journal of Chemical Physics*, 119(13):6840–6855, 2003.

[59] Andrea Zoia, Alberto Rosso, and Mehran Kardar. Fractional laplacian in bounded domains. *Physical Review E*, 76(2):021116, 2007.

[60] Hirotsugu Matsuda and Kazushige Ishii. Localization of normal modes and energy transport in the disordered harmonic chain. *Progress of Theoretical Physics Supplement*, 45:56–86, 1970.

[61] Nahuel Freitas and Juan Pablo Paz. Analytic solution for heat flow through a general harmonic network. *Phys. Rev. E*, 90:042128, Oct 2014.

[62] Jack Sherman and Winifred J. Morrison. Adjustment of an Inverse Matrix Corresponding to a Change in One Element of a Given Matrix. *The Annals of Mathematical Statistics*, 21(1):124 – 127, 1950.